CHAPTER (4)

RESULTS AND DISCUSSION

CHAPTER (4)

4. RESULTS AND DISCUSSION

This chapter is divided into four sections. In Section 1, the chemical structure conformation of the synthesized 3-mercaptoalkyloxy aniline surfactants and 3-mercaptoalkyloxy polyaniline surfactants are discussed. In Section 2 the self-assembling of these surfactants on silver nanoparticlies was studied. In Section 3 we discussed the surface properties of the synthesized surfactants. In section 4, The application of these surfactants and their nano structure with the prepared silver nanoparticles was investigated as corrosion inhibitors

4.1. Structure conformation of the synthesized surfactants

4.1.1. Structure conformation of the synthesized 3-mercapto alkyloxy aniline Surfactants

The chemical structure of the synthesized surfactants (C6M, C8M, C10M and C12M) as shown in scheme (3,4) was confirmed using FTIR, and ^{1}HNMR spectroscopy.

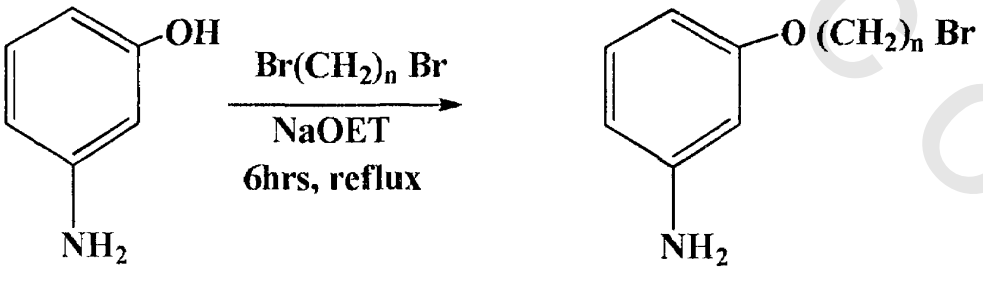

Where n = 6, 8, 10 and 12

Scheme3

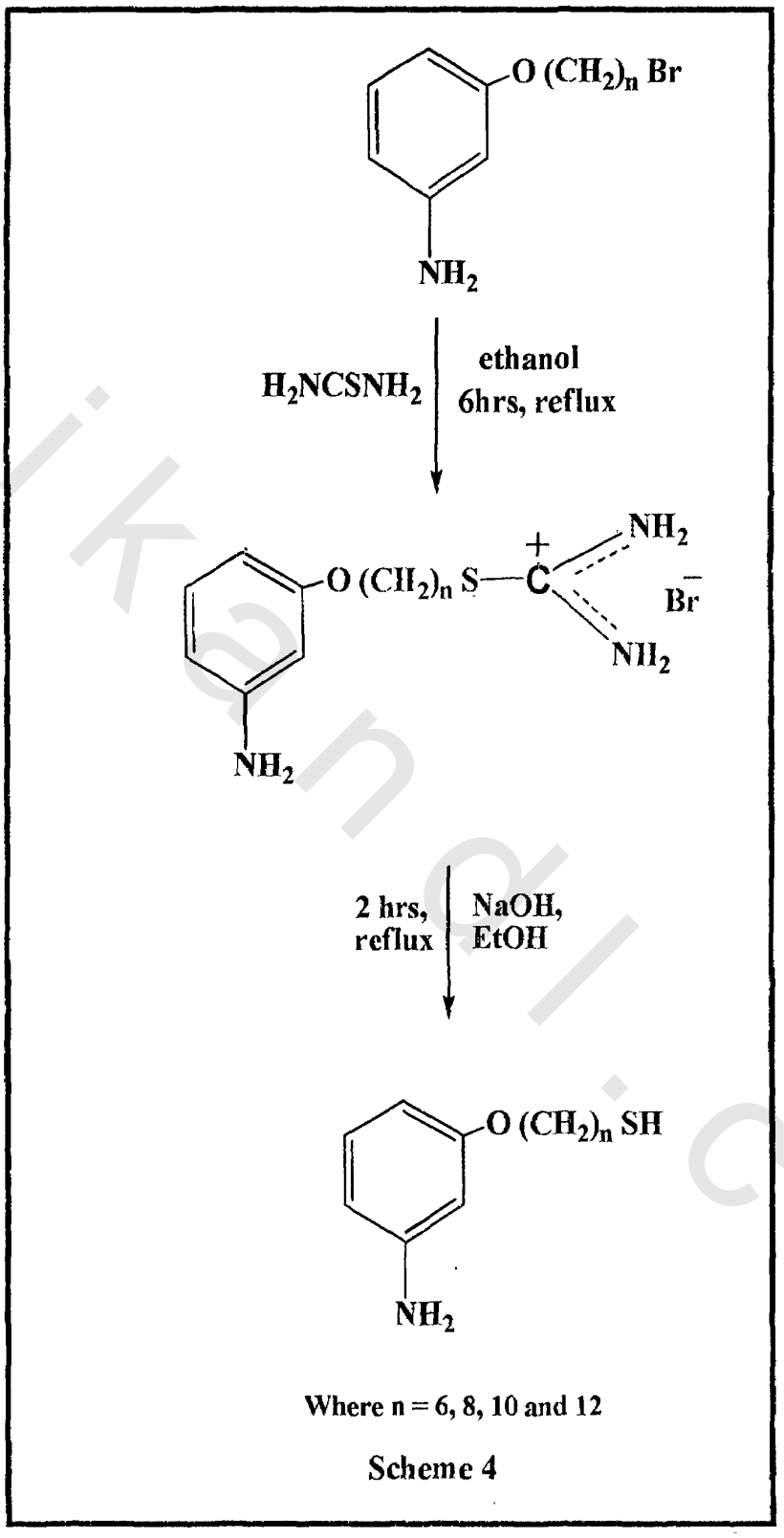

Where n = 6, 8, 10 and 12

Scheme 4

4.1.1.1. Fourier Transform Infrared Spectrometer (FTIR)

The FTIR data in Figures (3-6) and Table (3) show the peaks for the individual monomeric surfactants as follow ν_{sym} (NH_2) around 3450cm^{-1}. ν_{sym} (CH_2) around 2853 cm^{-1}, ν_{asym} (CH_2) around 2918 cm^{-1}, ν_{sym} (SH) around 2450 cm^{-1} ν (C=C)Ar around 1600 cm^{-1}, 1490 cm^{-1}, δ (CH_2) around 1461 cm^{-1}, 1318 cm^{-1}, ν_{asym} (COC) around 1250 cm^{-1}, ν (C-N) around 1152 cm^{-1}, ν_{sym} (COC) around 1021 cm^{-1}, meta substituted benzene ring around 580cm^{-1}, ν_{sym} (C-S) bands around 620 cm^{-1}. The shift and the intensity of the peaks depend on the difference in the alkyl chain length of C6M-C12M surfactants.

Table (3): FTIR spectroscopic data of C6M, C8M, C10M and C12M

Functional Group	I.R. Bands (cm^{-1})			
	C6M	C8M	C10M	C12M
$\nu_{sym}(NH_2)$	3442	3416	3450	3455
$\nu_{asym}(CH_2)$	2923	2922	2915	2917
$\nu_{sym}(CH_2)$	2852	2851	2850	2845
ν_{sym} (SH) weak band	2337	2464	2388	2419
ν (C=C) Ar	1560	1622	1504	1612
δ (CH2) bending	1455	1310	1392	1455
ν_{asym}(COC)	1250	1215	1240	1150
ν (C-N)	1119	1155	1150	1145
ν_{sym}(COC)	1045	1050	1053	1030
Meta substituted benzene ring	619	609	580	618
ν_{sym} (C-S)	657	640	590	618

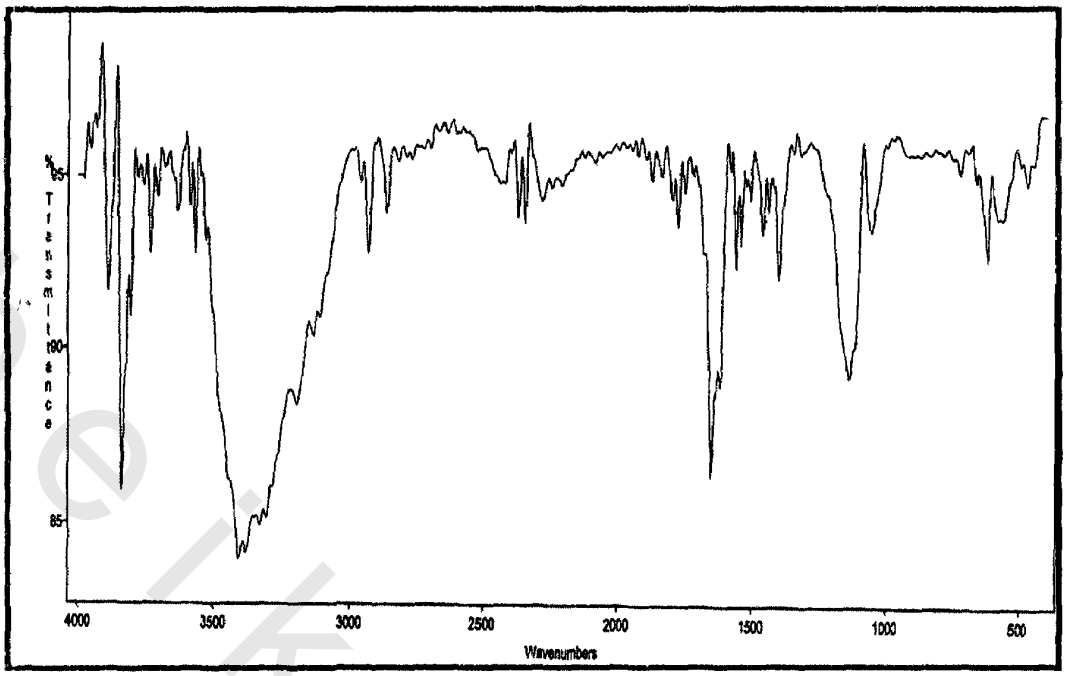

Figure (3) FTIR-spectrum of 6-(3-amino phenoxy) hexane-1- thiol(C6M)

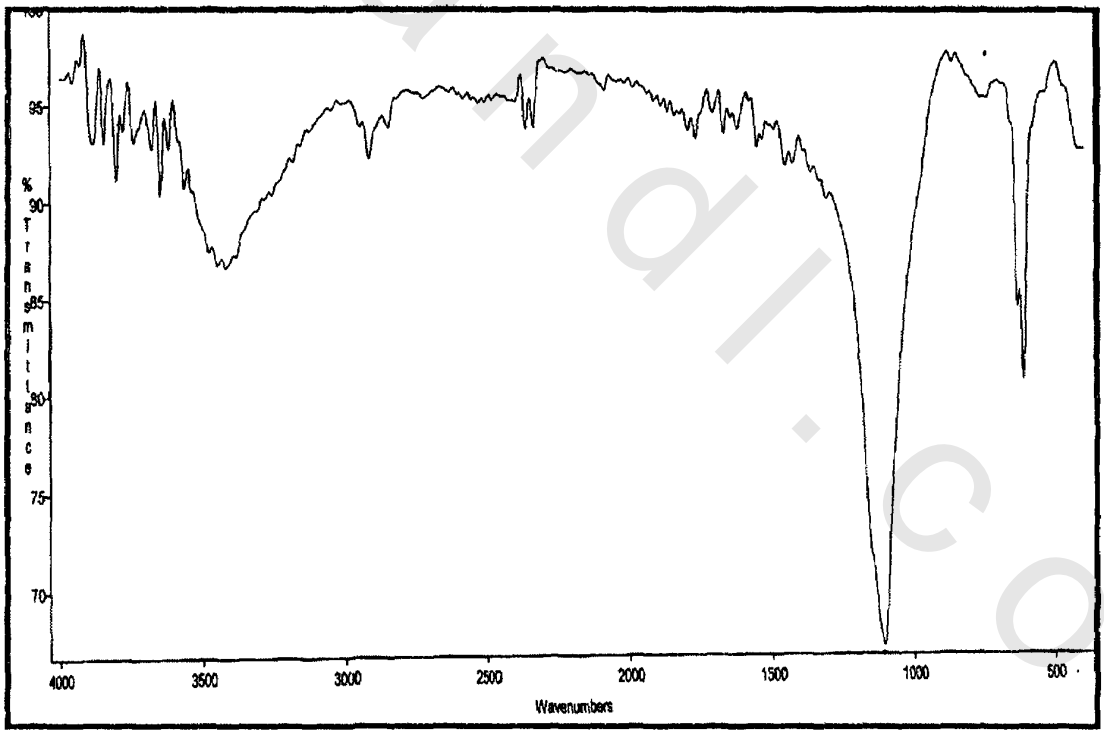

Figure (4) FTIR-spectrum of 8-(3-amino phenoxy) octane-1-thiol (C8M)

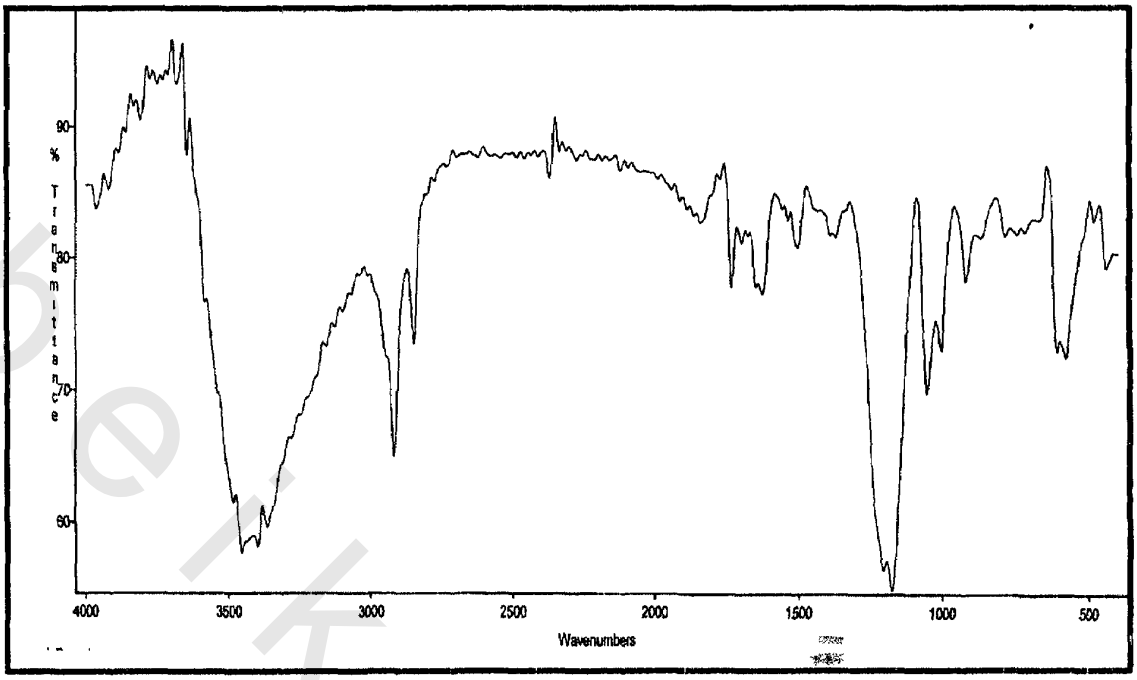

Figure (5) FTIR-spectrum of 10-(3-amino phenoxy) decane-1-thiol (C10M)

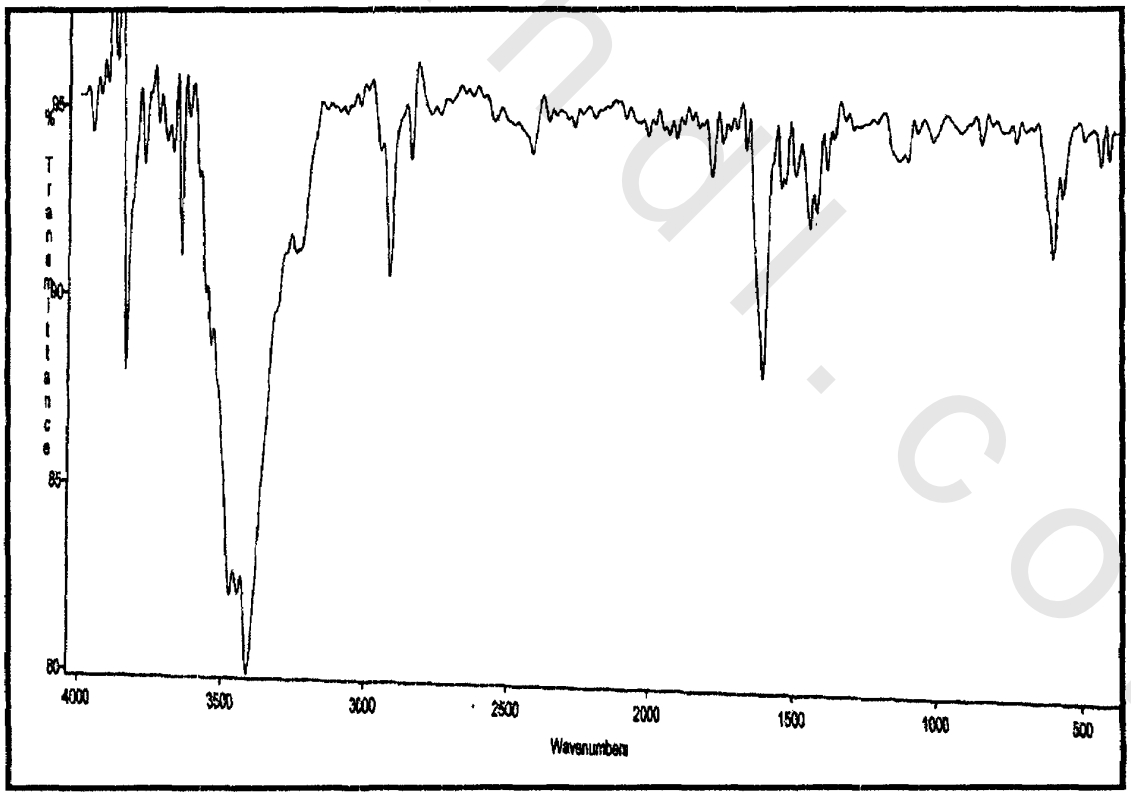

Figure (6) FTIR-spectrum of 12-(3-amino phenoxy) dodecane-1- thiol (C12M)

4.1.1.2. Proton Nuclear Magnetic Resonance (^{1}HNMR)

The ^{1}HNMR spectra of the synthesized monomeric surfactants in Figures (7-10) and Table (4) show the following δ values.

Table (4): ^{1}HNMR spectroscopy of C6M, C8M, C10M and C12M

Compound	^{1}HNMR spectra data (δ) ppm
C6M	1.3, 1.4, 1.5 (m, 8H, CH2), 2.5 (q, 2H, S-CH2), 3.9 (t, 2H, O-CH2), 6.5 (s, 1H, Ar), 7. (t, 1H, Ar), 6.8 (d, 2H, Ar).
C8M	1.23, 1.47 1.78 (m, 12H, CH2), 2.61 (q, 2H, S-CH2), 3.71 (t, 2H, O-CH2) and 7.26(m, 4H, Ar).
C10M	1.23, 1.47, 1.78 (m, 16H, CH2), 2.61 (q, 2H, S-CH2), 3.71 (t, 2H, O-CH2) and 7.26(m, 4H, Ar).
C12M	1.23, 1.47, 1.78 (m, 20H, CH2), 2.61 (q, 2H, S-CH2), 3.71 (t, 2H, O-CH2) and 7.26(m, 4H, Ar).

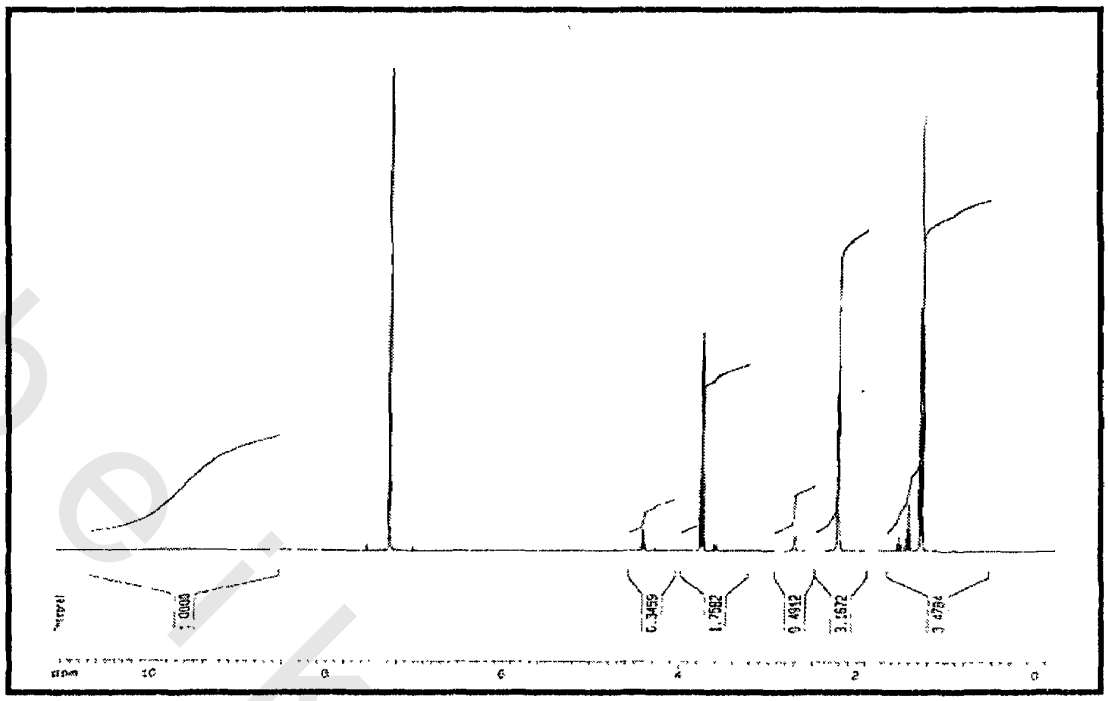

Figure (7): ^{1}HNMR -spectrum of 6-(3-amino phenoxy) hexane-1- thiol (C6M)

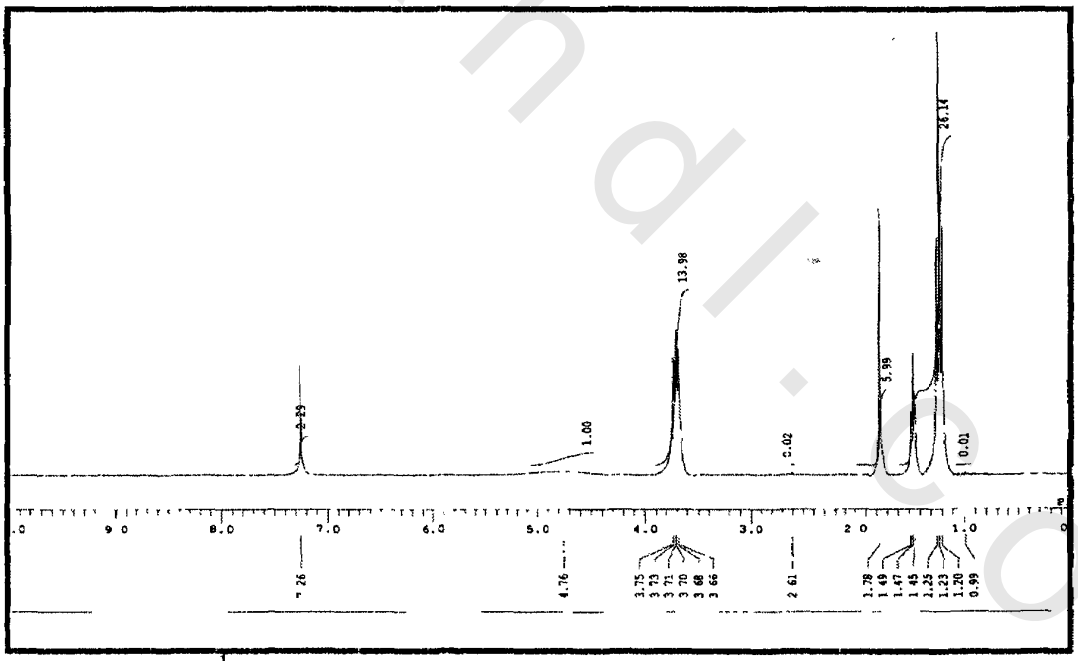

Figure (8): ^{1}HNMR-spectrum of 8-(3-amino phenoxy) octane thiol (C8M)

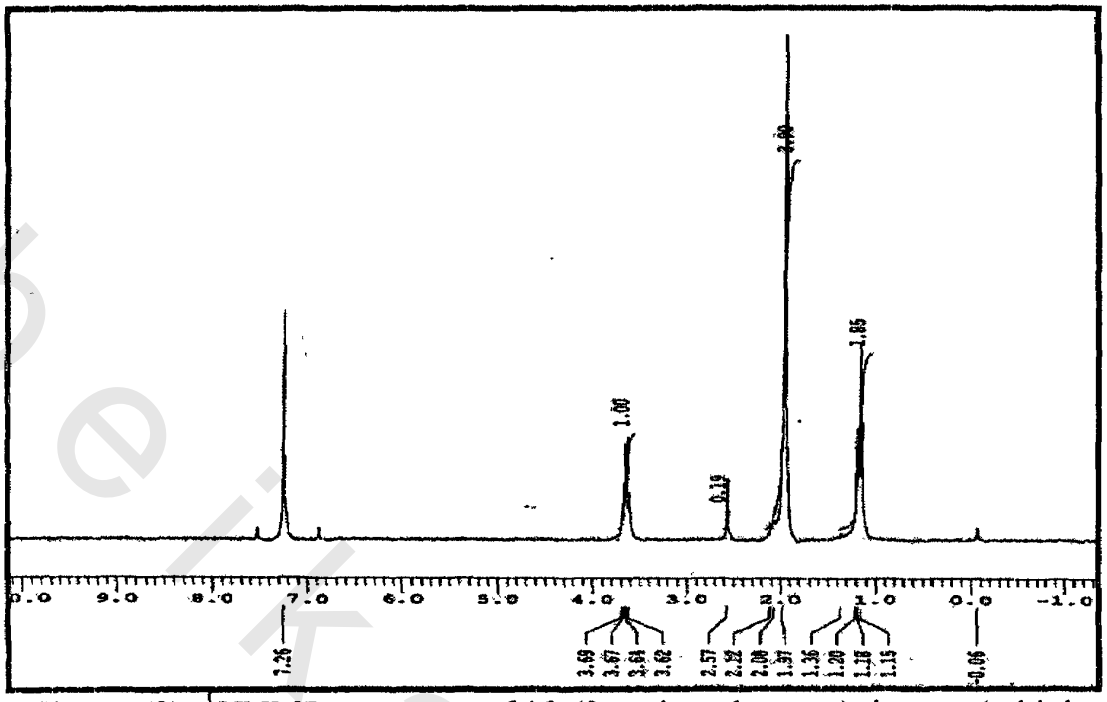

Figure (9): ^{1}HNMR-spectrum of 10-(3-amino phenoxy) decane-1-thiol (C10M)

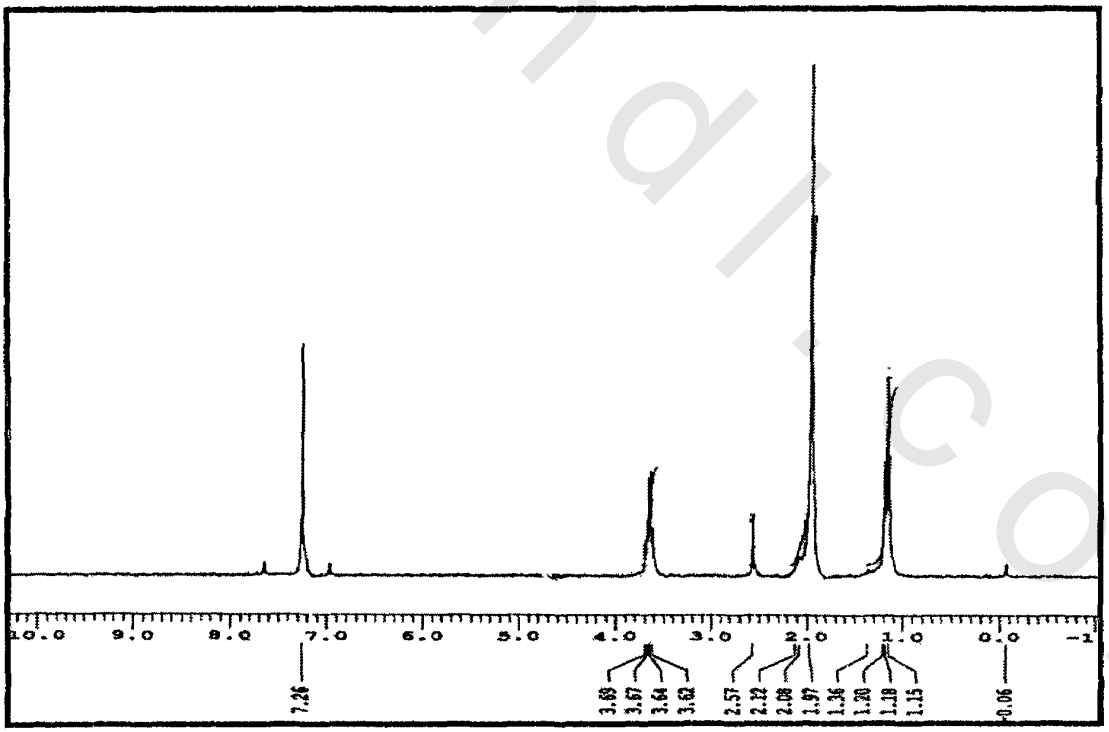

Figure (10): ^{1}HNMR-spectrum of 12-(3-amino phenoxy) dodecane-1-thiol (C12M)

4.1.2. Structure conformation of the synthesized 3- mercapto alkyloxy polyaniline thiol Surfactants

The chemical structure of the synthesized polymeric surfactants (C6P, C8P, C10P and C12P) as shown in scheme (5) was confirmed using FTIR, TGA, DSC and XRD.

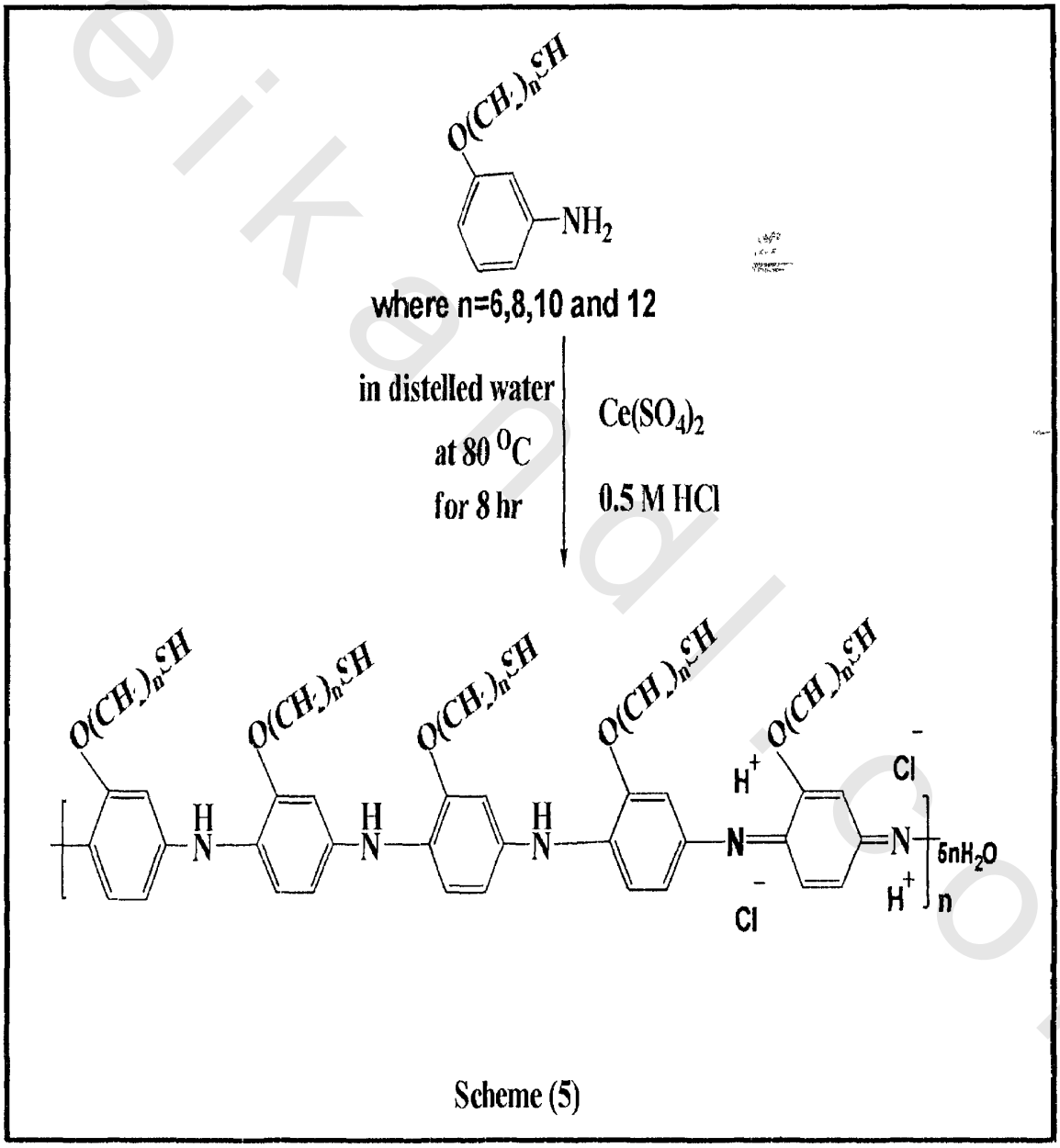

Scheme (5)

4.1.2.1. Fourier Transform Infrared Spectrometer (FTIR)

The FTIR spectra of the synthesized polymeric surfactants (C6P, C8P, C10P, and C12P) are represented in Figures (11-14) and Table (5) it is clear that the adsorption bands of these compounds are identical to those of their monomers that it is due to the similarity between their function groups. Also the adsorption band of the (–NH-) appeared around 3450 cm^{-1} as single band with slight shift compared with that of the (NH_2) group in monomeric surfactants.

Table (5): FTIR spectroscopic data of C6P, C8P, C10P and C12P

Functional Group	I.R. Bands (cm^{-1})			
	C6P	C8P	C10P	C12P
ν_{sym}(-NH-)	3442	3416	3450	3455
$\nu_{asym}(CH_2)$	2923	2922	2915	2917
$\nu_{sym}(CH_2)$	2852	2851	2850	2845
ν_{sym} (SH) weak band	2337	2464	2388	2419
ν (C=C) Ar	1560	1622	1504	1612
δ (CH2) bending	1455	1310	1392	1455
ν_{asym}(COC)	1250	1215	1240	1150
ν (C-N)	1119	1155	1150	1145
ν_{sym}(COC)	1045	1050	1053	1030
Meta substituted benzene ring	619	609	580	618
ν_{sym} (C-S)	657	640	590	618

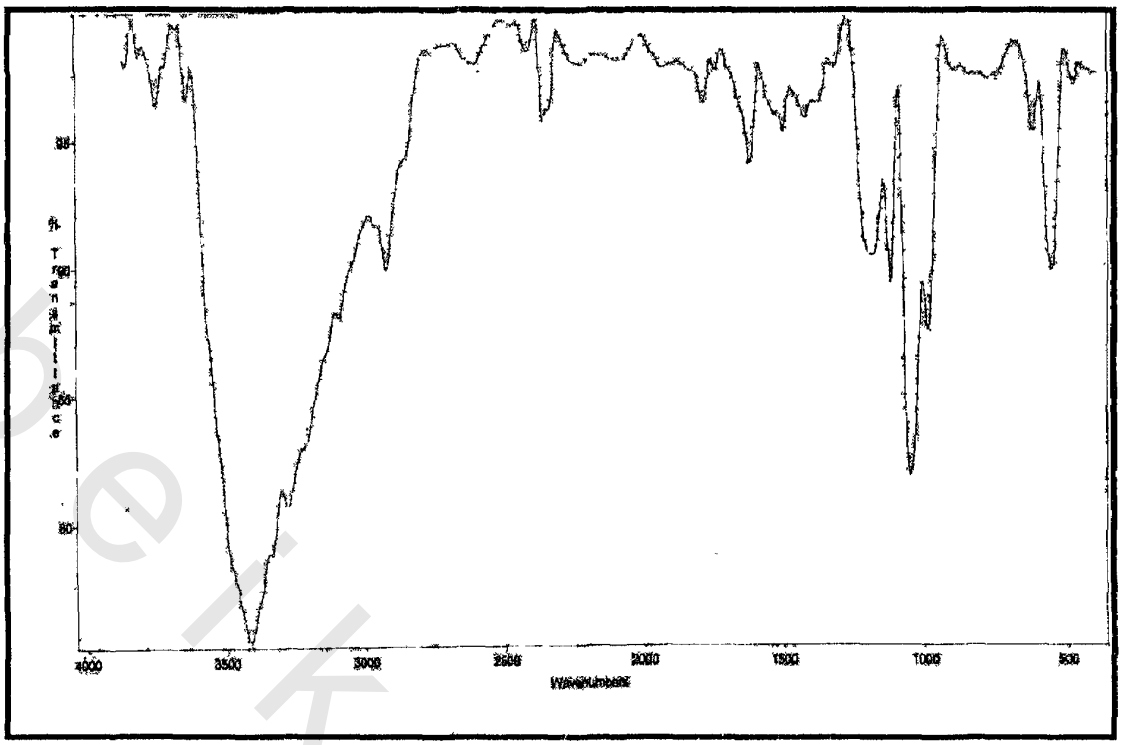

Figure (11) FTIR-spectrum of poly 6-(3-amino phenoxy) hexane-1- thiol (C6P)

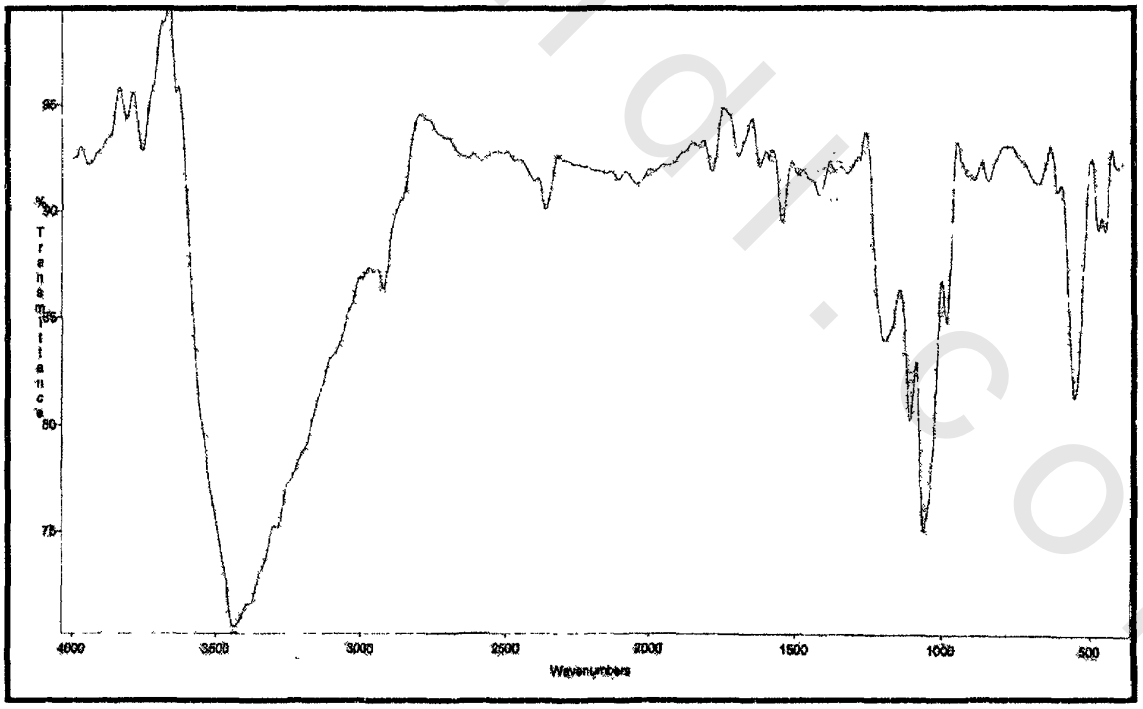

Figure (12) FTIR-spectrum of poly 8-(3-amino phenoxy) octane-1- thiol (C8P)

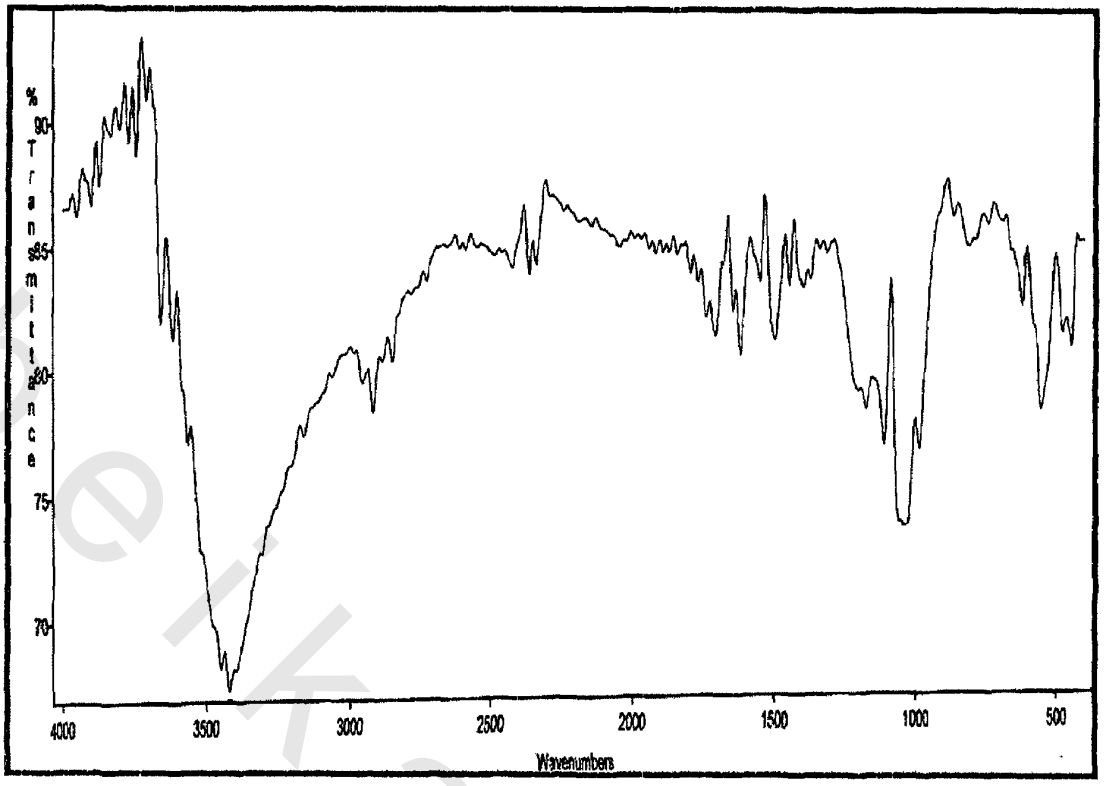

Figure (13) FTIR-spectrum of poly 10-(3-amino phenoxy) decane-1-thiol (C10P)

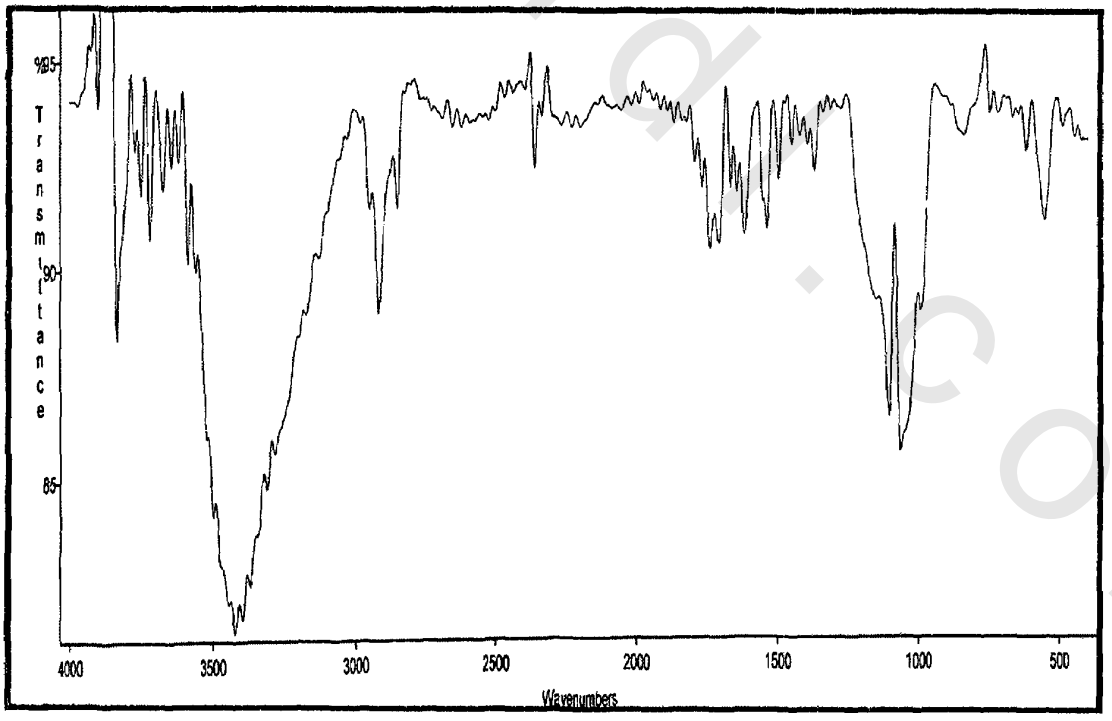

Figure (14) FTIR-spectrum of poly 12-(3-amino phenoxy) dodecane-1-thiol (C12P)

4.2.1.2. Thermal Gravimetric analysis (TGA) & Differential Scaning Colorimetry (DSC)

The thermogravimetric analysis (TGA) and Differential Scanning Colorimetry (DSC) for the synthesized polymeric surfactants are shown in Figures 15–18. The thermal behavior of the four polymers samples (C6P, C8P, C10P and C12P) is summarized as follow:-

The first stage:-This stage includes a loss of water of hydration in the four polymer samples at the temperature range from room temperature up to 150 ^{O}C. The estimated weight losses for this step were found to be 16.7%, 12.86%, 10.94% and 8.63% for C6P, C8P, C10P, and C12P, respectively. (Based on the repeat units in the suggested structures in Scheme (5) are 6.42%, 5.83%, and 4.94% for C6P, C8P, C10P, and C12P, respectively. This stage shows a broad endothermic peak in DSC curves starting at 46.09, 43.28, 66.11 and 63.13 ^{O}C for C6P, C8P, C10P, and C12P, respectively.

The second stage:-at the temperature range (150- 300 ^{O}C) from both TGA and DSC curves, the polymer samples show some thermal stability with no chemical or physical changes.

The Third stage:-at the temperature rang (300–400 ^{O}C) includes a loss of HCl molecules from each repeat unit in the four polymer samples associated with an endo-thermic peak on DSC curves. The weight loss in this stage is found to be 3.36, 4.68, 4.82, and 5.00%, for C6P, C8P, C10P, and C12P, respectively

The last stage:-at the temperature range (600–800 ^{O}C) includes the loss of all benzenoid alkyloxy groups except the (O-$(CH_2)_n$-SH) attached to the quinoid benzene ring. The estimated weight loss of this stage is found to be 13.73, 11.57, 10.09 and 9.18%, for C6P, C8P, C10P, and C12P,

respectively This stage is associated with an endothermic peak (1) followed by exothermic peak (2) on the DSC curves, which could be attributed to the break of covalent bond between benzene ring and ($O(CH_2)_nSH$) (peak 1) and the combination between the alkyloxy radicals respectively (peak 2) **[Sayyah et al., 2006].**

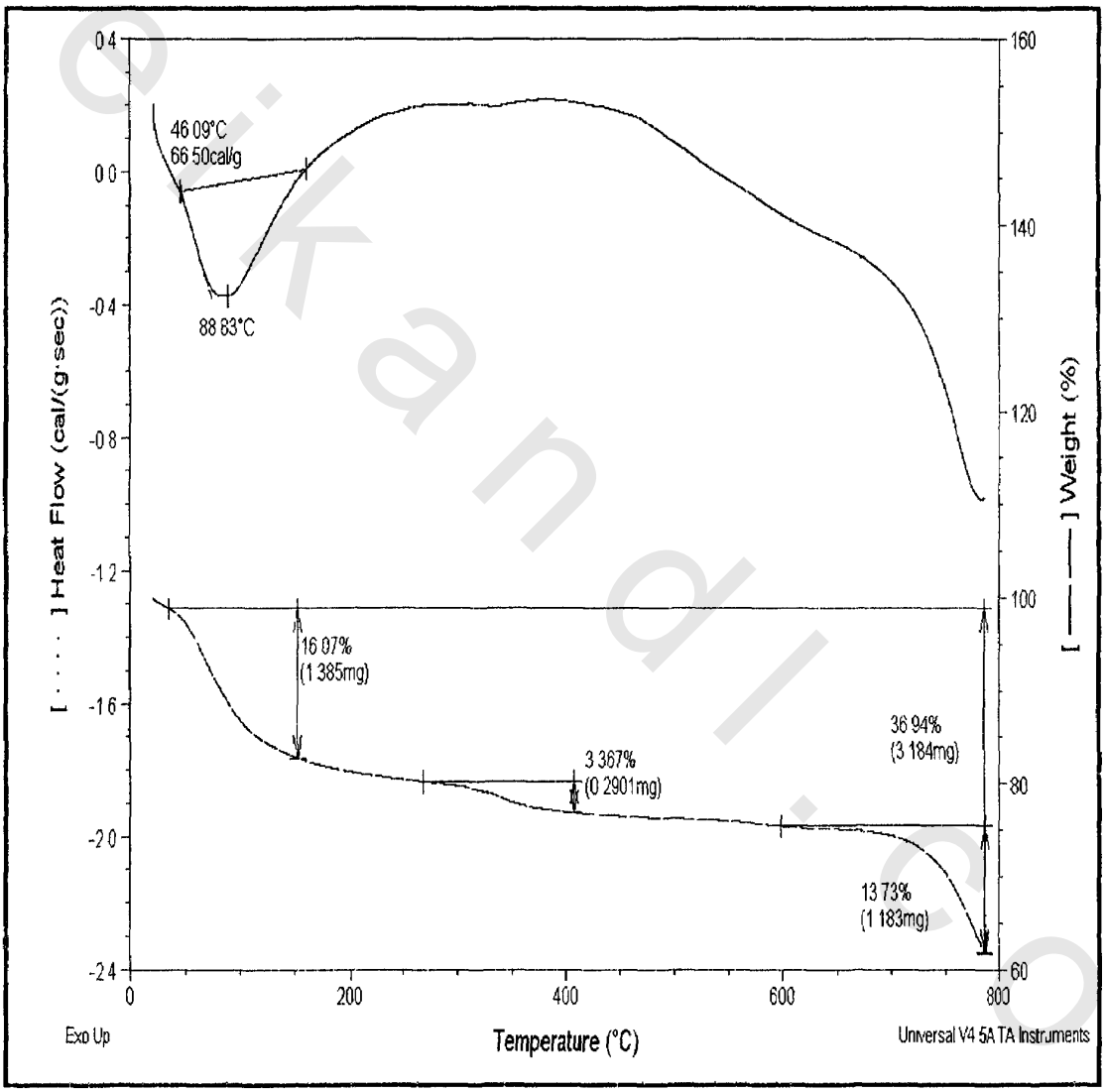

Figure (15) TGA &DSC Chart of poly 6-(3-amino phenoxy) hexane-1-thiol (C6P)

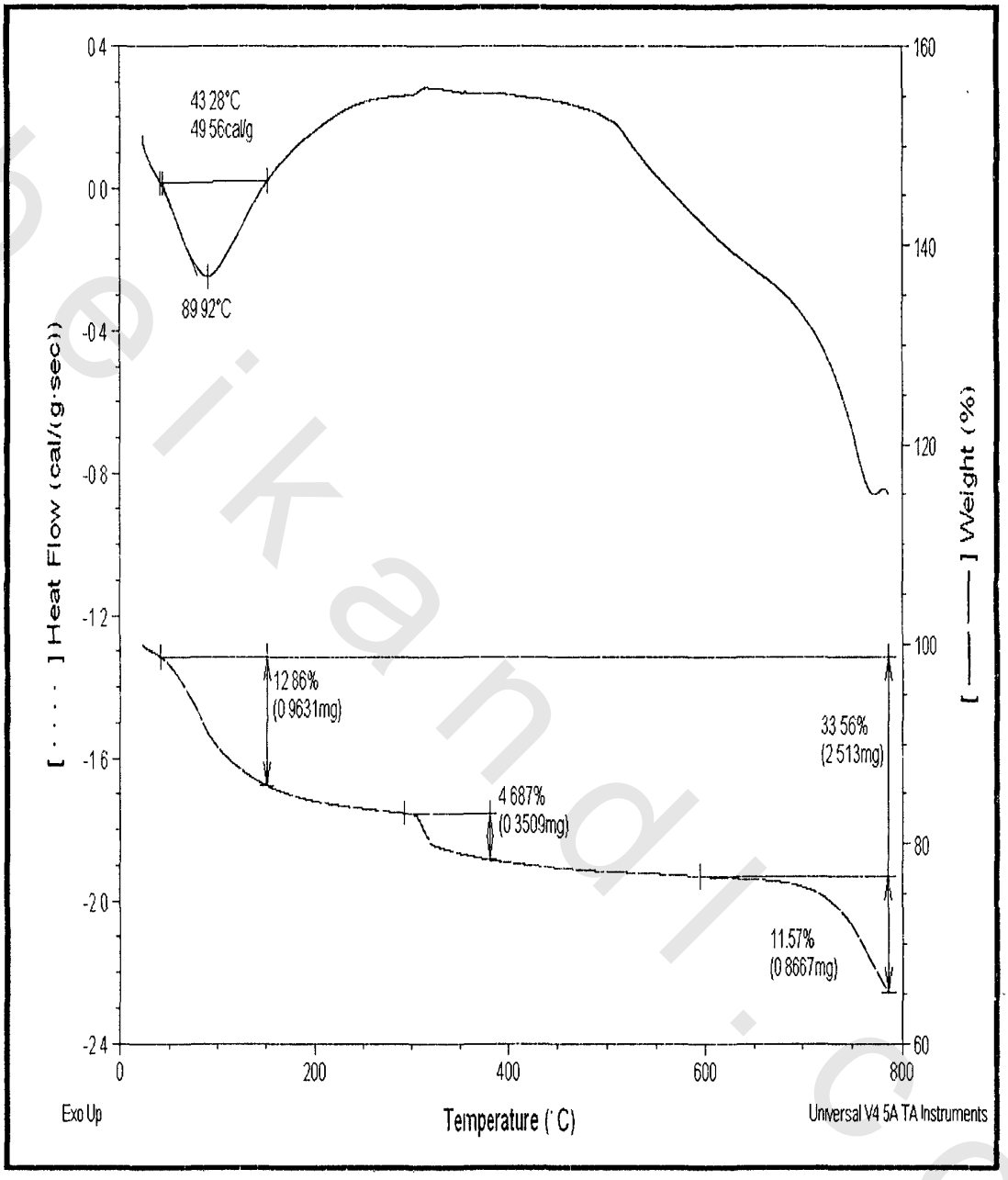

Figure (16) TGA &DSC Chart of poly 8-(3-amino phenoxy) octane-1-thiol (C8P)

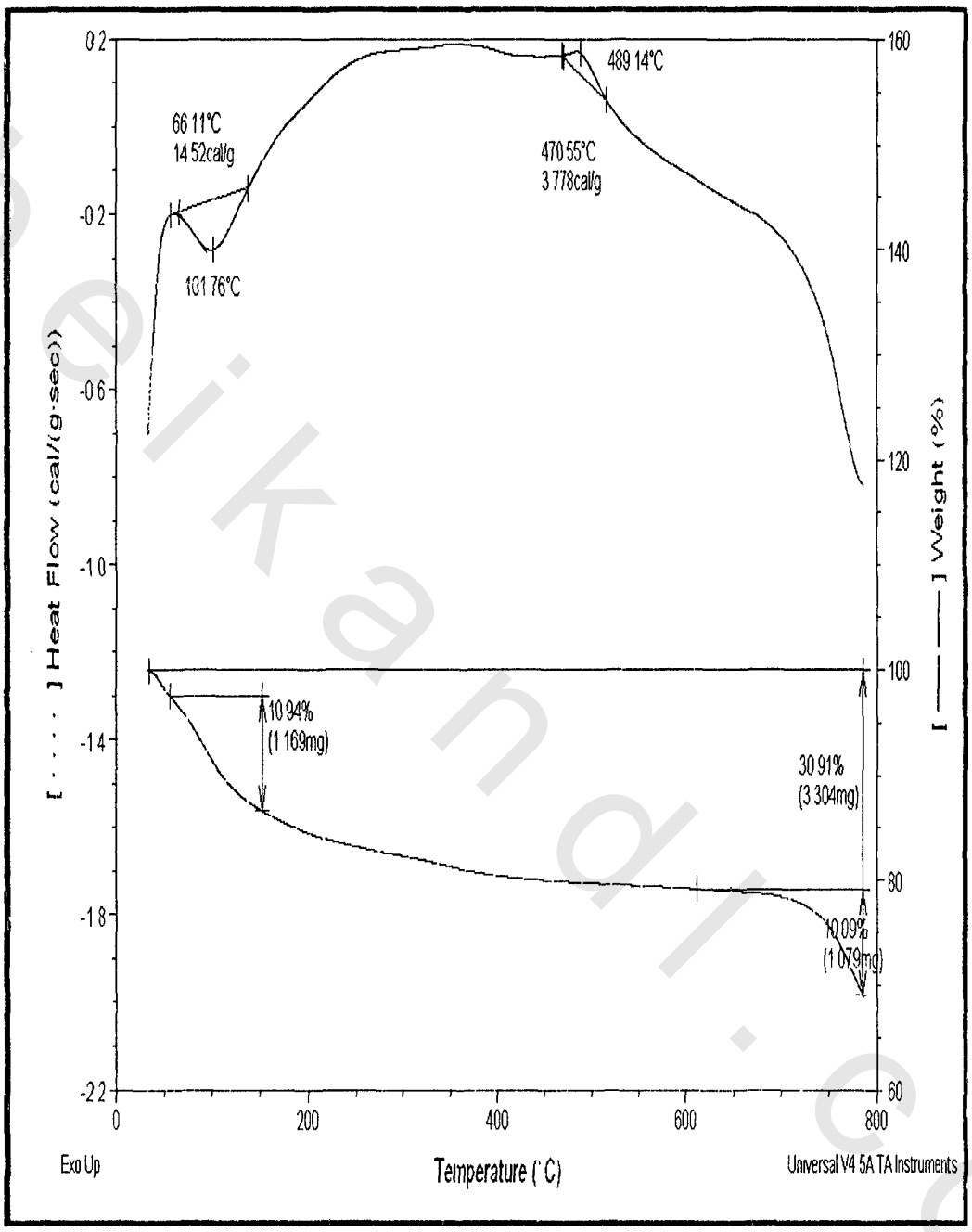

Figure (17) TGA &DSC Chart of poly 10-(3-amino phenoxy) decane-1-thiol (C10P)

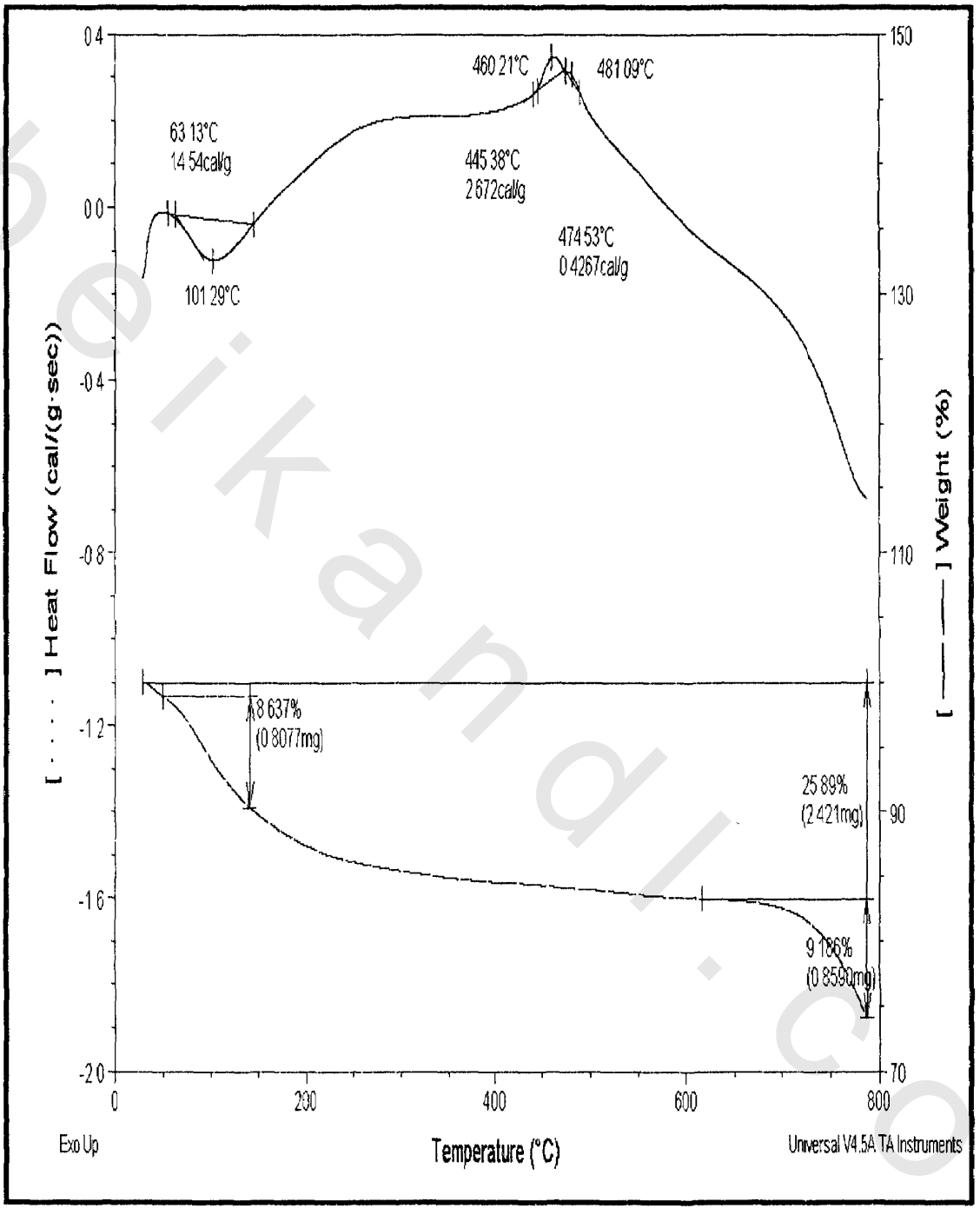

Figure (18) TGA &DSC Chart of poly 12-(3-amino phenoxy) dodecane-1- thiol (C12P)

X-Ray Diffraction Analysis (XRD)

The X-ray diffraction patterns of the four synthesized polymeric surfactants (C6P, C8P, C10P, and C12P) are represented in Figures (19-22). The figures show that the synthesized polymer samples are amorphous materials with slight portion of crystallinity that give a peak at 2θ about 25-32 degree with different intensity, which related to polyaniline derivatives **[Sayyah et al., 2006]**.

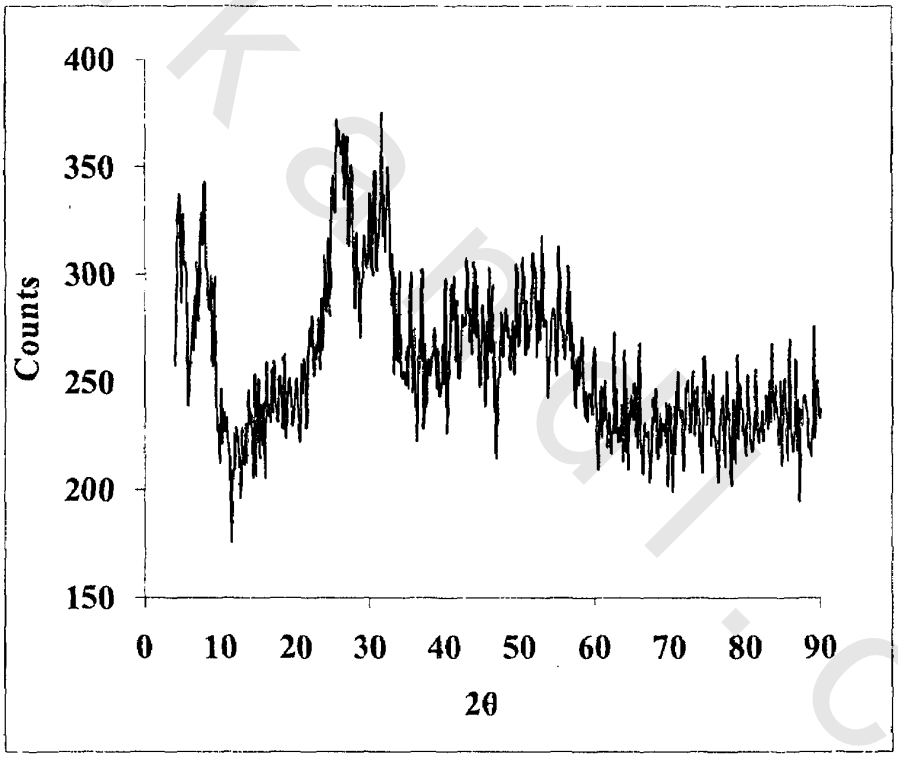

Figure (19) XRD spectra of poly 6-(3-amino phenoxy) hexane-1- thiol (C6P)

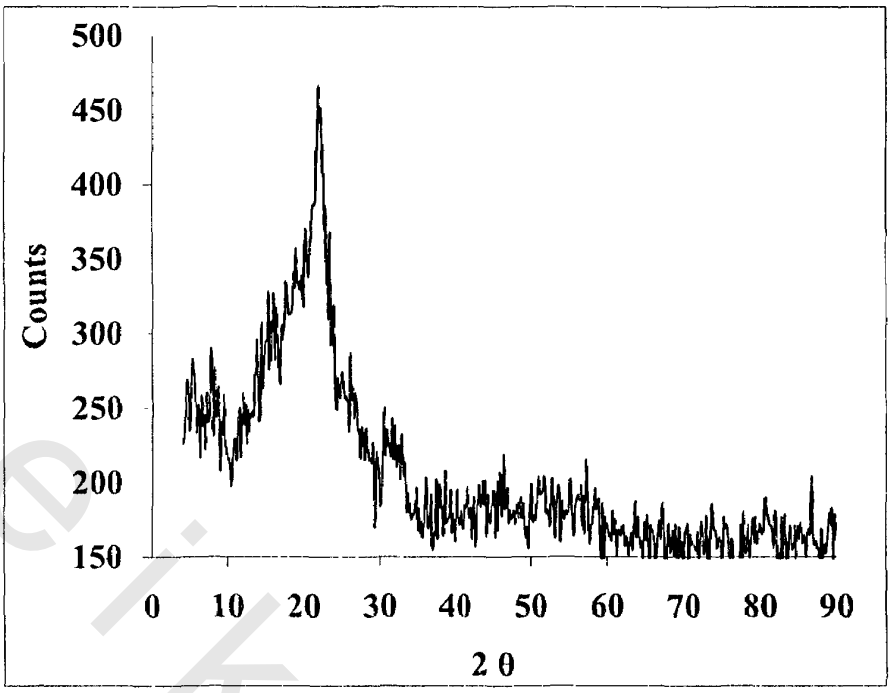

Figure (20) XRD spectra of poly 8-(3-amino phenoxy) octane-1- thiol (C8P)

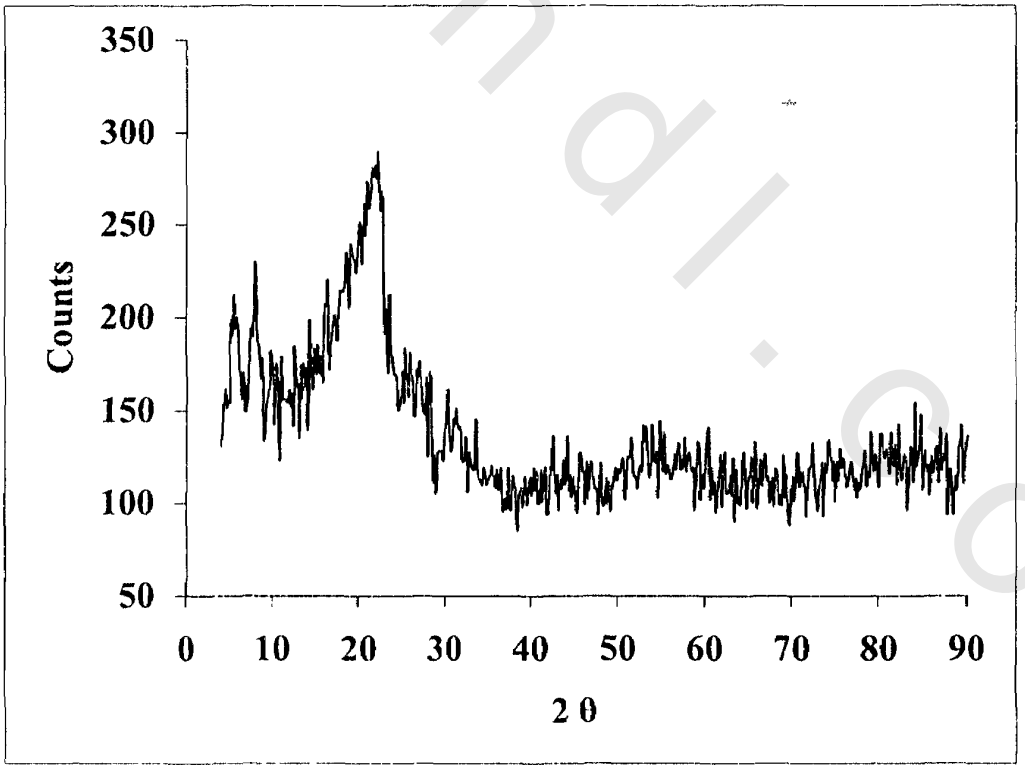

Figure (21) XRD spectra of poly 10-(3-amino phenoxy) decane-1- thiol (C10P)

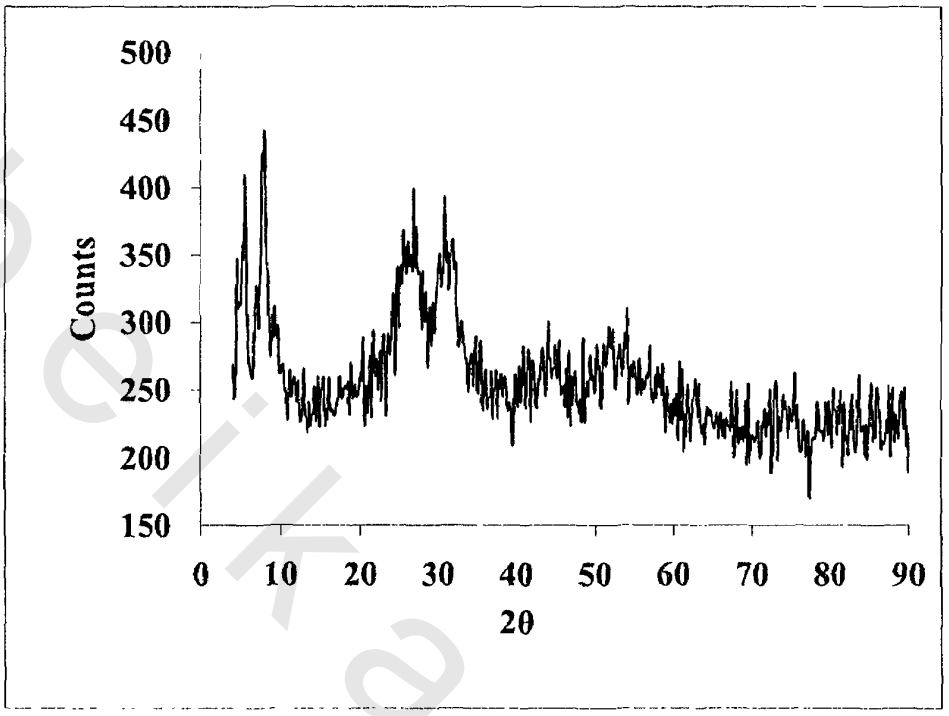

Figure (22) XRD spectra of poly 12-(3-amino phenoxy) dodecane-1-thiol (C12P)

4.2. Self-assembling of the synthesized surfactants

4.2.1. Self-assembling of the monomeric Surfactants (C6M-C12M) on AgNPs

The self-assembling of the synthesized monomeric surfactants on AgNPs was studies using FTIR, UV, XRD and TEM techniques as following

4.2.1.1. Fourier Transform Infrared Spectroscopy (FTIR)

One of the experimental techniques used in this work is the FTIR spectroscopy for confirmation of the self-assembling of the synthesized monomeric thiol surfactants on the silver nanoparticles. The FTIR data in Figures (23-26) for the nanostructure of these surfactants with the AgNPs show peaks similar to that of the individual surfactants in Figures (3-6). The shift in intensity and disappear the peaks depend on the difference in the alkyl chain length from C6M to C12M monomeric thiol surfactants. The shift and disappear of the peaks in FTIR spectra of the nanostructure of these surfactants with the silver nanoparticles Figures (23-26) from that of their individual structure without the silver nanoparticles Figures (3-6) may be related to the orientation of the surfactant molecules when assembled on the silver nanoparticles that leads to this shift in the FTIR peaks. Comparing, between the FTIR results of the individual monomeric thiol surfactants and their nanostructure with the silver nanoparticles, the self-assembling of the prepared monomeric thiol surfactants on the silver nanoparticles can be confirmed.

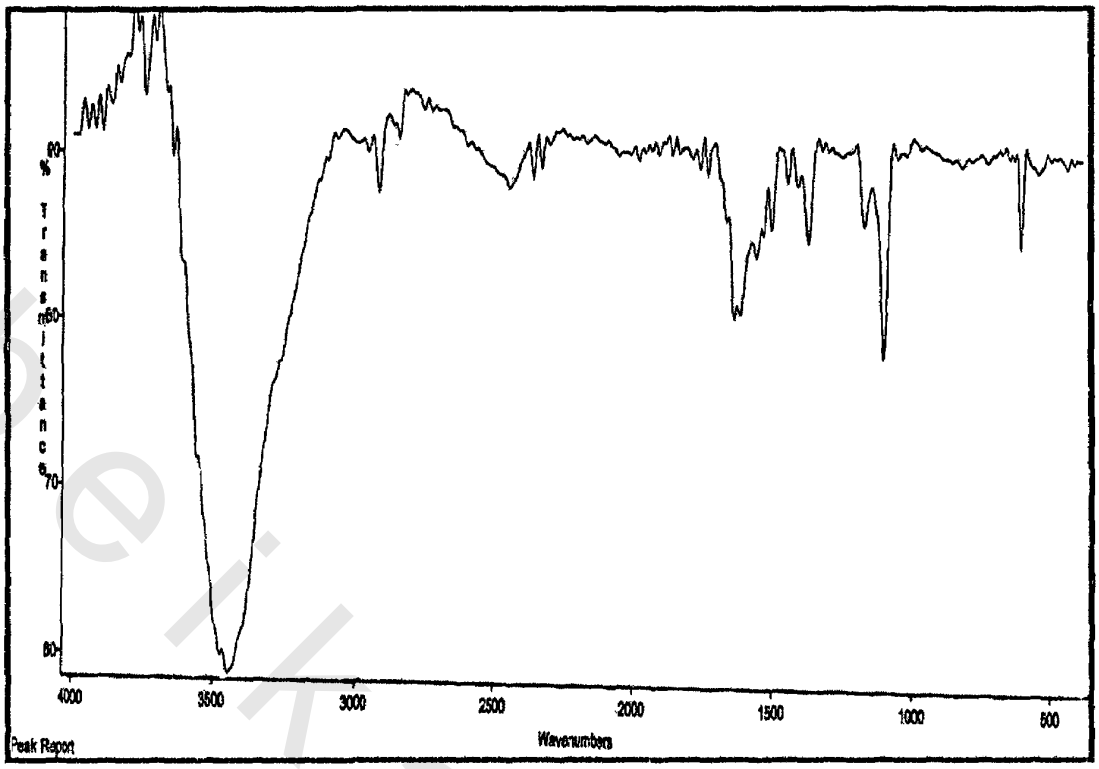

Figure (23) FTIR-spectrum of 6-(3-amino phenoxy) hexane-1- thiol (C6M) with AgNPs

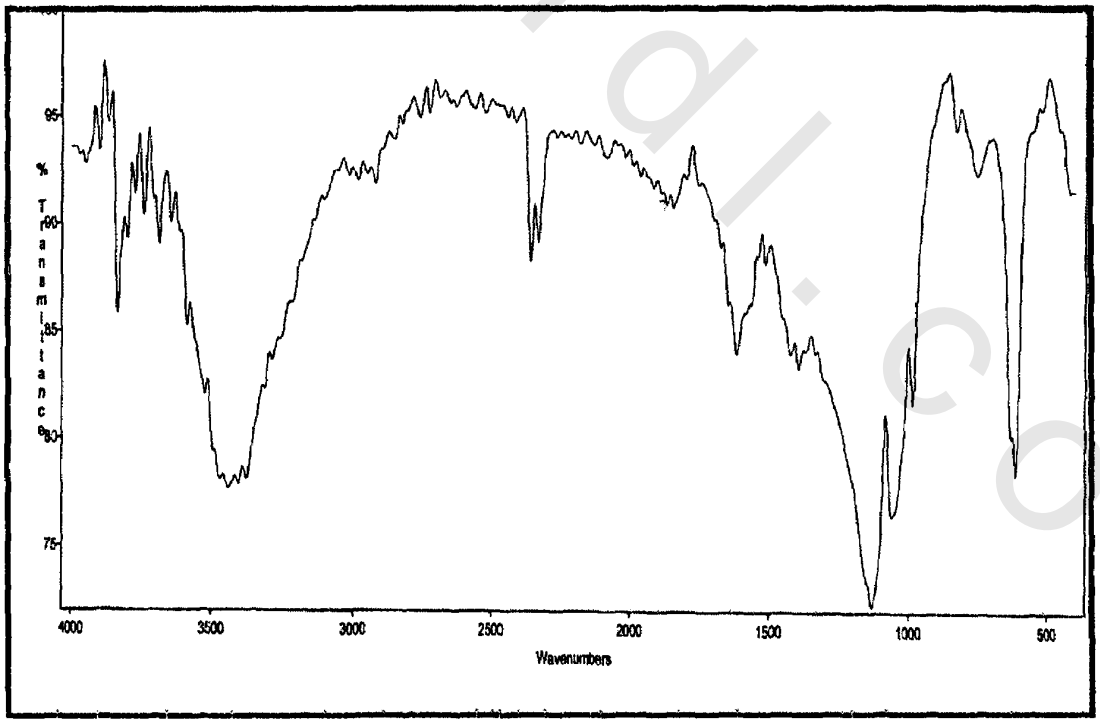

Figure (24) FTIR-spectrum of 8-(3-amino phenoxy) octane-1- thiol (C8M) with AgNPs

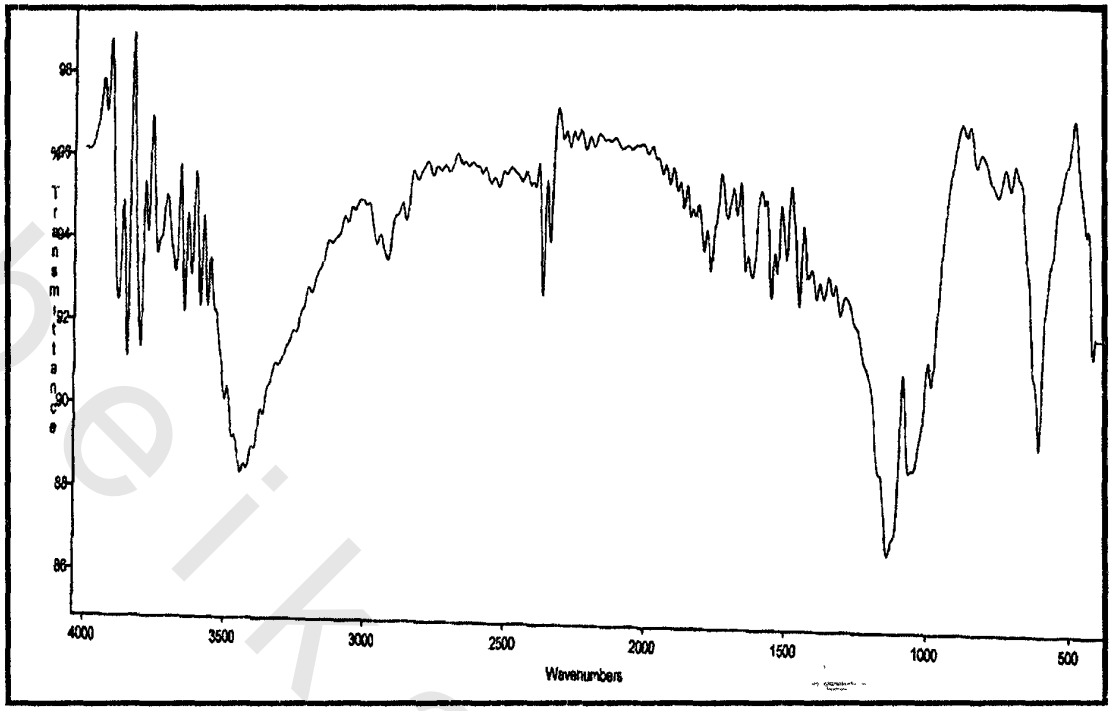

Figure (25) FTIR-spectrum of 10-(3-amino phenoxy) decane-1- thiol (C10M) With AgNPs

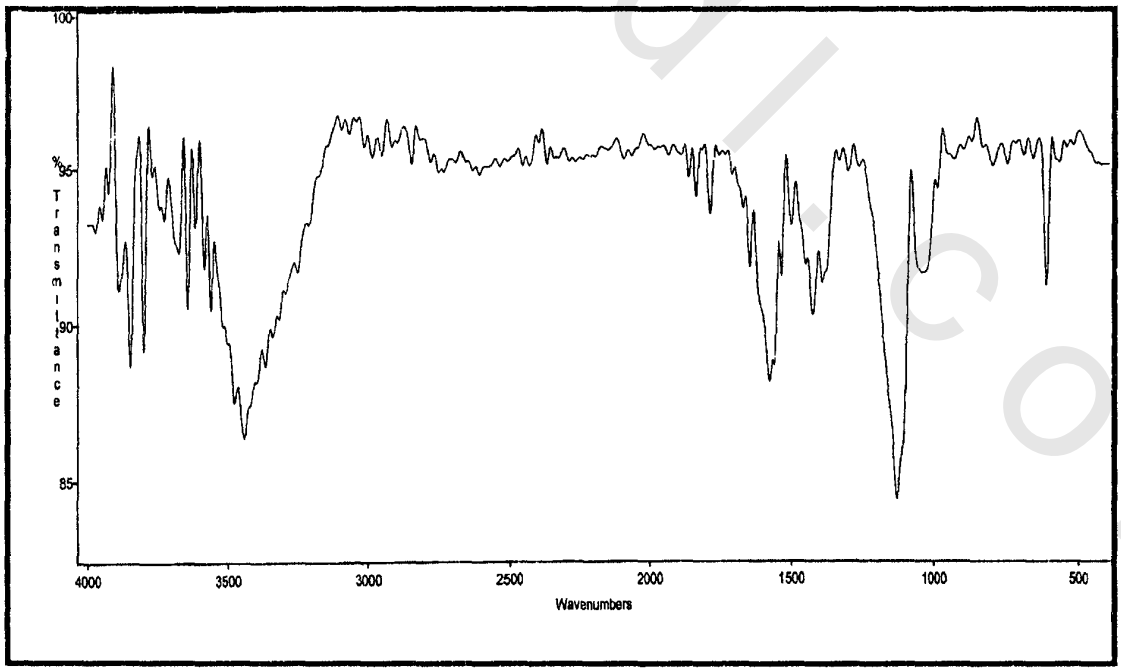

Figure (26) FTIR-spectrum of 12-(3-amino phenoxy) dodecane-1- thiol (C12M) With AgNPs

4.2.1.2. Ultraviolet Spectroscopy (UV)

UV absorption spectra have been proved to be quite sensitive to the formation of silver colloids because silver nanoparticles exhibit an intense absorption peak due to the surface plasmon **[Sileikaite et al., 2006]** by using the data of UV absorption in Figures 27-31 it was shown that the silver nanoparticles have a peak absorbance at (wavelength 430 nm, intensity 0.48) as shown in Figure 27. After addition of the synthesized monomeric thiol surfactants (C6M-C12M) to the silver nanoparticles solution the above peak was disappeared as shown in Figures 27-31. These results show the reduction of the negative charge of the colloidal particles. Namely, metal particles in aqueous colloidal dispersions usually bear a negative charge due to adsorbed anions. The addition of neutral adsorbate molecules such as the synthesized monomeric thiol surfactants, which displace the adsorbed ions, thus reducing the charge on the particles to the point where collisions occur as a result of diffusion motion due to the formation of nano shell of the thiol surfactants self-assembled on the AgNPs

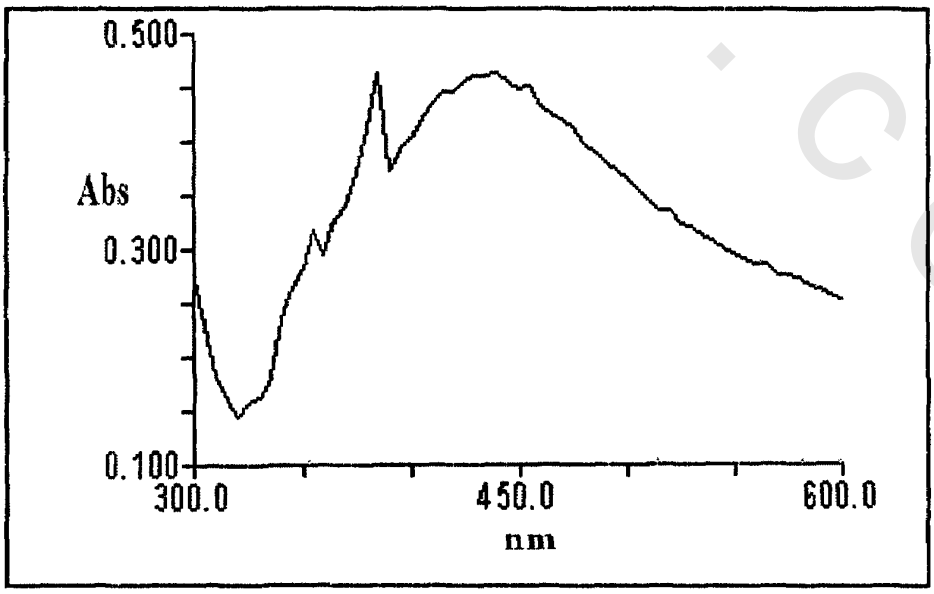

Figure (27) UV spectra of the prepared silver nanoparticles (AgNPs)

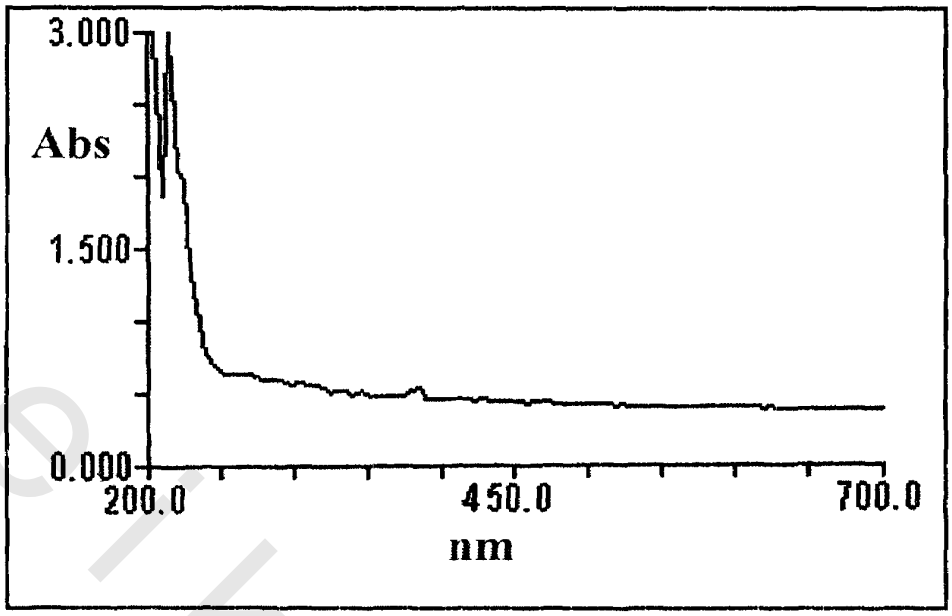

Figure (28) UV-spectrum of 6-(3-amino phenoxy) hexane-1- thiol with AgNPs (C6M+AgNPs)

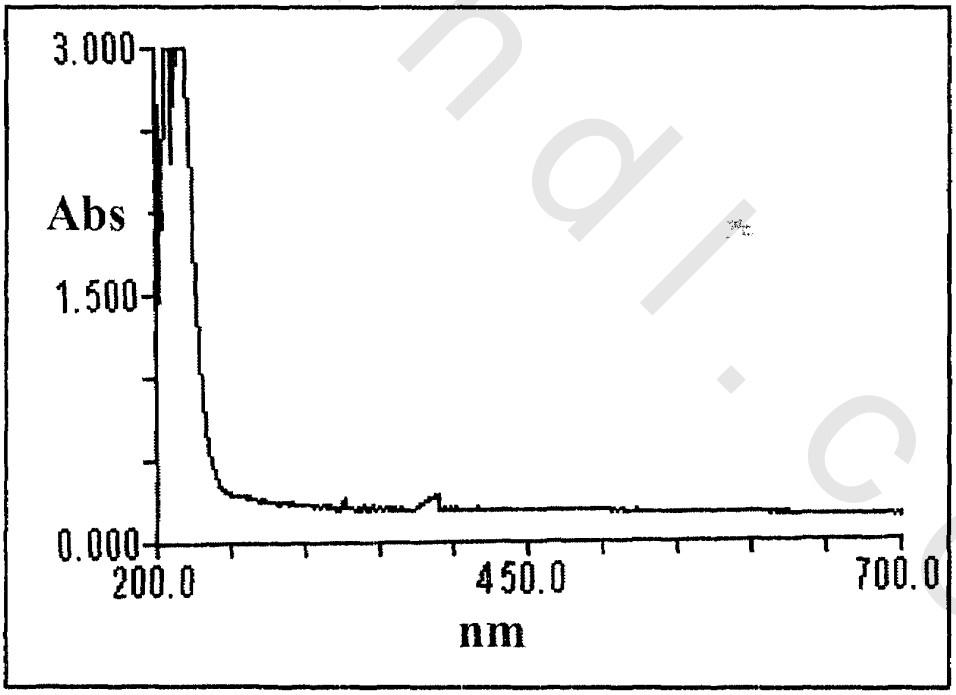

Figure (29) UV -spectrum of 8-(3-amino phenoxy) octane-1- thiol with AgNPs (C8M+AgNPs)

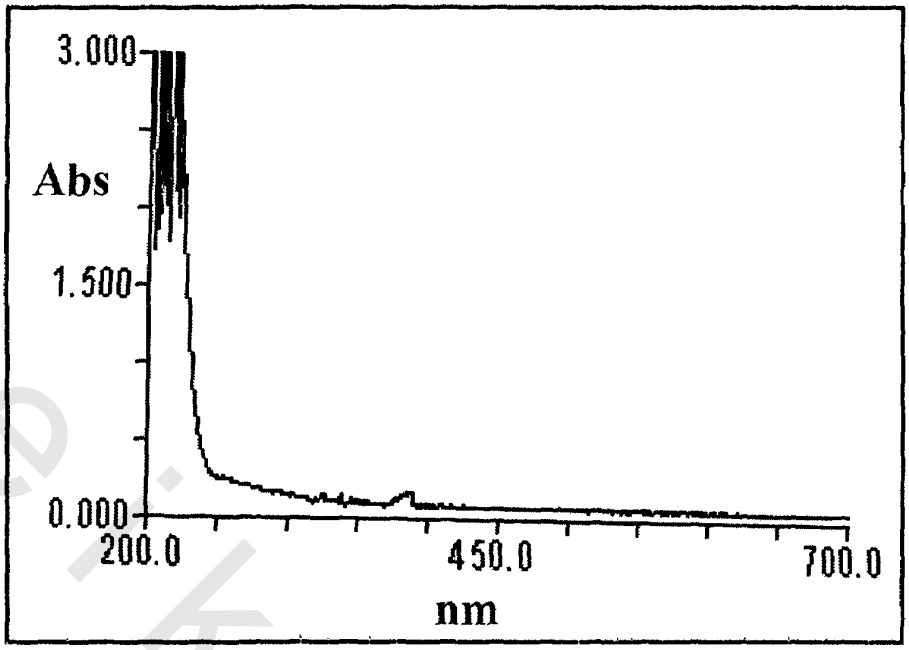

Figure (30) UV -spectrum of 10-(3-amino phenoxy) decane-1- thiol With AgNP (C10M+AgNPs)

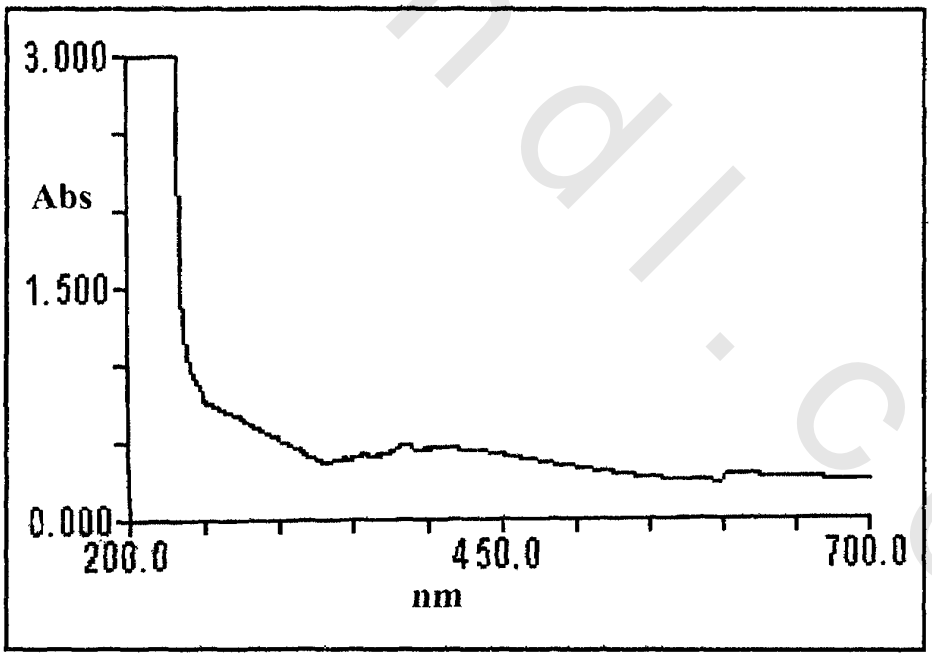

Figure (31) UV -spectrum of 12-(3-amino phenoxy) dodecane-1- thiol With AgNPs (C12M+AgNPs)

4.2.1.3. Transmission Electron Microscope (TEM) and Electron Diffraction (ED)

The size and morphology of silver nanoparticles and the nanostructure of the synthesized monomeric thiol surfactants (C6M-C12M) with AgNPs were investigated by TEM (transmission electron microscope) and ED (electron diffraction) as shown in Figures 32-36. The TEM image indicates that the silver particles are spherical shape and ED image reveals that the silver nanoparticles are polycrystalline structure **[Chun-Hua et al., 2007]**. Figures 33-36 show the spherical silver nanoparticles with a corona of the monomeric thiol surfactant ligands, which related to the self-assembling of the surfactant molecules on the silver nanoparticles. The TEM images further revealed the stabilization of silver nanoparticles due to interaction with the surfactant molecules. It is clear from the TEM images in Figure 33-36 the effect of the alkyl chain of the synthesized surfactants on the stabilization of the AgNPs, as the alkyl chain increase the aggregation of the AgNPs decrease and cause more stabilization of these particles.

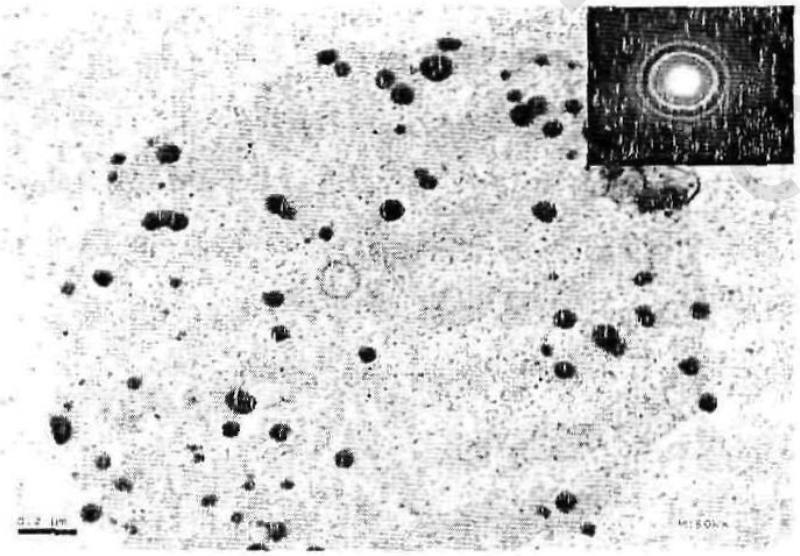

Figure (32) TEM image of the silver nanoparticles (AgNPs)

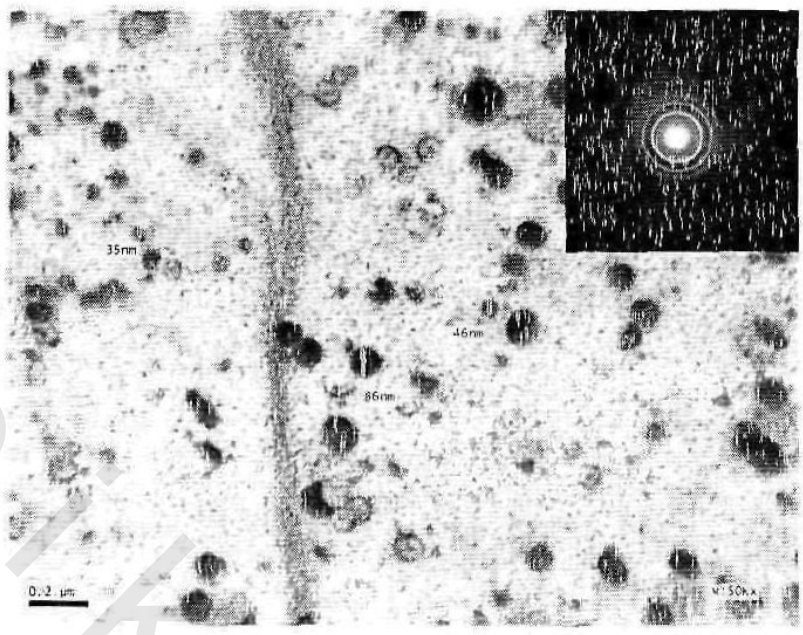

Figure (33) TEM image of 6-(3-amino phenoxy) hexane-1- thiol (C6M+AgNP)

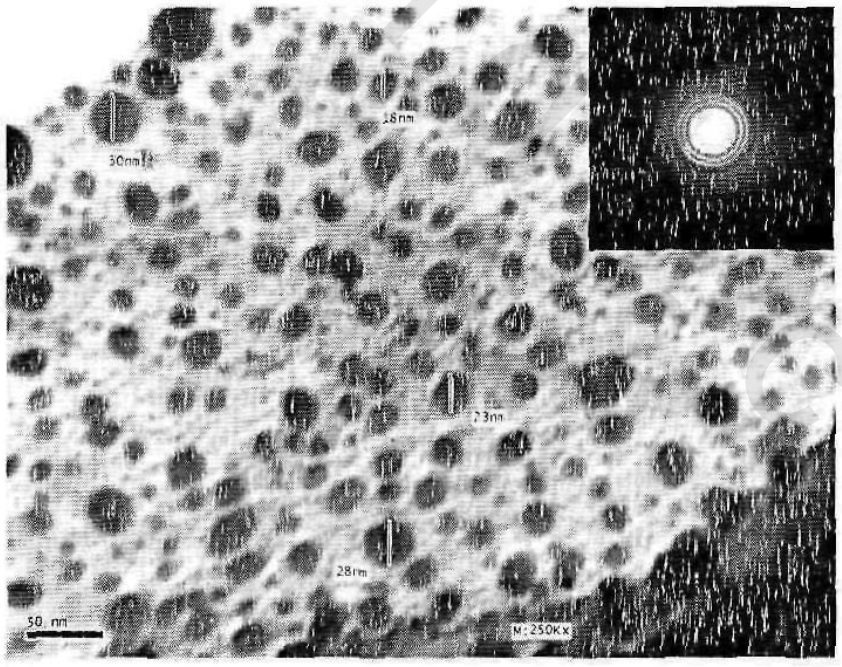

Figure (34) TEM image of 8-(3-amino phenoxy) octane-1- thiol with AgNPs (C8M+AgNPs)

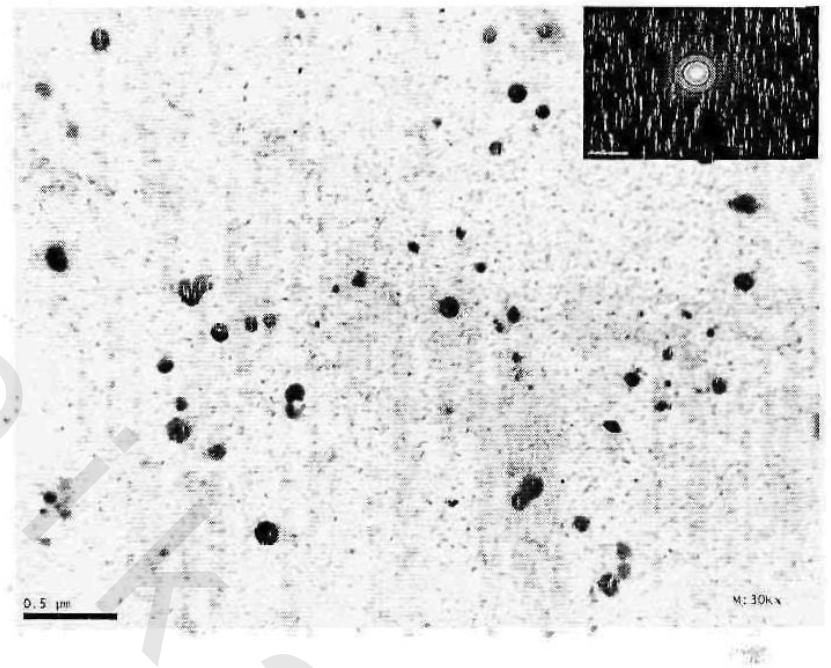

Figure (35) TEM image of 10-(3-amino phenoxy) decane-1- thiol With AgNPs (C10M+AgNPs)

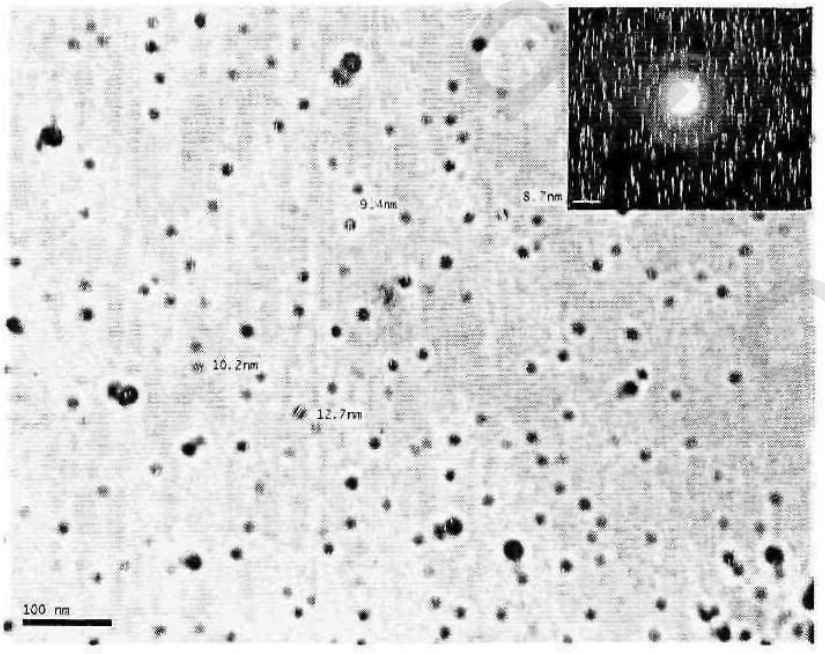

Figure (36) TEM image of 12-(3-amino phenoxy) dodecane-1- thiol With AgNPs (C12M+AgNPs)

4.2.1.4. X-Ray Diffraction (XRD)

The typical powder XRD pattern of the prepared silver nanoparticles is shown in Figure 37. The data shows diffraction peaks at $2\theta = 38.2°$, 44.4°, 64.6°, 77.5°, and 81.7°, which can be indexed to (111), (200), (220), (311), and (222) planes of pure silver . It confirmed that the main composition of the nanoparticles was silver **[Chun-Hua et al., 2007]**.Figure 38-41 represent the powder XRD pattern of the nanostructure for the synthesized monoeric thiol surfactants with the AgNPs. It is also found that there are some peaks appear in addition to the peaks of AgNPs which confirm the formation of nanoshell according to the self-assembling of the synthesized monoeric thiol surfactants on the AgNPs.

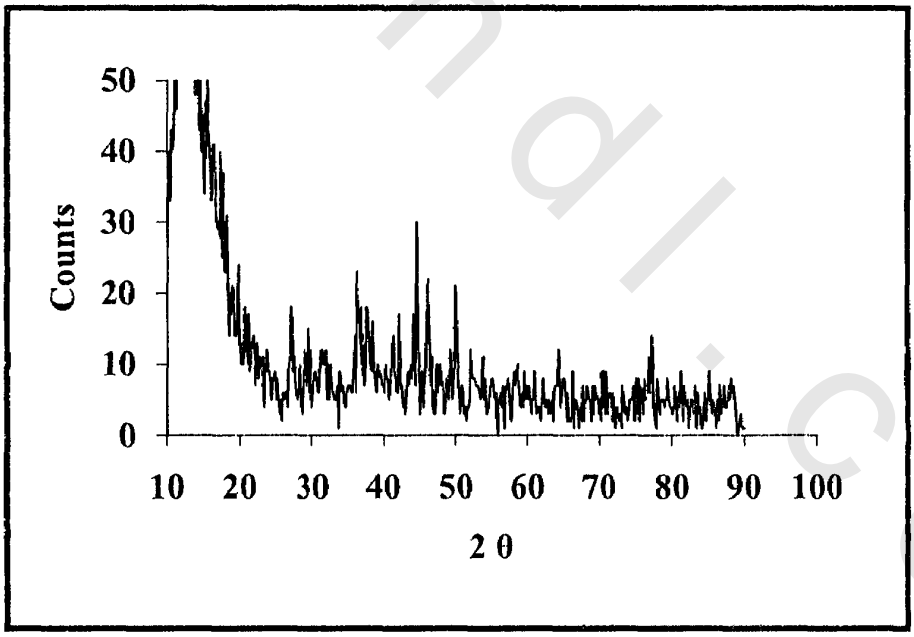

Figure (37) XRD spectra of the prepared Silver nanoparticles (AgNPs)

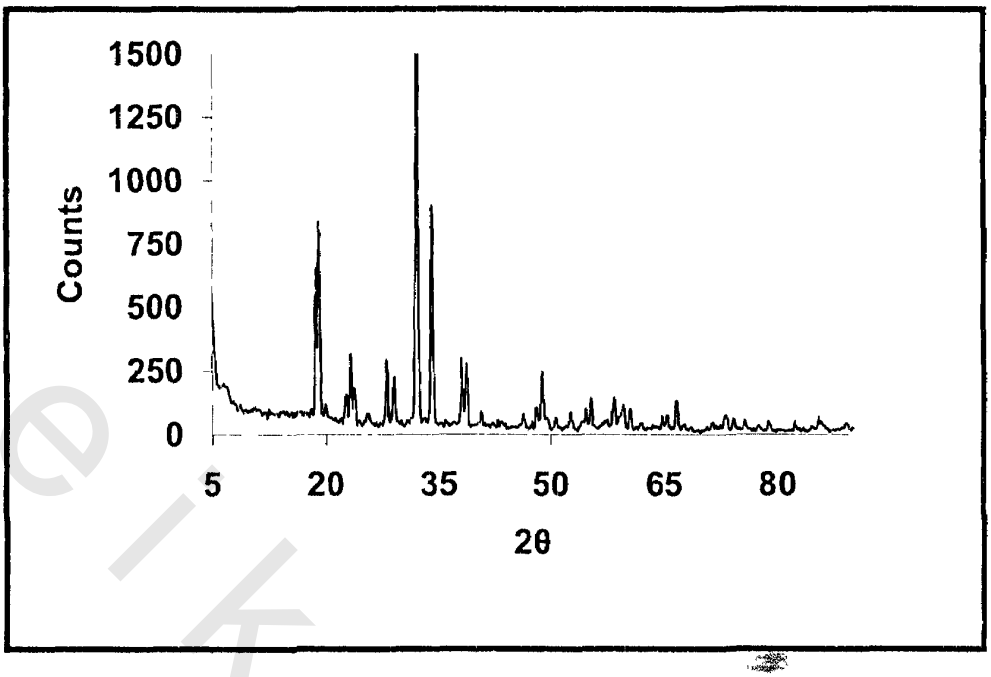

Figure (38) XRD spectra of 6-(3-amino phenoxy) hexane-1- thiol with AgNP (C6M+AgNPs)

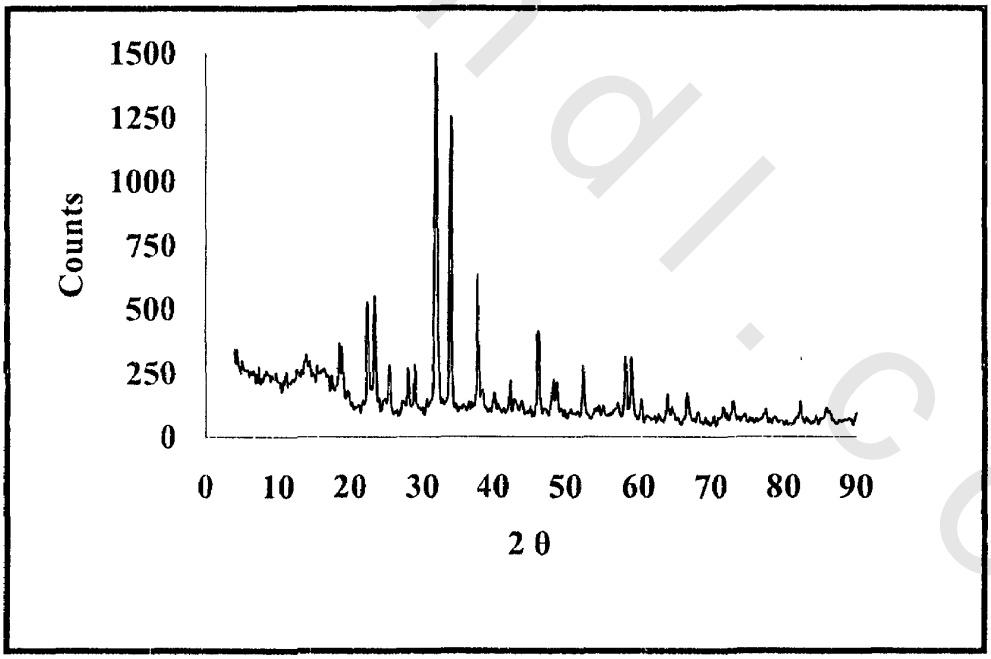

Figure (39) XRD spectra of 8-(3-amino phenoxy) octane-1- thiol with AgNPs (C8M+ AgNPs)

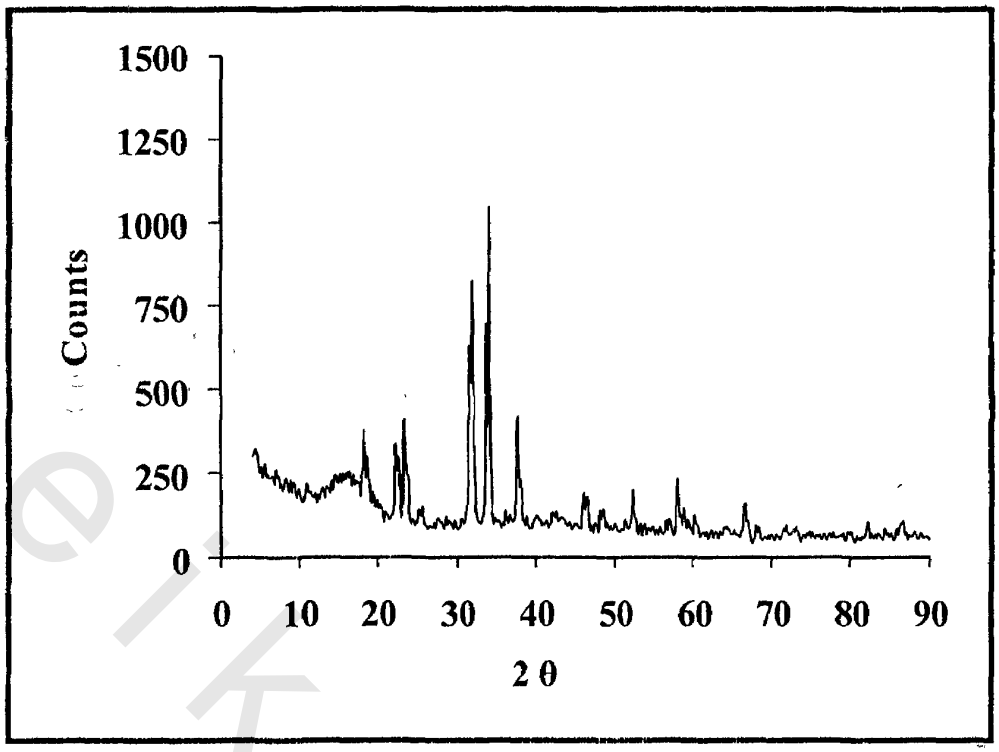

Figure (40) XRD spectra of 10-(3-amino phenoxy) decane-1- thiol with AgNPs (C10M+AgNPs)

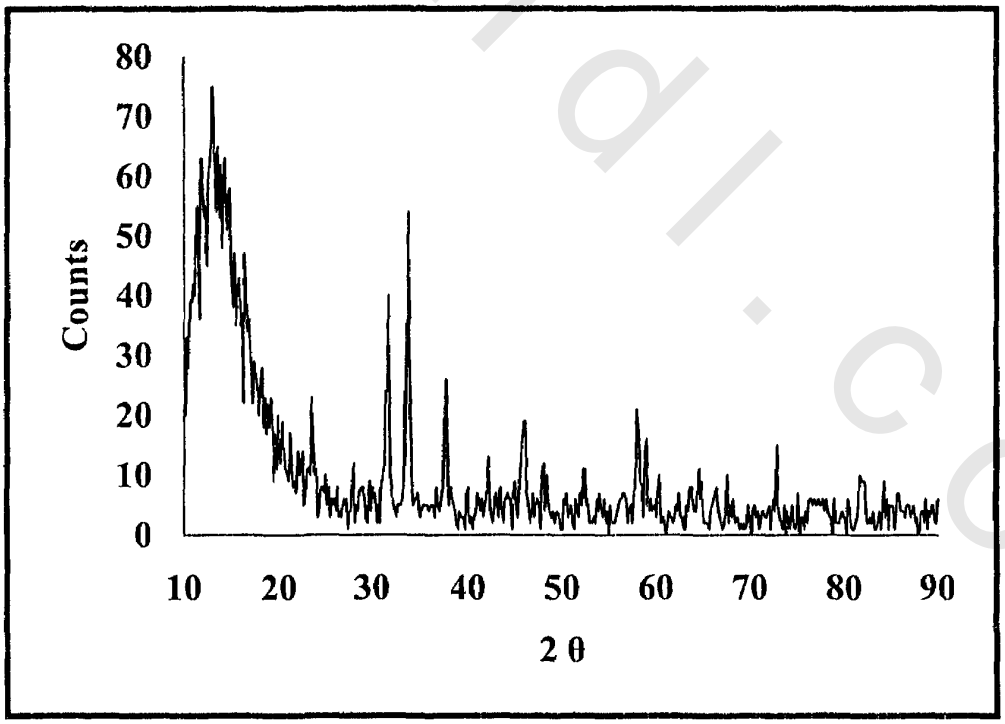

Figure (41) XRD spectra of 12-(3-amino phenoxy) dodecane-1- thiol With AgNPs (C12M+AgNPs)

4.2.2. Self-assembling of the synthesized polymeric Surfactants (C6P-C12P) on AgNPs

Self-assembling of synthesized polymeric surfactants on AgNPs was studied using FTIR, UV, XRD and TEM techniques as follow.

4.2.2.1. Fourier Transform Infrared Spectroscopy (FTIR)

The FTIR data in Figures (42-45) for the nanostructure of the polymeric thiol surfactants with the AgNPs show peaks similar to that of the individual polymeric thiol surfactants in Figures (11-14). The shift of the intensity and disappear the peaks depend on the difference in the alkyl chain length from C6P to C12P polymeric thiol surfactants. The shift of the peaks in FTIR spectra of the nanostructure of these surfactants with the silver nanoparticles Figures (42-45) from that of their individual structure without the silver nanoparticles Figures (11-15) may be related to the orientation of the surfactant molecules when assembled on the silver nanoparticles that leads to this shift in the FTIR peaks. The above FTIR results of the individual polymeric thiol surfactants and their nanostructure with the silver nanoparticles indicate the self-assembling of the prepared polymeric thiol surfactants on the silver nanoparticles.

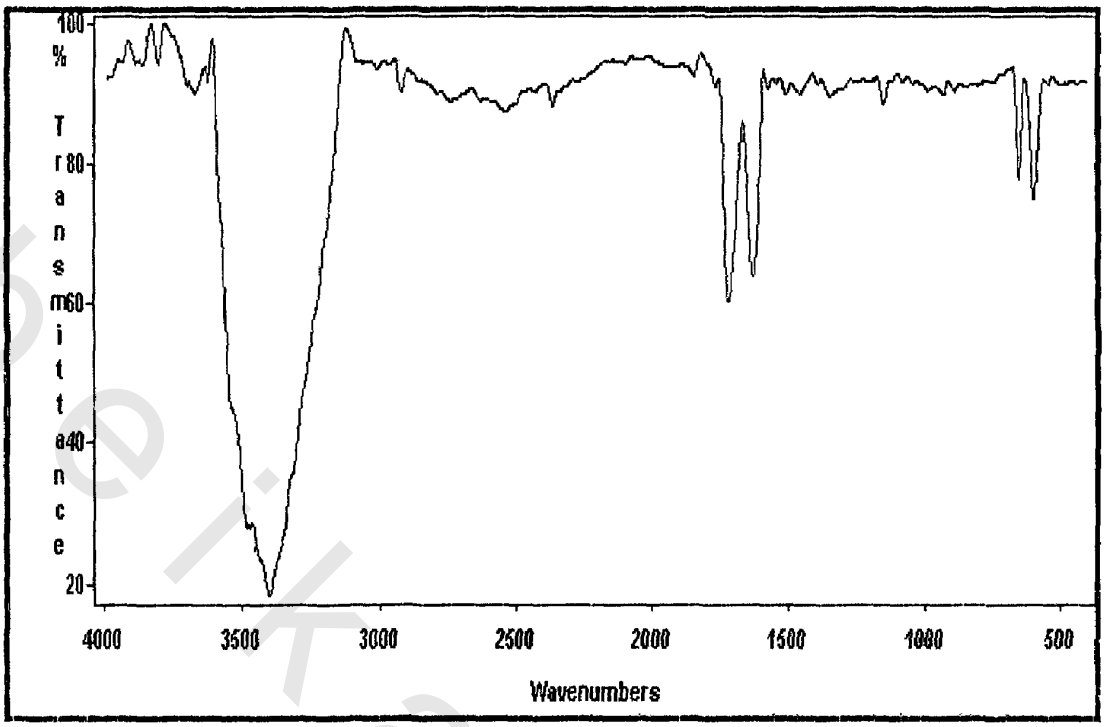

Figure (42) FTIR-spectrum of poly 6-(3-amino phenoxy) hexane-1- thiol with AgNPs (C6P+AgNPs)

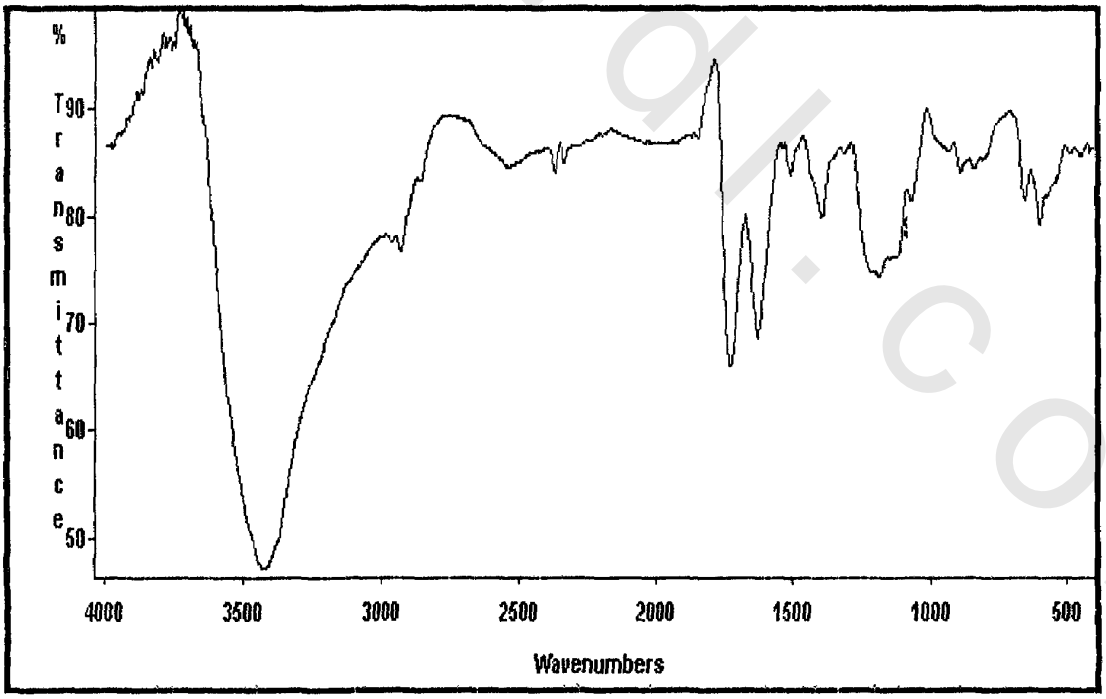

Figure (43) FTIR-spectrum of poly 8-(3-amino phenoxy) octane-1- thiol with AgNPs (C8P+AgNPs)

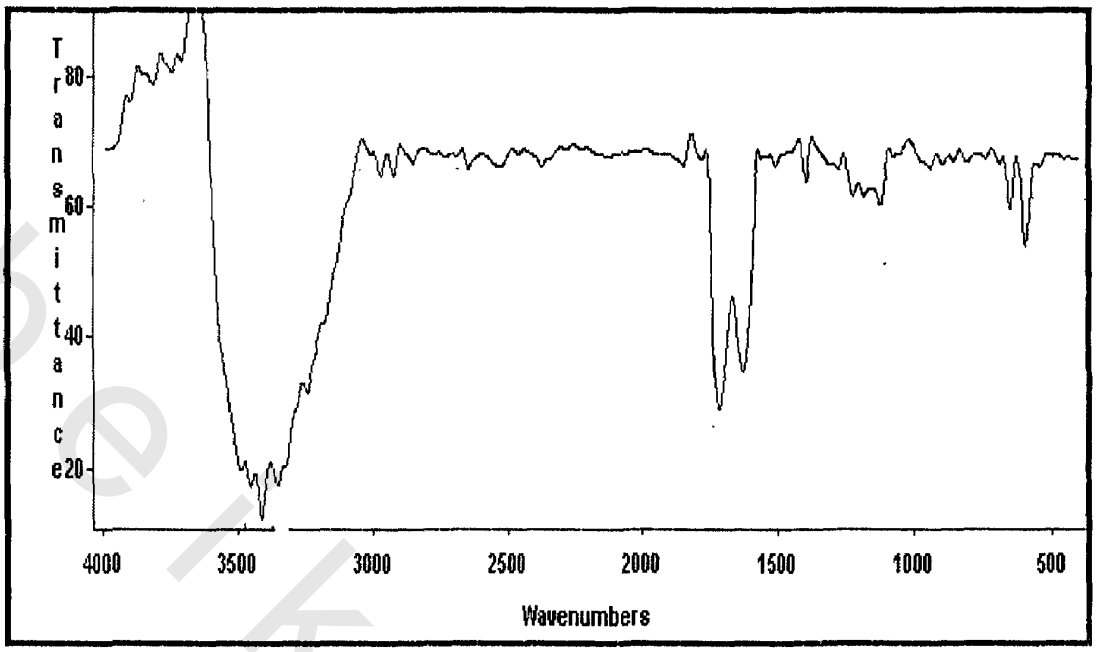

Figure (44) FTIR-spectrum of poly 10-(3-amino phenoxy) decane-1-thiol With AgNPs (C10P+AgNPs)

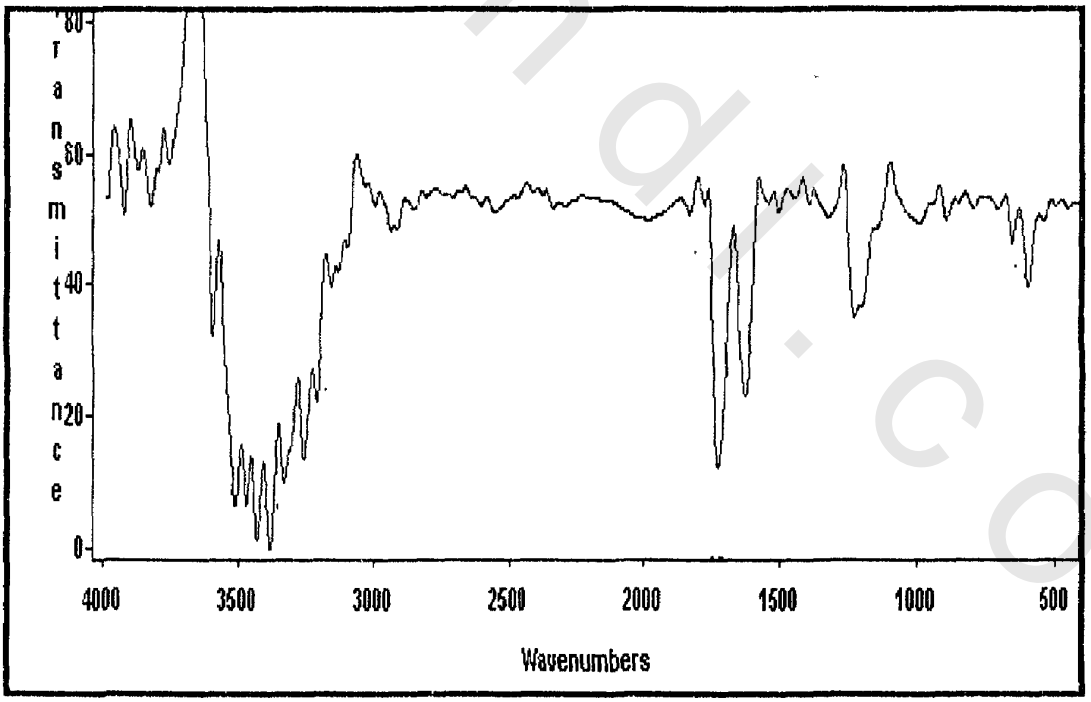

Figure (45) FTIR-spectrum of poly 12-(3-amino phenoxy) dodecane-1-thiol with AgNPs (C12P+AgNPs)

4.2.2.2. Ultraviolet Spectroscopy (UV)

After addition of the synthesized polymeric thiol surfactants (C6P-C12P) to the silver nanoparticles the peak at 430 nm of silver nanoparticlies was disappeared. These results show that the synthesized polymeric surfactants have attached to the surface of the silver nanoparticles and form nano shells structure **[Azzam et al., 2009]**

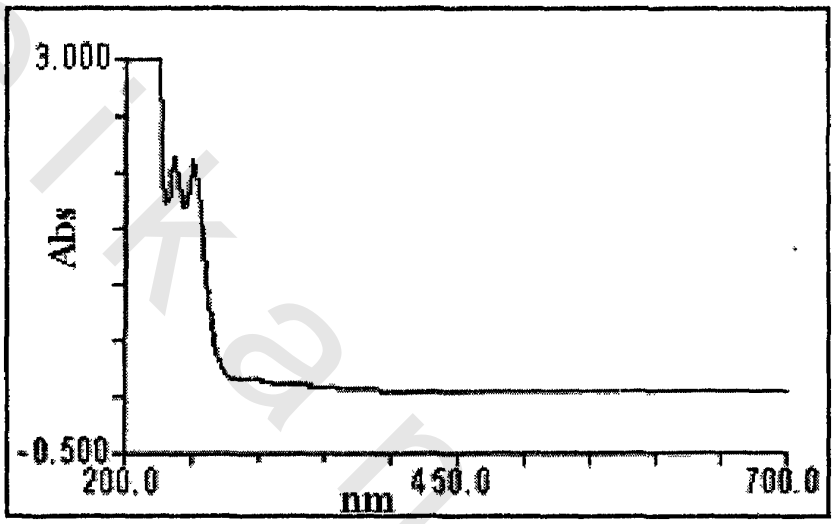

Figure (46) UV-spectrum of poly 6-(3-amino phenoxy) hexane-1- thiol with AgNPs (C6P+AgNPs)

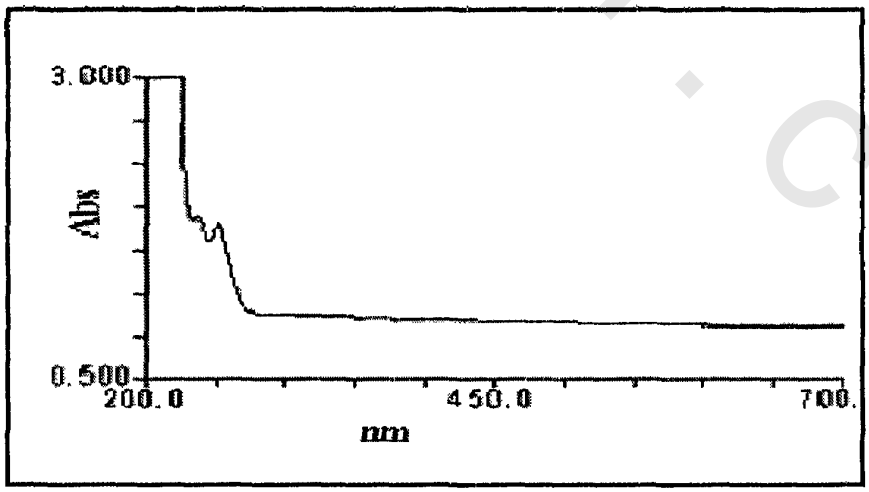

Figure (47) UV-spectrum of poly 8-(3-amino phenoxy) octane-1- thiol with AgNPs (C8P+AgNPs)

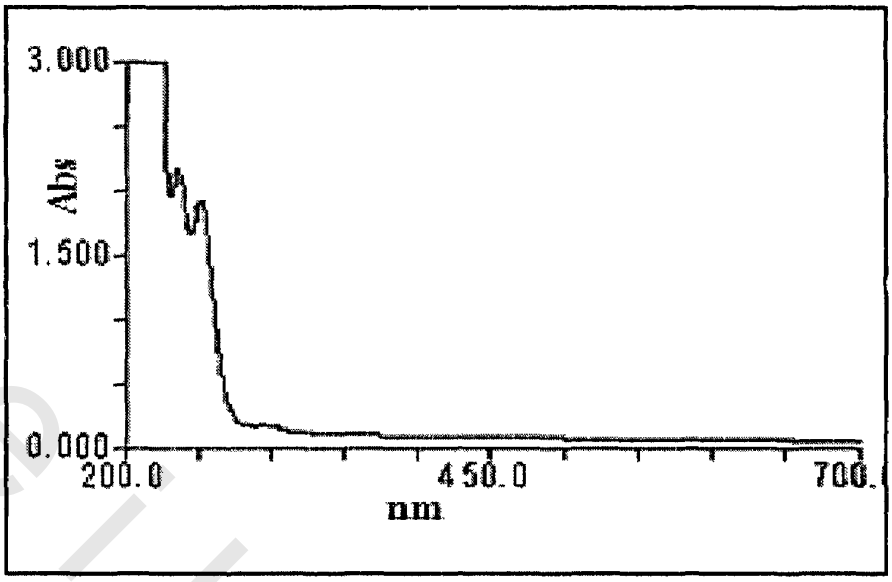

Figure (48) UV-spectrum of poly 10-(3-amino phenoxy) decane-1- thiol With AgNPs (C10P+AgNPs)

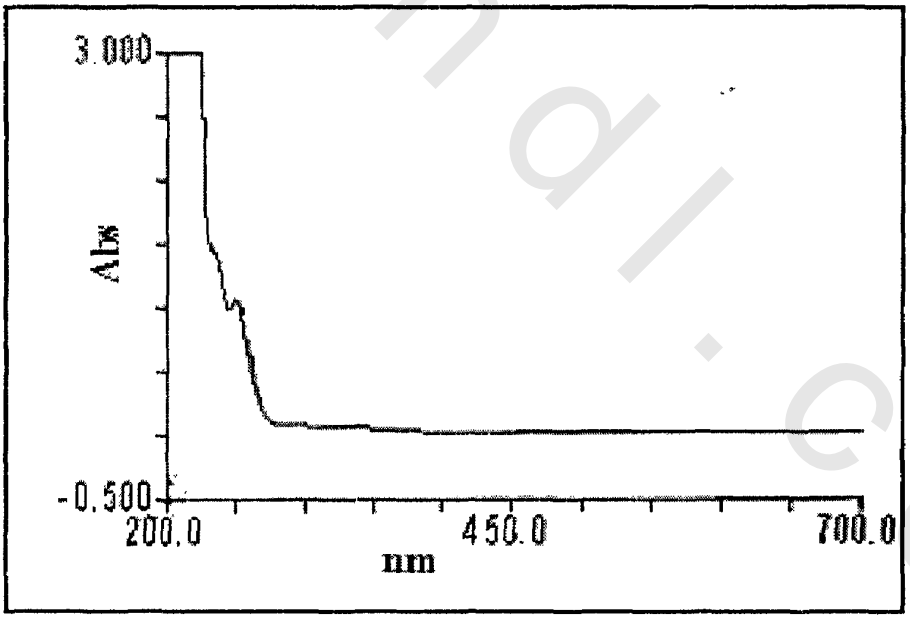

Figure (49) UV-spectrum of poly 12-(3-amino phenoxy) dodecane-1-thiol with AgNPs (C12P+AgNPs)

4.2.2.3. Transmission Electron Microscope (TEM) and Electron Diffraction (ED)

Figures 50-53 show the spherical silver nanoparticles with a corona of the polymeric thiol surfactant ligands (C6P, C8P, C10P and C12P), which related to the self-assembling of the polymeric thiol surfactant molecules on the silver nanoparticles. The TEM images further revealed the stabilization of silver nanoparticles due to interaction with the surfactant molecules. It is clear from the TEM images in Figure 50-53 the effect of the alkyl chain of the synthesized surfactants on the stabilization of the AgNPs, as the alkyl chain increase, the aggregation of the AgNPs decrease and cause more stabilization of these particles **[Azzam et al., 2009]**.

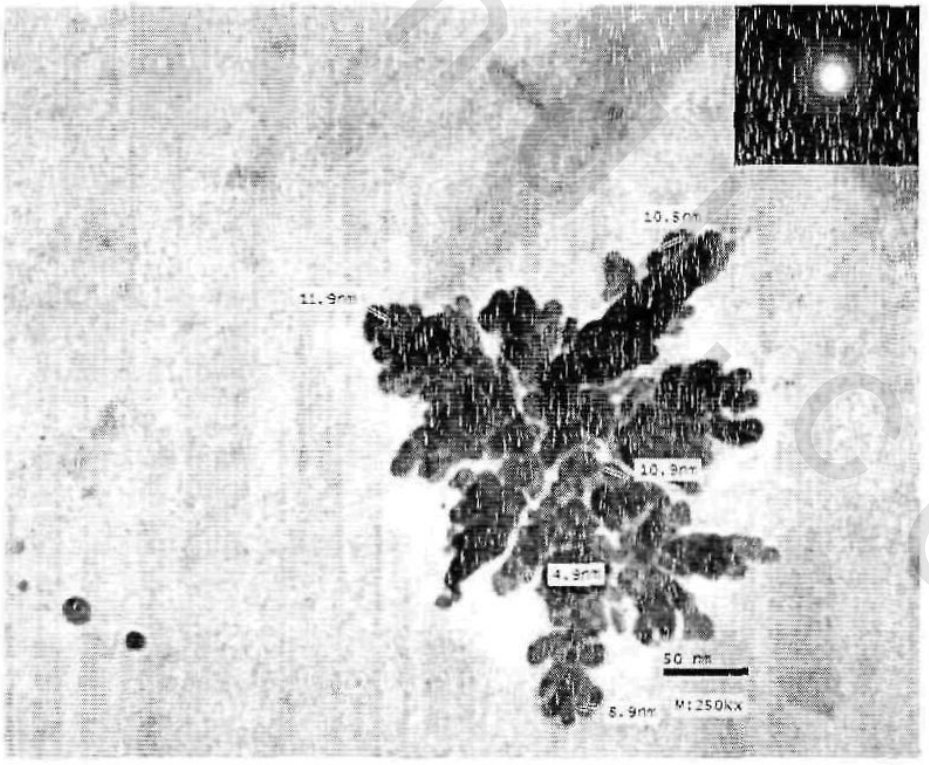

Figure (50) TEM image of poly 6-(3-amino phenoxy) hexane-1- thiol with AgNPs (C6P+AgNPs)

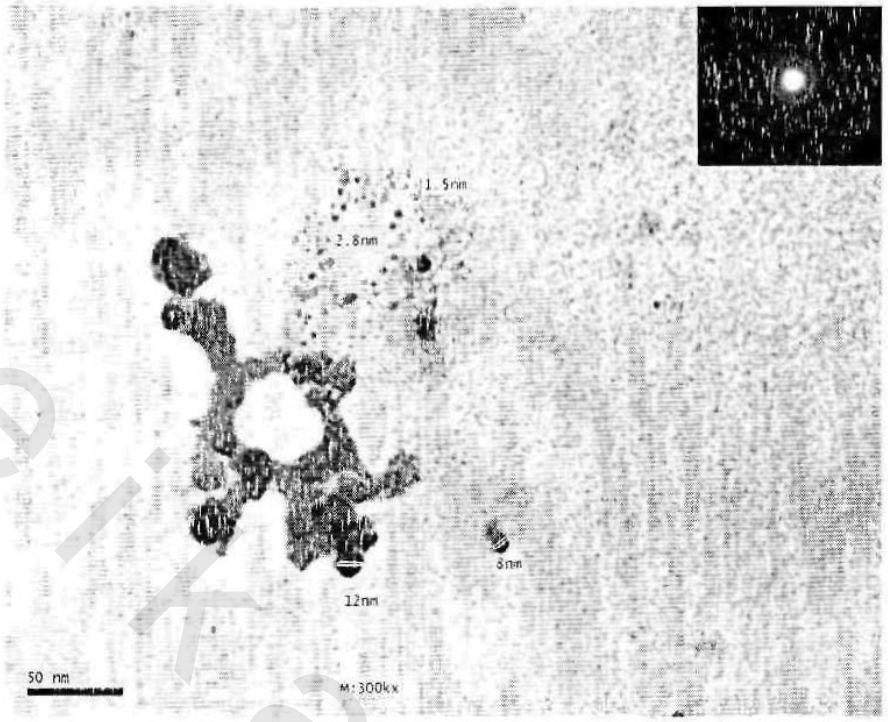

Figure (51) TEM image of poly 8-(3-amino phenoxy) octane-1- thiol with AgNPs (C8P+AgNPs)

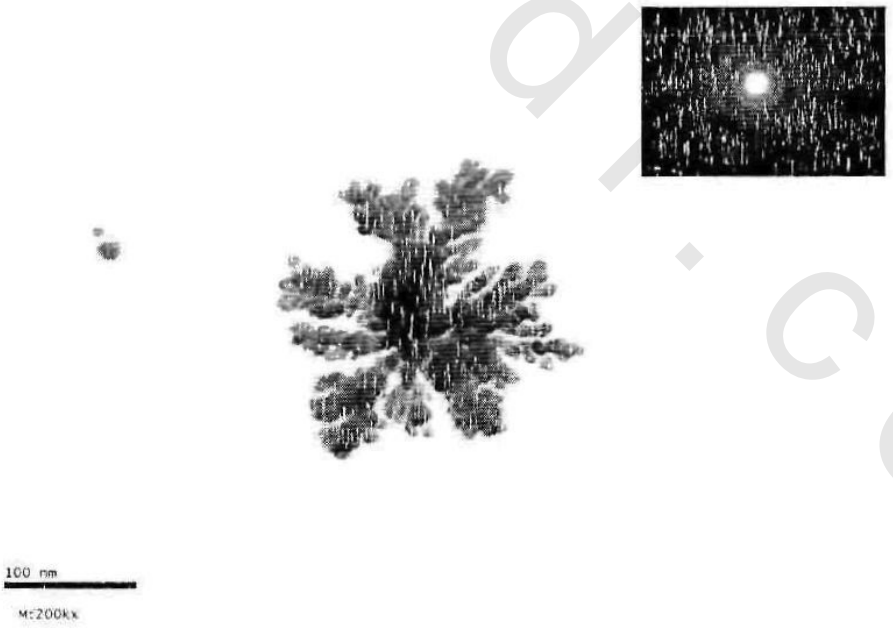

Figure (52) TEM image of poly 10-(3-amino phenoxy) decane-1- thiol With AgNPs (C10P+AgNPs)

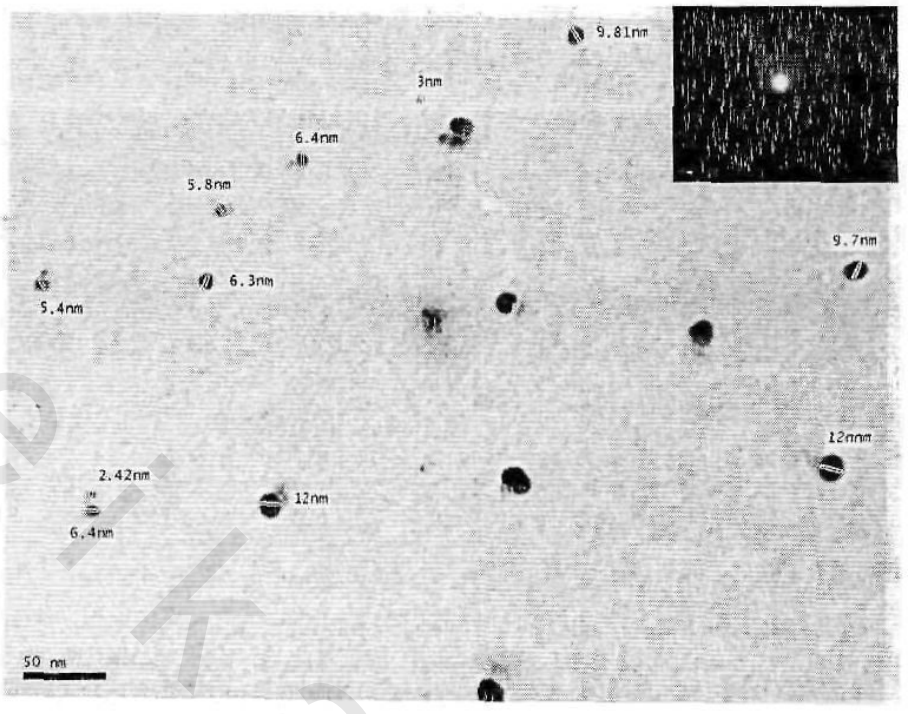

Figure (53) TEM image of poly 12-(3-amino phenoxy) dodecane-1- thiol with AgNPs (C12P+AgNPs)

4.2.2.4. X-Ray Diffraction (XRD)

The powder XRD pattern of the nanostructure for the synthesized polymeric thiol surfactants (C6P, C8P, C10P and C12P) with the AgNPs are representing in Figures 54-57. It was noted that there are some peaks appear in addition to the peaks of AgNPs which confirm the formation of nanoshell according to the self-assembling of the synthesized polymeric thiol surfactants on the AgNPs and these new peaks indicate that there is more crystalnilty than that amorphous structure of the individual polymers.

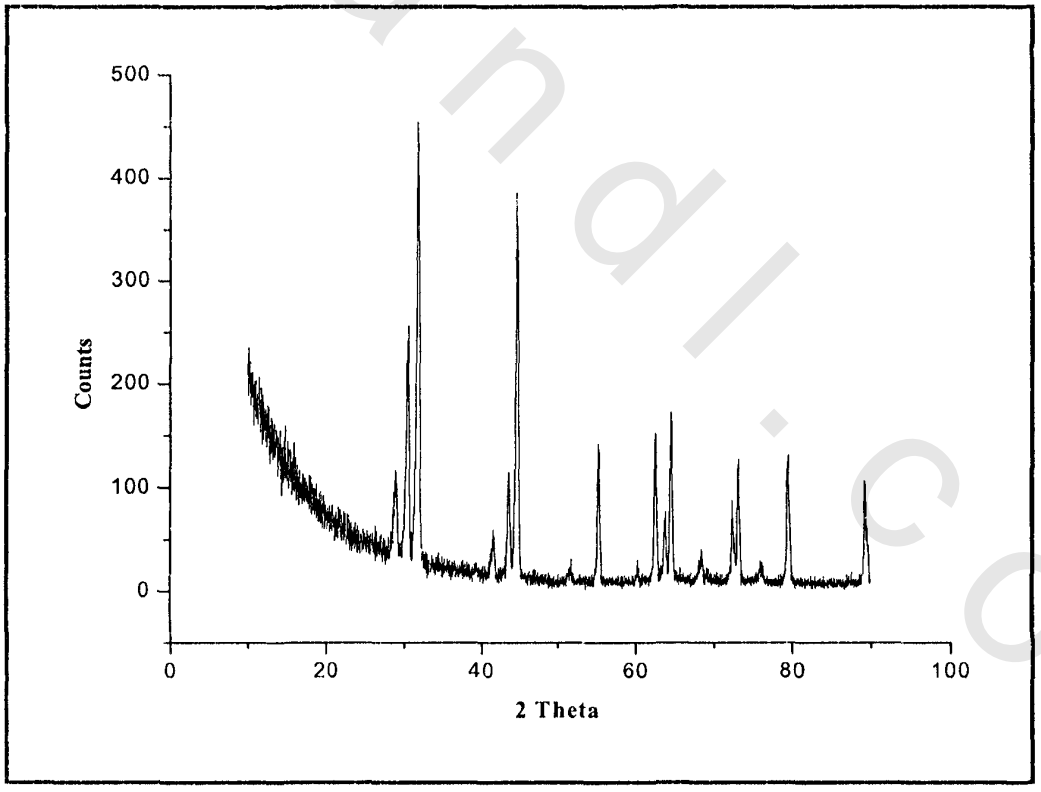

Figure (54) XRD-spectrum of poly 6-(3-amino phenoxy) hexane-1- thiol with AgNPs (C6P+AgNPs)

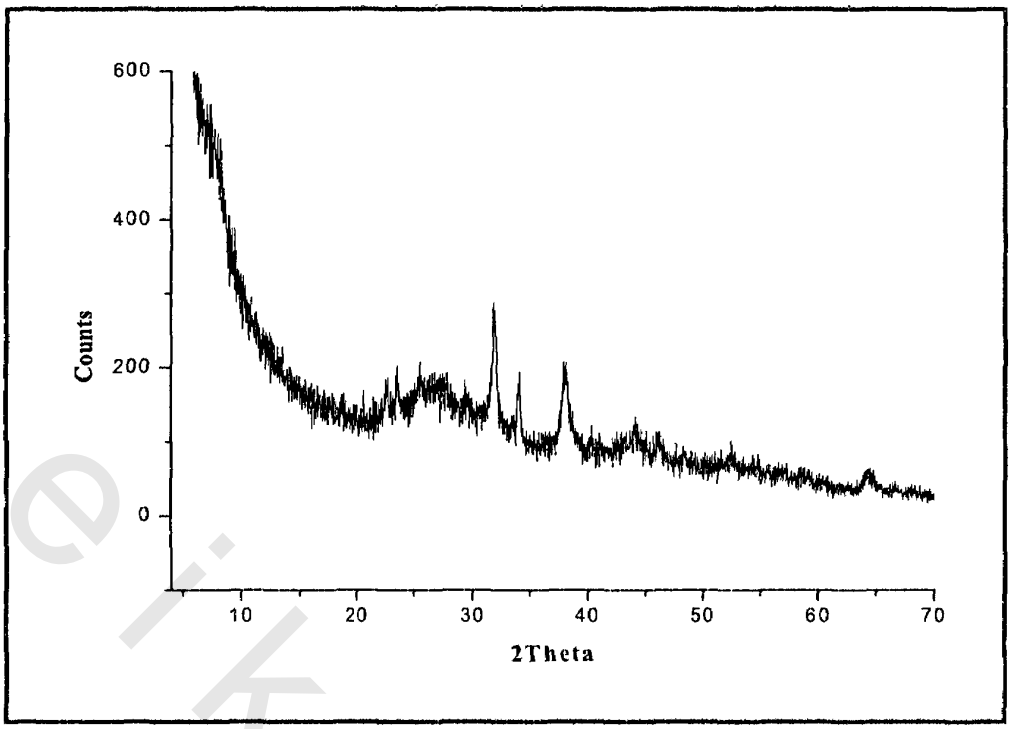

Figure (55) XRD-spectrum of poly 8-(3-amino phenoxy) octane-1- thiol with AgNPs (C8P+AgNPs)

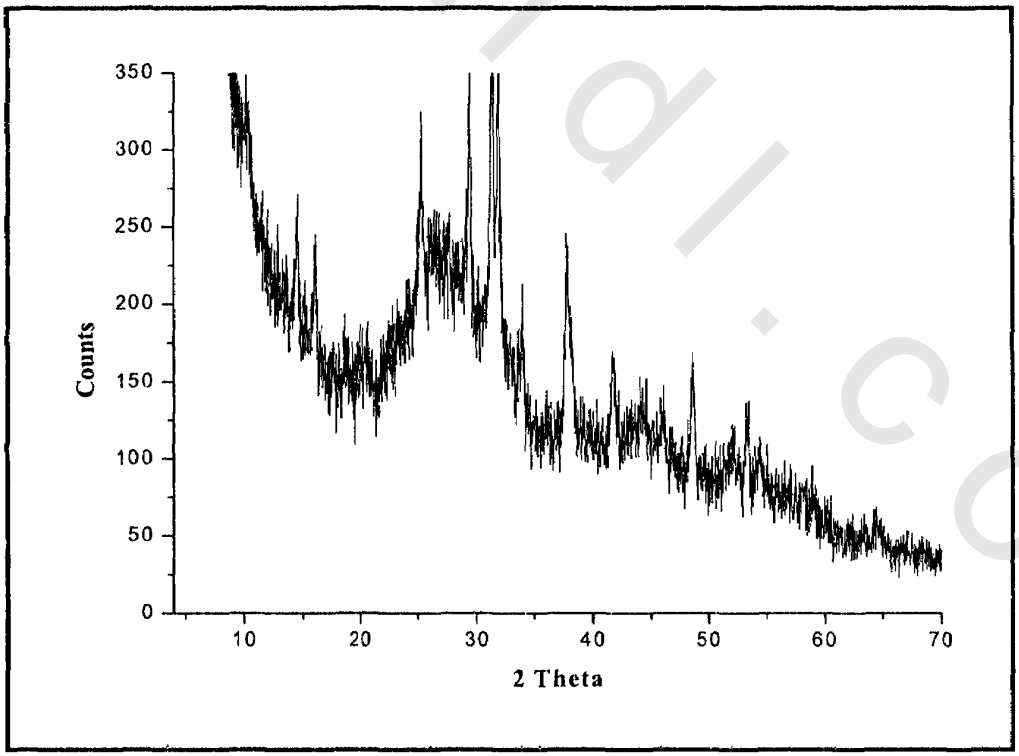

Figure (56) XRD-spectrum of poly 10-(3-amino phenoxy) decane-1-thiol With AgNPs (C10P+AgNPs)

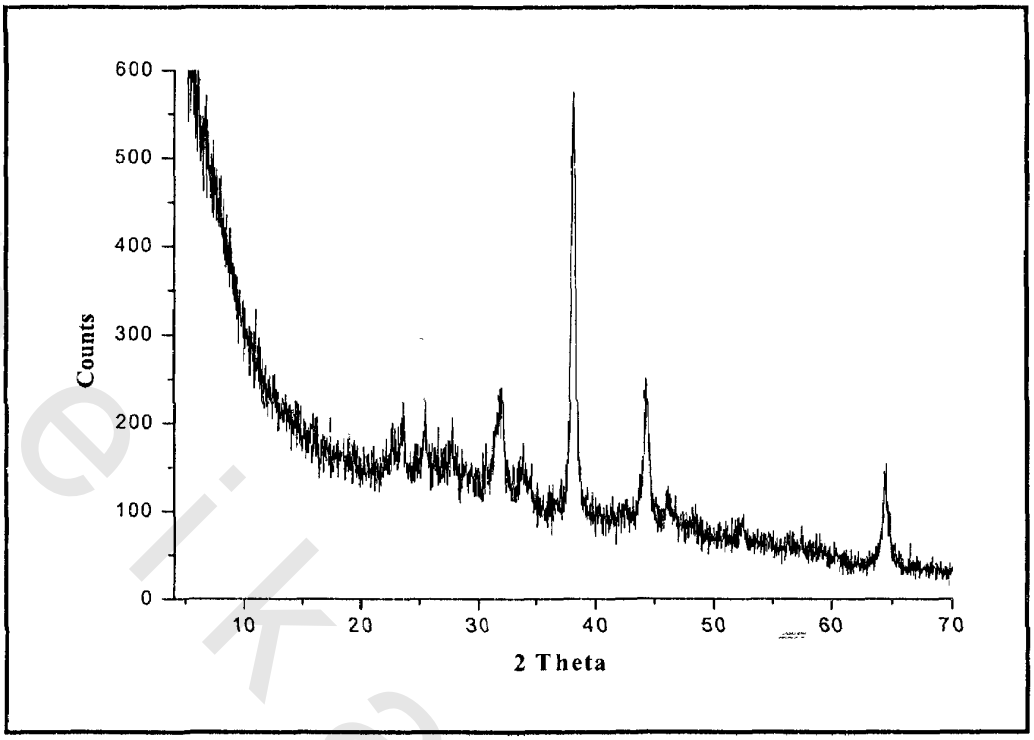

Figure (57) XRD-spectrum of poly 12-(3-amino phenoxy) dodecane-1-thiol with AgNPs (C12P+AgNPs)

4.3. The effect of the silver nanoparticles on the surface, the interfacial tension and the emulsion stability of the synthesized monomeric and polymeric surfactants

Reduction of surface and interfacial tension is one of the most commonly measured properties of surfactants in solution, since it depends directly on the replacement of molecules of solvent at the interface by molecules of surfactants.

Surface tension values are represented in Figures 58-61. The results indicated a considerable reduction in surface tension by increasing the length of hydrophobic moiety of the synthesized monomeric and polymeric surfactants. It was noticed from Figures 58-61 that the nanostructure of these surfactants with AgNPs has more reduction in surface tension than the individual surfactants. This is related to the ability of the nanoparticles to adsorb at interface and decrease the surface tension **[Wang et al., 2007]**. Although, the critical micelle concentration (cmc) are approximately the same value for all surfactants but the effectiveness (π_{cmc}) values increase as the alkyl chain increase and these values also increase with the synthesized polymeric surfactants more than that of the monomeric surfactants as shown in Table 6. This behavior of the polymeric surfactants may be related to the ability of these surfactants to adsorb at the interface and decrease the surface tension than the monomeric surfactants because of they have more hydrophobic and hydrophilic groups in their chemical structure **[Sayyah, et al, 2005].** The data in Table 5 also shows that the nanostructure of the surfactants under investigation with the AgNPs have the ability to make a reduction in the surface tension more than the investigating individual surfactants which clear from the increase in the effectiveness (π_{cmc}) values of the

nanostructure of these surfactants than that of the individual surfactants. The data of the interfacial tension of the individual surfactants under investigation and their nanostructures with the silver nanoparticles in Table 6 shows that, the interfacial tension of these surfactants with paraffin oil decreases as the alkyl chain moiety increases from C6 to C12. In addition, the polymeric surfactants (C6P-C12P) have the ability to decrease the interfacial tension with paraffin oil than the monomeric surfactants (C6M-C12M). It was noticed from Table 5 that, the interfacial tension of the nanostructure of these surfactants with the AgNPs decreases more than that of the individual surfactants which shows the effect of the AgNPs on the decreasing of the interfacial tension of the synthesized surfactants with the paraffin oil. This effect may be related to the formation of the nanoshells between the synthesized surfactants and the silver nanoparticles which effects on the interfacial tension of these surfactants with the paraffin oil **[Azzam et al., 2009].** The results of the emulsion stability in Table 5 show that, the emulsion stability of the all individual synthesized surfactants from C6M to C12P with the paraffin oil increase as the alkyl chain of these surfactants increases. Also, the emulsion stability of the nanostructure of the synthesized surfactants with the silver nanoparticles increases than that of the individual surfactants which shows the effect of the silver nanoparticles on the emulsion stability of the synthesized surfactants with the paraffin oil. From the conclusion of the above results it is clear the effect of the AgNPs in the improvement of the surface activity of the polymeric and monomeric surfactants under investigation.

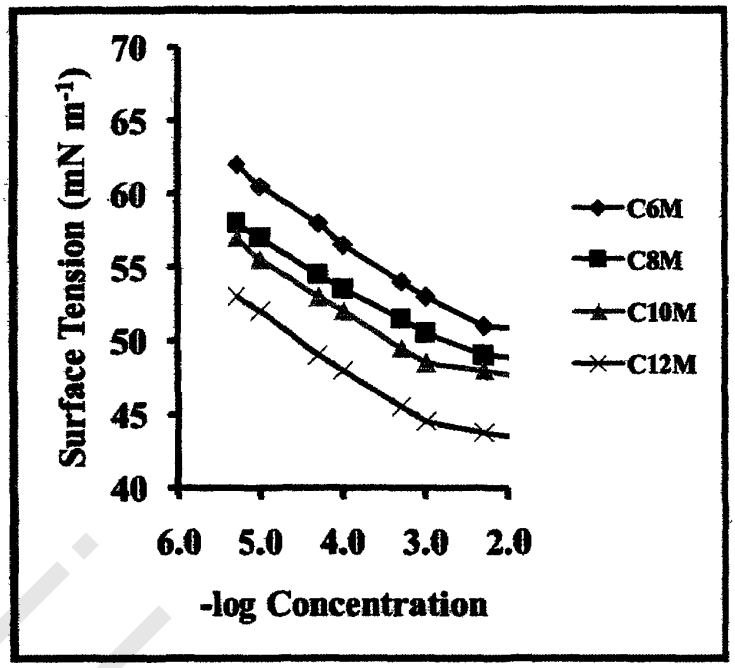

Figure (58) Relationship between surface tension and –logarithm concentration of the synthesized monomeric thiol surfactants

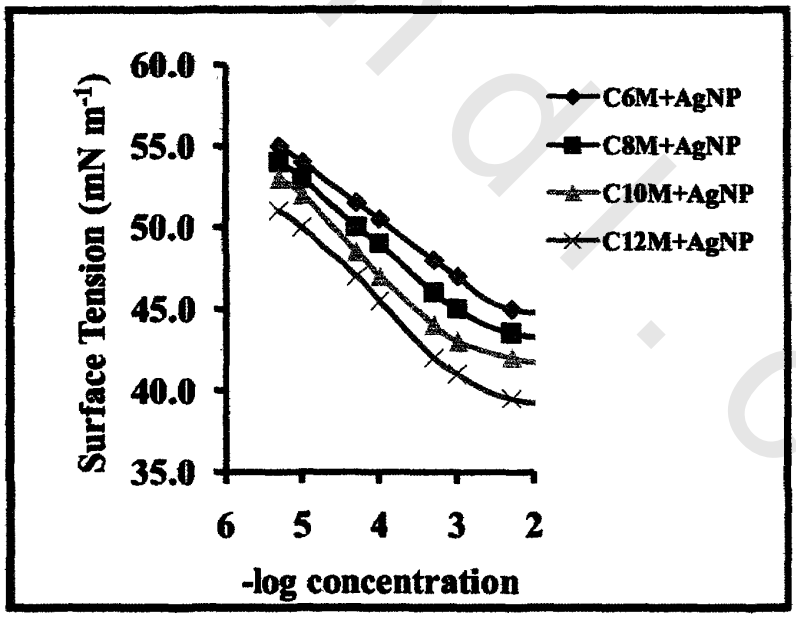

Figure (59) Relationship between surface tension and –logarithm concentration of the synthesized monomeric thiol surfactants with silver nanoparticles

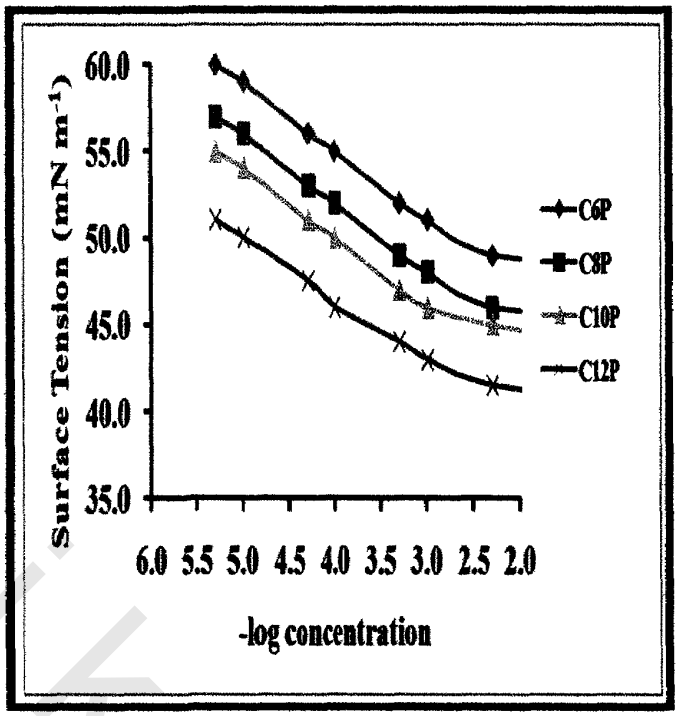

Figure (60) Relationship between surface tension and –logarithm concentration of the synthesized polymeric thiol surfactants

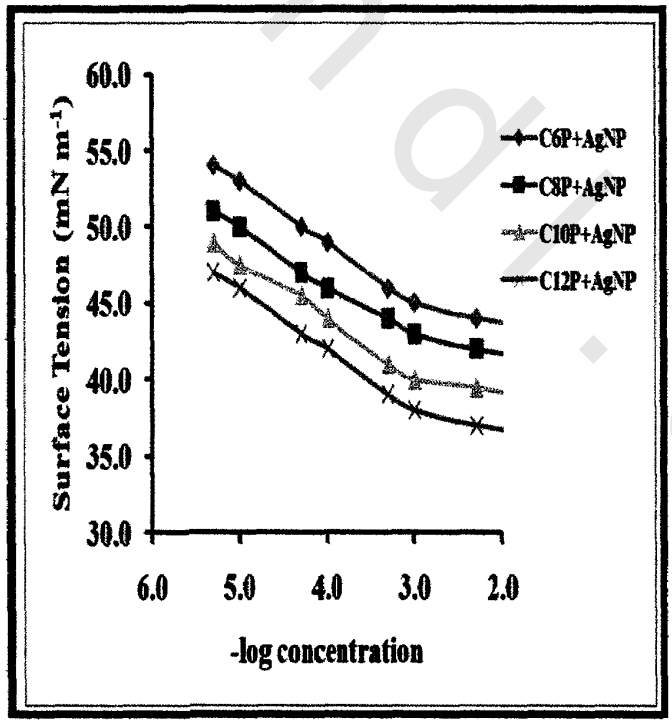

Figure (61) Relationship between surface tension and –logarithm concentration of the synthesizedpolymeric thiol surfactants with silver nanoparticles

Table (6): Critical micelle concentration (cmc), effectiveness (π_{cmc}), surface tension at cmc (γ_{cmc}), Interfacial tension and emulsion stability of the synthesized monomeric and polymeric surfactants and their nanostructure with silver nanoparticles

Sample	CMC Mol L^{-1}	π_{cmc} mN m^{-1}	γ_{cmc} mN m^{-1}	Interfacial tension mN m^{-1}	Emulsion stability (sec)
C6M	2.5×10^{-3}	16	56	13	44 sec
C8M	1×10^{-3}	18.5	53.5	10	56 sec
C10M	1×10^{-3}	20	52	8	68 sec
C12M	1×10^{-3}	23	49	6	79 sec
C6M + AgNPs	1×10^{-3}	21	51	10	58 sec
C8M + AgNPs	1×10^{-3}	23.3	48.7	9	70 sec
C10M+AgNPs	1×10^{-3}	25	47	7.5	81 sec
C12M+AgNPs	1×10^{-3}	26.5	45.5	5	92 sec
C6P	1×10^{-3}	18	54	11	56 sec
C8P	1×10^{-3}	20	52	9	62 sec
C10P	1×10^{-3}	22	50	7.5	78 sec
C12P	1×10^{-3}	26	46	5	90 sec
C6P + AgNPs	1×10^{-3}	23	49	10	68 sec
C8P + AgNPs	1×10^{-3}	25.5	46.5	8.5	75 sec
C10P +AgNPs	1×10^{-3}	28	44	6.5	85 sec
C12P +AgNPs	1×10^{-3}	30	42	4	100 sec

4.4. Evaluation of the synthesized surfactants and their nanostructure with silver nanoparticlies (AgNPs) as Corrosion Inhibitors

Corrosion protection of steel in acidic media is great important both for industrial facilities and theoretical aspects. The use of inhibitor is one of the most practical methods for protection of steel against corrosion in acidic media. Among all inhibitors, the most important are the organic ones, also called adsorption inhibitors. They control corrosion, acting over the anodic or the cathodic surface or both. Most commercial acid inhibitors are organic compounds containing hetero atoms such as nitrogen (N), oxygen (O), sulphur (S), phosphor (P) atoms, by which the inhibitor molecules are adsorbed on the metal surface in acidic media, thus resulting adsorption film acts as a barrier separating the metal from the corrosive medium and blocks the active sites. As a representative type of these organic inhibitors, quaternary ammonium salts have been demonstrated to be highly cost-effective and used widely in various industrial processing for preventing corrosion of iron and steel in acidic media.

Three different techniques used in this work to determine the corrosion rate and corrosion inhibition efficiency.

4.4.1. Wight Loss Technique

4.4.1.1. Corrosion rate of the synthesized surfactants

The corrosion rate of carbon steel sheet was calculated from the following equation:

$$CR = W/At \quad (6)$$

where CR is corrosion rate, W is the average weight loss of three parallel carbon steel samples by mg, A is the total area of the specimen by cm^2 and t is immersion time by hour.

The corrosion rate data of carbon steel sample with and without addition of the synthesized monomeric and polymeric thiol surfactants and their nanostructure with silver nanoparticlies in corrosive medium 1M HCl at 25^{O}C are shown in Tables (7-10) and Figures (62-65). From the data in these tables it is clear that the corrosion rate values in mg cm^{-2} h^{-1} decrease with increasing inhibitors concentration also the corrosion rate values in mg cm^{-2} h^{-1} decrease with increasing hydrocarbon chain length of the synthesized surfactants then by addition of the inhibitor the corrosion rate value decrease gradually by increasing the concentration of the inhibitor reached to value 0.26 mg cm^{-2} h^{-1} at concentration of (375 ppm) of compound (C6M). This behavior is the same for all synthesized surfactants (C8M, C10M, C12M, C6P, C8P, C10P and C12P). Comparing between the data in Table (6) and Table (8), it is clear that the corrosion rate with the polymeric thiol surfactants (C6P-C12P) is relatively decrease than that of the monomeric thiol surfactants(C6M-C12M). This may be related to that the polymeric thiol surfactants have more hydrophobic (alkyl chain) and hydrophilic groups (SH) in their chemical structure which make more adsorption and more protective films on the surface of steel than the monomeric thiol surfactants. It was noted from the results in Tables (8,10) that the nanostructure of the prepared monomeric and polymeric thiol surfactants with the AgNPs have lower corrosion rate than the individual surfactants without the AgNPs which indicate the enhancement of the corrosion inhibition of these surfactants in the presence of AgNPs. This behavior of the nanostructure of the synthesized surfactants with the AgNPs is related to the protective film which formed according to the adsorption of AgNPs on the steel surface and prevents the corrosion **[Migahed et al., 2009]**.In addition, from Table (8,10) it is clear that the lowest corrosion rate is

0.112 (mg cm^{-2} h^{-1}) at concentration of 375 ppm of the nanostructure of compound C12P with AgNPs.

Table (7): Corrosion rate of carbon steel with and without addition of the synthesized monomeric thiol surfactants as corrosion inhibitor in 1M HCl at 25^{O}C

Concentration, (ppm)	Corrosion Rate (mg cm^{-2} h^{-1})			
	C6M	C8M	C10M	C12M
blank	0.89	0.89	0.89	0.89
75	0.47	0.42	0.41	0.39
150	0.34	0.37	0.35	0.32
225	0.32	0.30	0.27	0.25
300	0.29	0.27	0.25	0.22
375	0.26	0.23	0.22	0.18

Table (8): Corrosion rate of carbon steel with and without addition of the synthesized monomeric thiol surfactants with silver nanoparticlies as corrosion inhibitor in 1M HCl at 25 ^{O}C

Concentration, (ppm)	Corrosion Rate (mg cm^{-2} h^{-1})			
	C6M+ AgNPs	C8M+ AgNPs	C10M+ AgNPs	C12M+ AgNPs
blank	0.89	0.89	0.89	0.89
75	0.39	0.38	0.35	0.38
150	0.34	0.34	0.31	0.30
225	0.27	0.26	0.23	0.22
300	0.25	0.23	0.21	0.19
375	0.19	0.18	0.15	0.15

Table (9): Corrosion rate of carbon steel with and without addition of the synthesized polymeric thiol surfactants as corrosion inhibitor in 1M HCl at 25 ^{O}C

Concentration, (ppm)	Corrosion Rate (mg cm^{-2} h^{-1})			
	C6P	C8P	C10P	C12P
blank	0.89	0.89	0.89	0.89
75	0.44	0.39	0.38	0.36
150	0.37	0.34	0.31	0.29
225	0.29	0.27	0.24	0.22
300	0.27	0.24	0.22	0.19
375	0.23	0.2	0.19	0.15

Table (10): Corrosion rate of carbon steel with and without addition of the synthesized polymeric thiol surfactants with silver nanoparticlies as corrosion inhibitor in 1M HCl at 25 ^{O}C

Concentration, (ppm)	Corrosion Rate (mg cm^{-2} h^{-1})			
	C6P+ AgNPs	C8P+ AgNPs	C10P+ AgNPs	C12P+ AgNPs
blank	0.89	0.89	0.89	0.89
75	0.36	0.35	0.32	0.31
150	0.31	0.29	0.27	0.25
225	0.24	0.23	0.2	0.18
300	0.22	0.20	0.19	0.15
375	0.16	0.14	0.12	0.11

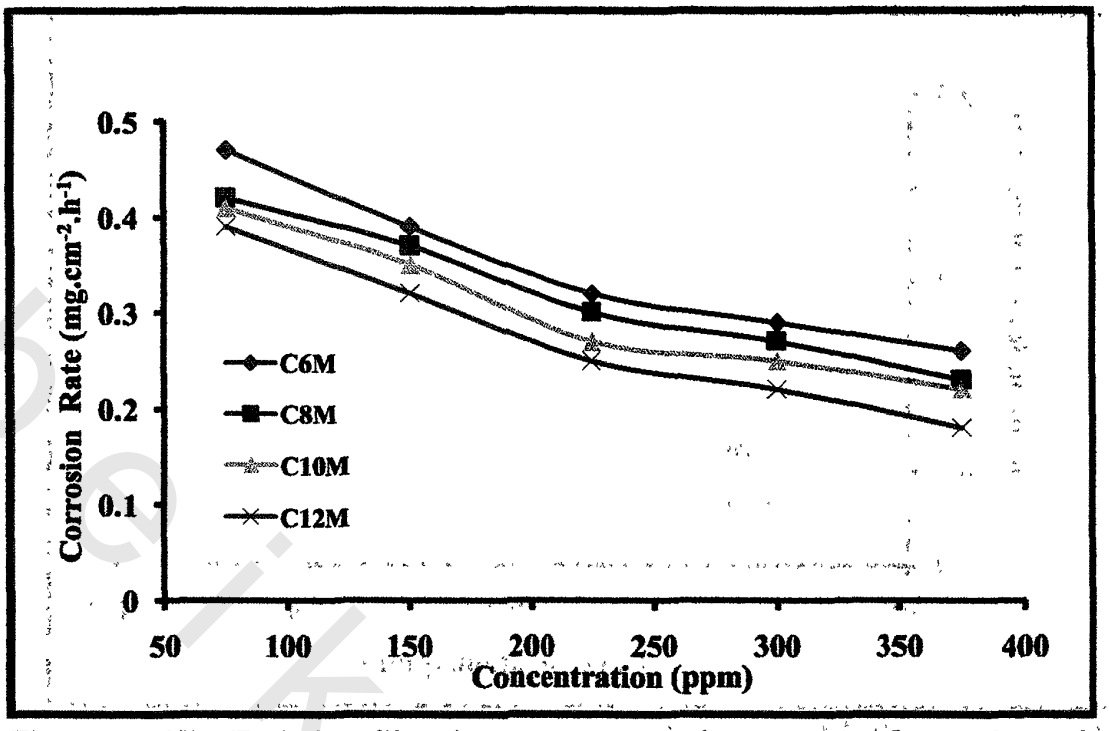

Figure (62) Relationship between corrosion rate of steel and concentration of the synthesized monomeric thiol surfactants

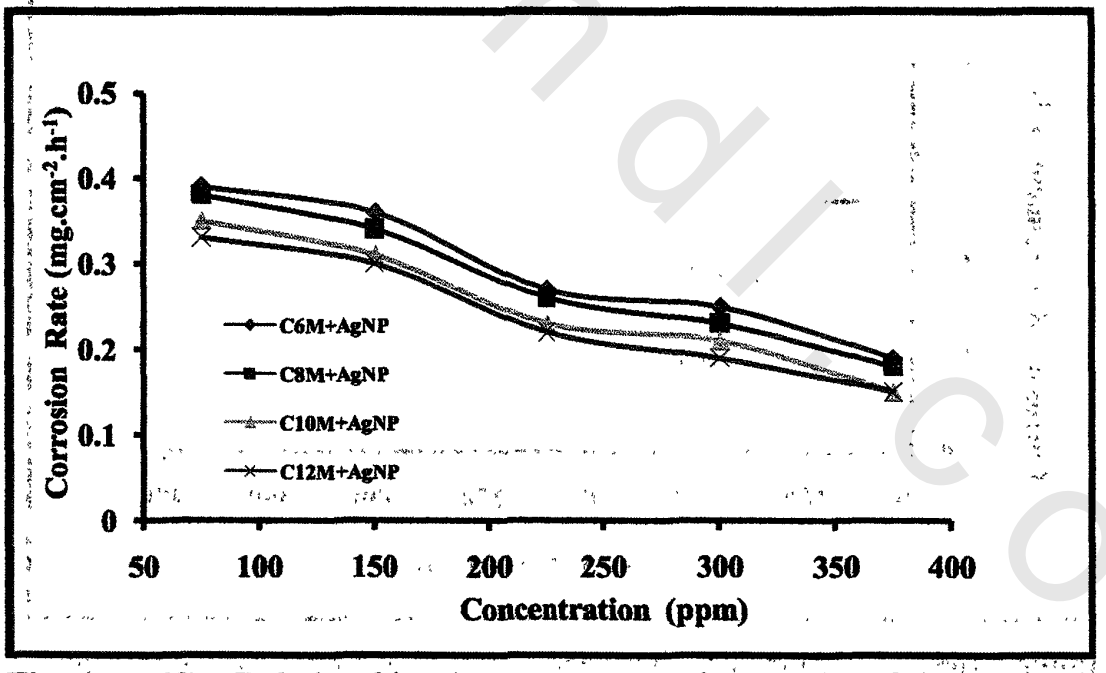

Figure (63) Relationship between corrosion rate of steel and concentration of the synthesized monomeric thiol surfactants with silver nanoparticles

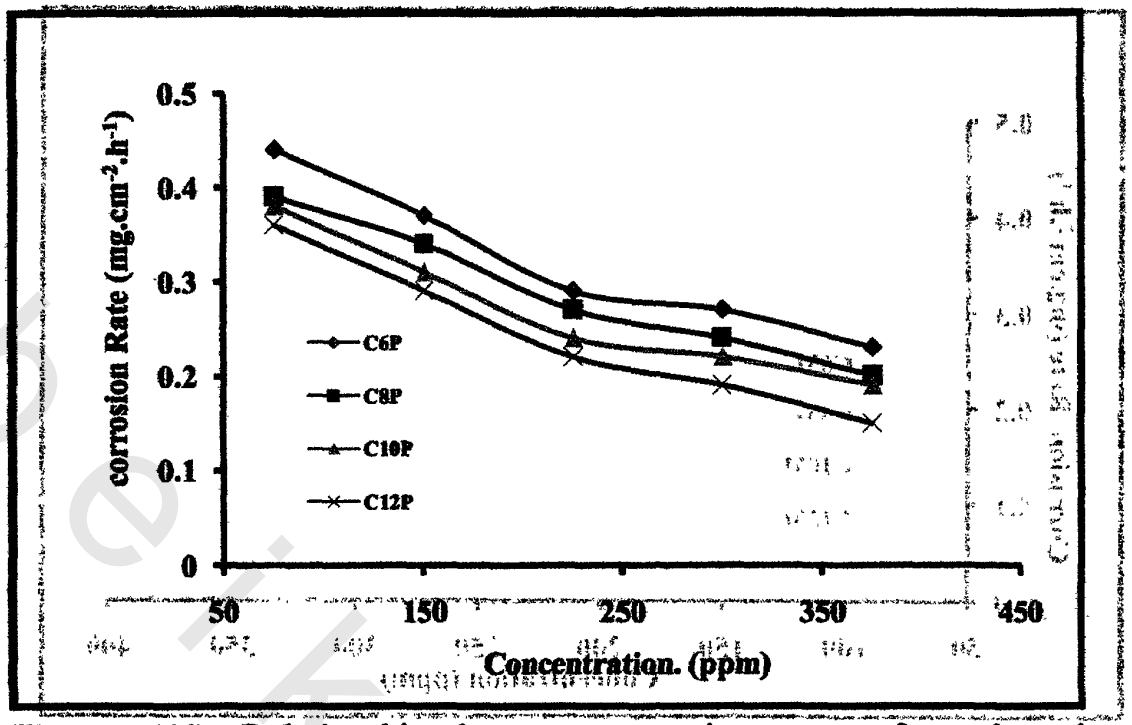

Figure (64) Relationship between corrosion rate of steel and concentration of the synthesized polymeric thiol surfactants

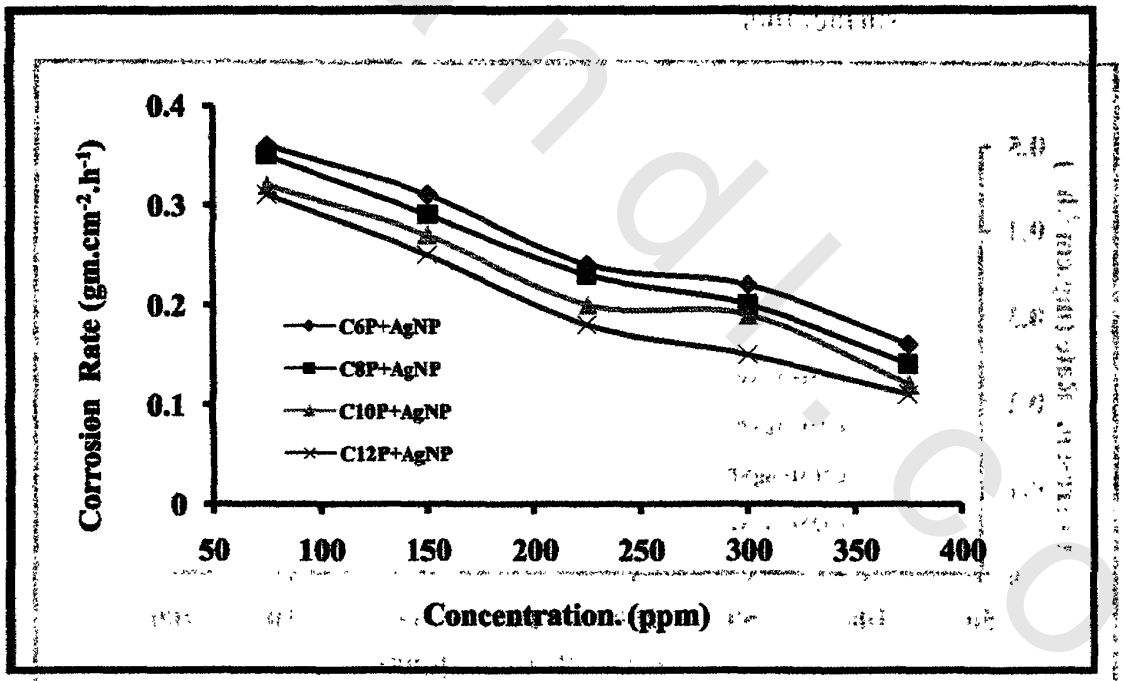

Figure (65) Relationship between corrosion rate of steel and concentration of the synthesized polymeric thiol surfactants with silver nanoparticles

4.4.1.2. The inhibition Efficiency of the synthesized surfactants as corrosion inhibitors

The inhibition efficiency (η %) of an inhibitor calculated from the following equation

$$\eta\ \% = (CR - CR^{\backslash}) / CR \times 100 \qquad (7)$$

where **CR** and **CR** $^{\backslash}$ are corrosion rate values of carbon steel in absence and presence of inhibitor respectively

The inhibition efficiency of the organic compounds depends on many factors including the number of adsorption sites and their charge density, molecular size, heat of hydrogenation, mode of interaction with the metal surface and formation of metallic complexes **[Fouda et al., 1986]**. The inhibition of a corrosion process by addition of surfactants may take place through two effects, namely blocking and hydrophobic effects. The former occurs when the inhibitor molecule is adsorbed on the metal surface through the adsorption centers in the molecules. In the investigated surfactants there are Nitrogen (N), oxygen (O) and sulfur (S) atoms which can act as adsorption centers in the molecule. Adsorptions of cationic inhibitor prevent contact between the steel surface and the acid solution. It exists at the interface and attaches or adsorb to the metal surface. The adsorption takes place by head group (SH) and tail group (hydrocarbon chain) of each molecule forming barrier film. The adsorption takes place by dipole induced interaction with the steel surface as a result of π electron polarization **[Hajjaji et al., 1993].** Charge and mass transfer are inhibited due to hydrophobizing the metal surface by inhibitor molecules. Surfactants have a characteristic structure consisting of a structural group that has very little attraction for the solvent, known as a hydrophobic group, together with a polar head. When the surfactant is dissolved in water, the presence of the hydrophobic group in the

solvent causes a distortion of the solvent liquid structure, increasing the free energy of the system. As compromise, the surfactant concentrates at the interface because there the thermodynamically best arrangement is possible. At the metal solution interface the surfactant molecules orientate their polar heads toward the metal and are adsorbed on its surface. The hydrophobic part is oriented away into the solution, repelling thus, the aqueous fluid. Under such conditions a diffusion barrier to chemical and / or electrochemical attack of the solution on the metal surface is established. The inhibiting effect increases with an increase of surfactant concentration **[Koopal and Ralstan, 1986].** At low surfactant concentration the adsorption takes place by horizontal adsorpation to hydrophobic region. This adsorption is a competitive one because the inhibitor displaces progressively the water molecules and other ions adsorbed. When surfactant concentration increases, a perpendicular adsorption takes place as a result of an inter-hydrophobic chain interaction **[Elachouri et al., 1996].**

Inspection of the data in Tables (11-14) and Figures (66-69), it is obvious the inhibition efficiency of the prepared inhibitors increases with increasing concentration of the prepared inhibitor.

For comparing of synthesized monomeric thiol surfactants as corrosion inhibitor it was found that the inhibition of these compounds increase in the order C6 <C8 < C10< C12 due to increasing in hydrocarbon chain length and by comparing synthesized monomeric thiol surfactants with assembling on silver nanoparticlies . It is clear that the efficiency in presence of silver nanoparticlies is more than that without silver nanoparticlies in the same order of monmeric surfactants this is due

to adsorption of silver on the surface of metal which lead to formation of protective film on steel surface and causes inhibition **[Li et al., 2006].**

The data in Tables (11-14) also show that the nanostructure of synthesized polymeric thiol surfactants with AgNPs have more efficiency than that of the individual surfactants which related to the protective film on steel formed by AgNPs. It is clear from the results in Tables (11-14) and Figures (66-69) that the polymeric thiol surfactants and their nanostructure with the AgNPs have more efficiency than the monomeric thiol surfactant due to the polymeric thiol surfactants have more hydrophobic and hydrophilic moiety in their chemical structure which enhancement their adsorption on steel and their corrosion inhibition.

Table (11): Inhibition efficiency of the synthesized monomeric surfactants in 1M HCl for the carbon steel sample at 25 ^{O}C and different concentrations

Concentration, (ppm)	Inhibition efficiency η (%)			
	C6M	C8M	C10M	C12M
75	47.40	53.26	54.50	57.00
150	55.60	58.40	61.80	64.40
225	64.70	66.60	70.40	72.10
300	66.90	70.40	71.60	75.10
375	71.20	74.30	75.90	79.40

Table (12): Inhibition efficiency of the synthesized monomeric surfactants with silver nanoparticles in 1M HCl for the carbon steel sample at 25 ^{O}C and different concentrations

Concentration, (ppm)	Inhibition efficiency η (%)			
	C6M+ AgNPs	C8 M+ AgNPs	C10 M+ AgNPs	C12M+ AgNPs
75	56.60	58.30	60.90	61.80
150	61.80	62.60	66.10	66.90
225	70.38	71.20	73.80	75.50
300	72.10	74.20	75.96	79.30
375	78.50	80.70	82.80	83.70

Table (13): Inhibition efficiency of the synthesized polymeric surfactants in 1M HCl for the carbon steel sample at 25^{O}C and different concentrations

Concentration , (ppm)	Inhibition efficiency η (%)			
	C6P	C8P	C10P	C12P
75	50.90	56.70	58.00	60.40
150	59.00	61.80	65.20	68.00
225	68.10	70.40	73.80	75.50
300	70.30	73.80	75.10	78.50
375	74.60	77.70	79.30	82.80

Table (14) Inhibition efficiency of the synthesized polymeric surfactants with silver nanoparticles in 1M HCl for the carbon steel sample at 25 ^{O}C and different concentrations

Concentration , (ppm)	Inhibition efficiency η (%)			
	C6P+ AgNPs	C8P+ AgNPs	C10P+ AgNPs	C12P+ AgNPs
75	60.10	61.80	64.30	65.20
150	65.20	66.10	69.50	70.30
225	73.80	74.60	77.70	78.96
300	75.50	77.70	79.30	82.30
375	81.90	84.10	86.30	87.59

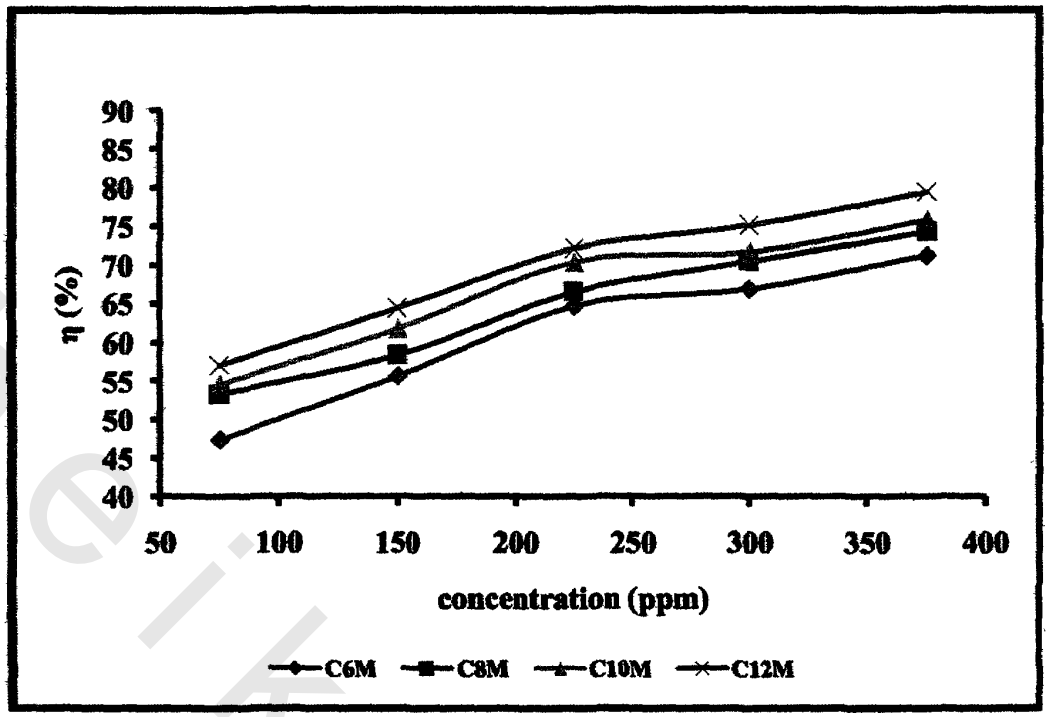

Figure (66). The Relation between inhibition efficiency and concentration of the synthesized monomeric thiol surfactants in 1 M HCl for the carbon steel sample at 25^{o}C

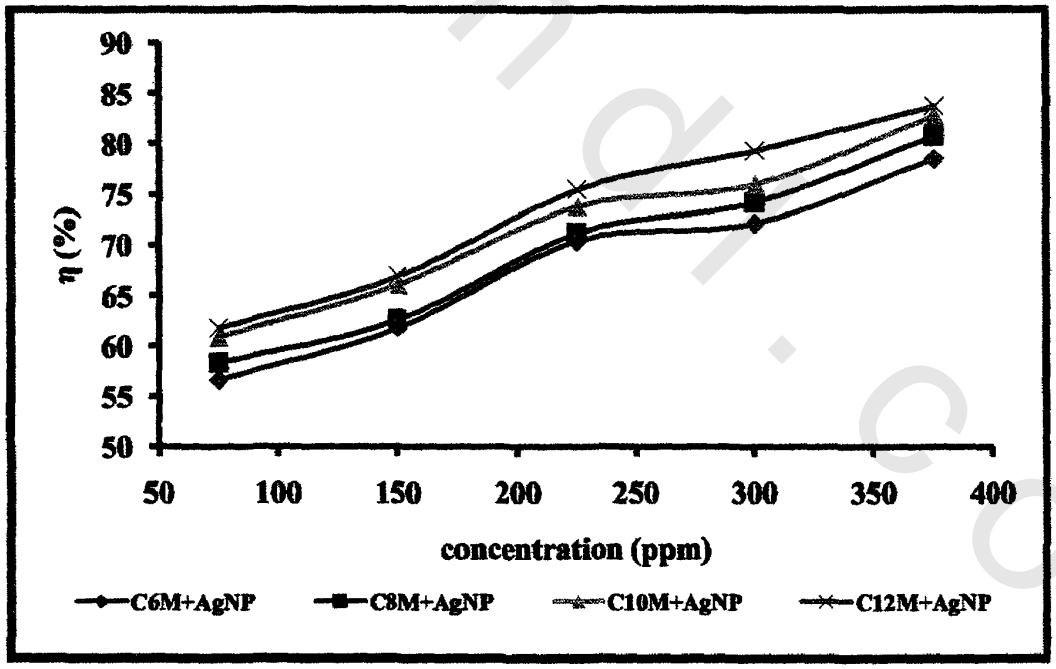

Figure (67). The Relation between inhibition efficiency and concentration of the synthesized monomeric thiol surfactants with silver nanoparticles in 1 M HCl for the carbon steel sample at 25^{o}C

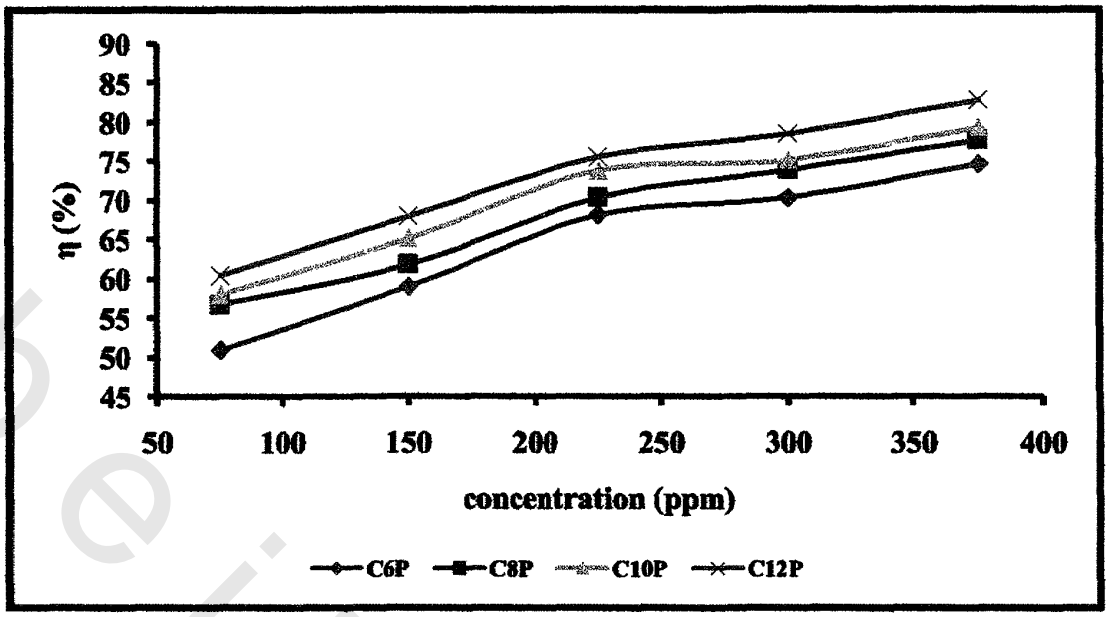

Figure (68) The Relation between inhibition efficiency and concentration of the synthesized polymeric thiol surfactants in 1 M HCl for the carbon steel sample at 25^{O}C

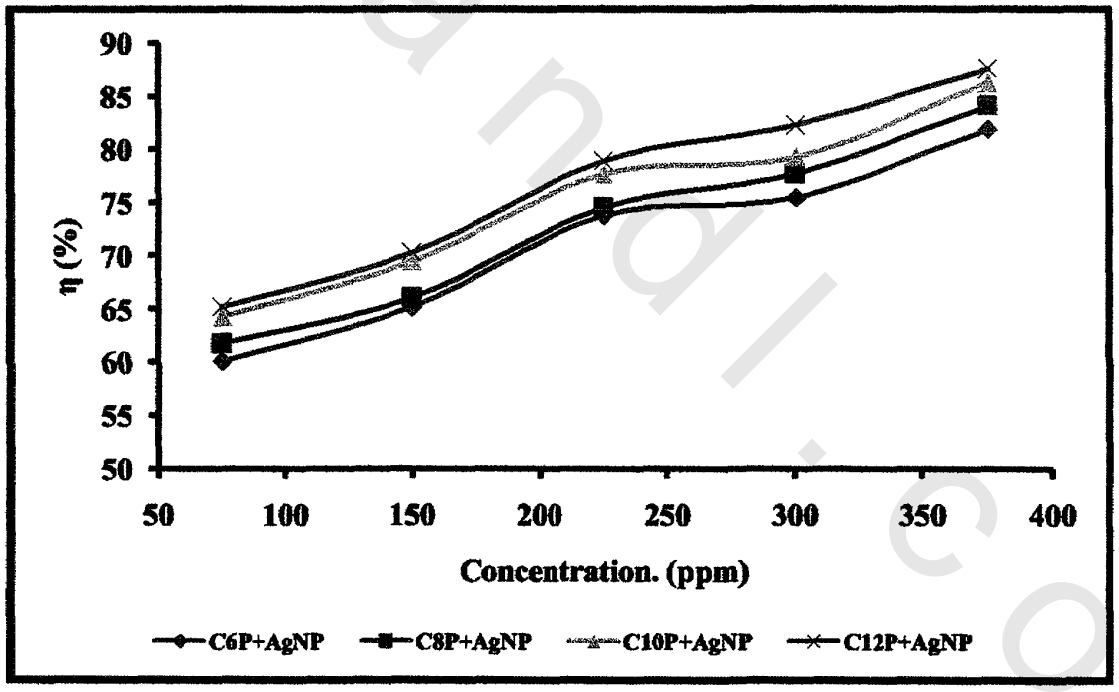

Figure (69) The Relation between inhibition efficiency and concentration of the snthesized polymeric thiol surfactants with silver nanoparticles in 1 M HCl for the carbon steel sample at 25^{O}C.

4.4.2. Tafel Polarization Measurements

The generation of polarization curves continues to be important in aqueous corrosion research. The time-consuming potentiostatic method has been largely replaced by the potentiodynamic approach where the potential (E) of the corroding metal is automatically varied with the time. The current (I) needed to maintain the metal (working electrode) at each applied potential is ascertained and the potential/current data is plotted to give the experimental polarization curve. Extrapolation of Tafel lines is one of the most popular direct current (DC) techniques for estimation of corrosion rate. The extrapolation of anodic and/or cathodic Tafel lines for charge transfer controlled reactions gives the corrosion current density, I_{corr}, at the corrosion potential, E_{corr}.

Corrosion current densities were obtained from the polarization curves by linear extrapolation of the Tafel curves. Since the corrosion rate is directly related to the corrosion current I_{corr}, the inhibition efficiency η % at different inhibitor concentrations were calculated from the equation(8)

$$\eta\ \% = \{(I_{corr} - I'_{corr}) / I_{corr}\} \times 100 \quad (8)$$

where I_{corr} and I'_{corr} are the corrosion current densities (mA cm^{-2}) with and without addition of inhibitor, respectively.

According to the weight loss and the efficiency inhibition results which indicate that the synthesized 12-(3-amino phenoxy) dodecane-1-thiol (C12M) and poly 12-(3-amino phenoxy) dodecane-1- thiol (C12P) and their nanostructure with AgNPs gives the best corrosion inhibition for steel. The corrosion inhibition of C12M and C12P and their nanostructure with AgNPs was investigated using Tafel polarization and EDAX as follow.

The anodic and cathodic polarization curves for carbon steel in 1M HCl at different concentrations of the synthesized C12M and C12P and thier nanostructure with AgNPs are shown in Figurs (70-73) It is clear that the presence of inhibitor causes a markedly decrease in the corrosion rate, i.e. shifts the anodic curves to more positive potentials and the cathodic curves to more negative potentials. This may be ascribed to adsorption of inhibitor over the corroded surface **[Gomma and. Wahdan, 1995]**. The values of corrosion current densities (I_{corr}), corrosion potential (E_{corr}), the cathodic Tafel slope (bc), anodic Tafel slope (ba), and the inhibition efficiency (η %) as functions corrosion inhibitors concentrations, were calculated from the curves of Figures (70-73) and given in Tables (15-18).Tables (15-18) reveals that the corrosion current decreases obviously and efficiency η % increases with the inhibitor concentration. The presence of corrosion inhibitors does not remarkably shift the corrosion potential, while the anodic and cathodic Tafel slopes change upon addition of increasing inhibitor concentration. Therefore, these corrosion inhibitors can be acts as mixed-type inhibitor in 1M HCl Similar results have been reported with other organic compounds in acidic medium [**Bentiss et al.,2000, Tang et al., 2003**]. From Tables (15-18), it can be concluded that inhibition efficiencies obtained from weight loss and electrochemical polarization curves are in good agreement. Also the nanostructure of the synthesized monomeric and polymeric thiol surfactants with AgNPs has more inhibition efficiency which gives a clear indication about the effect of AgNPs in the inhancement of the inhibition efficiency for these surfactants.

Table (15): Potentiodynamic polarization parameters of compound C12M in 1M HCl 25 ^{o}C

Sample		E_{corr} (i=0) mV	I_{corr} mA cm^{-2}	b_a mV	b_c mV	η%
C12M	Blank (1M)HCl	-569.600	0.233	166.700	-120.700	0.000
	75 ppm	-531.100	0.136	114.600	-127.800	41.630
	150 ppm	-553.700	0.121	161.700	-122.300	48.069
	225 ppm	-539.600	0.116	123.200	-123.700	50.215
	300 ppm	-585.000	0.073	95.600	-106.900	68.670
	375 ppm	-585.600	0.065	96.600	-106.400	72.103

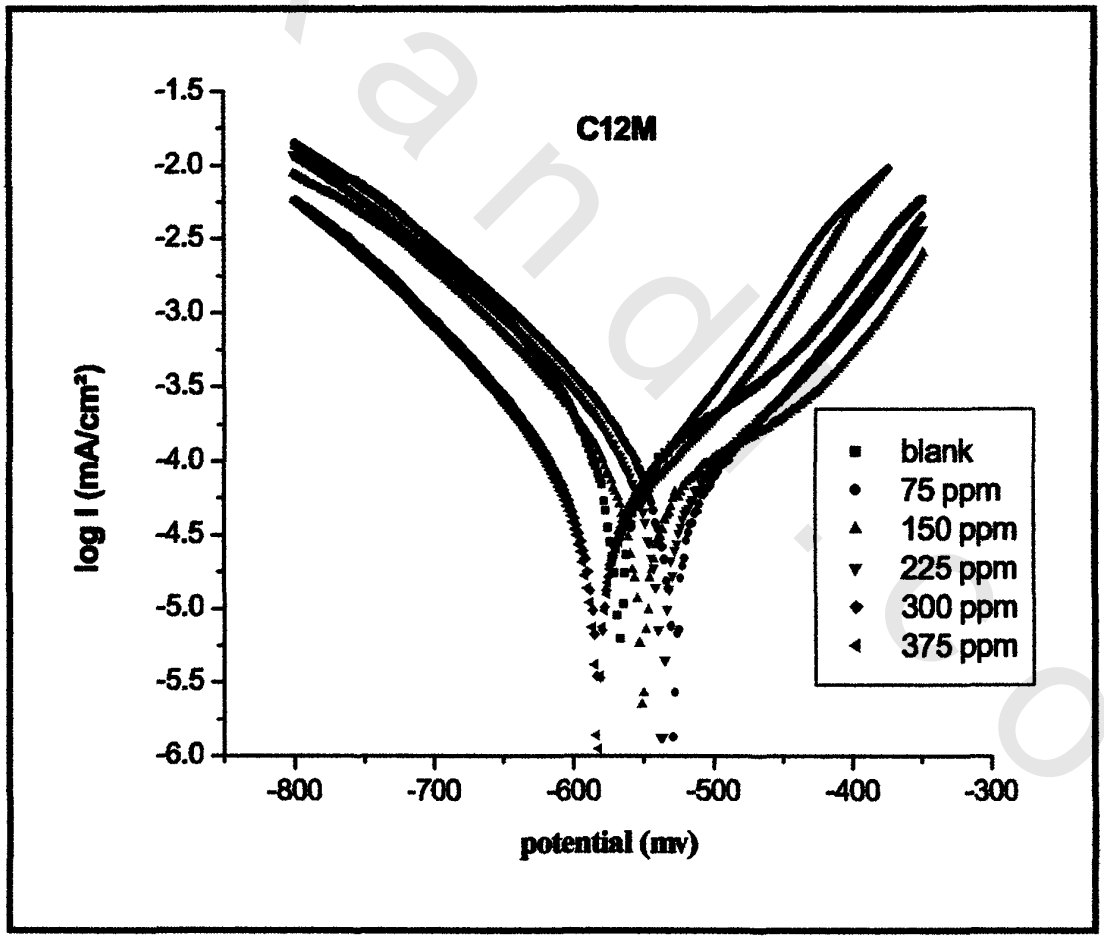

Figure (70). Tafel line for the carbon steel sample in 1 M HCl and at different concentrations of compound C12M

Table (16): Potentiodynamic polarization parameters of compound C12M with AgNP in 1M HCl at 25 ^{o}C

Sample		E_{corr} (i=0) mV	I_{corr} mA/ cm²	b_a mV	b_c mV	η%
C12M+AgNPs	Blank (1M)HCl	-569.600	0.233	166.700	-120.700	0.000
	75 ppm	-603.500	0.122	123.100	-101.400	47.682
	150 ppm	-557.800	0.112	293.600	-120.200	51.974
	225 ppm	-581.100	0.087	100.300	-106.200	62.790
	300 ppm	-579.800	0.067	113.000	-114.300	71.373
	375 ppm	-586.300	0.057	103.900	-111.200	.75.536

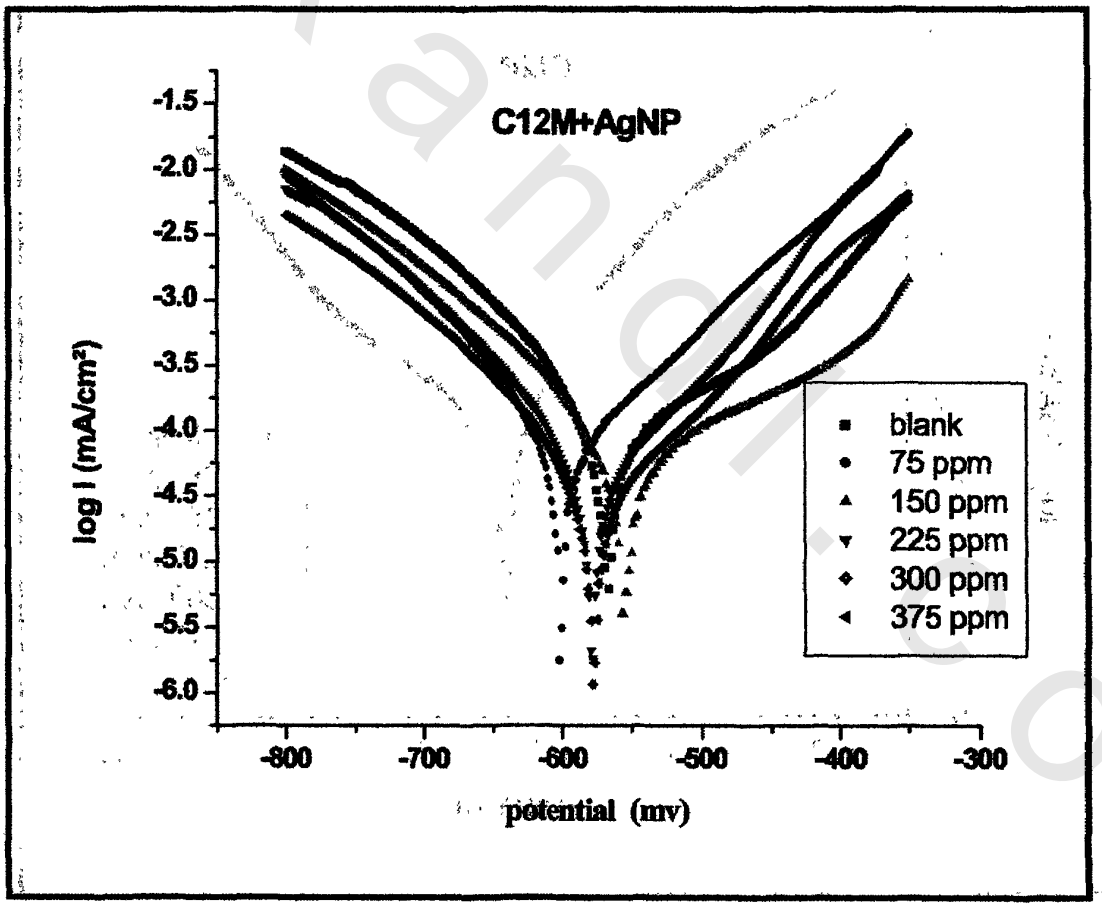

Figure (71). Tafel line for the carbon steel sample in 1 M HCL and at different concentrations of compound C12Mwuth AgNPs

Table (17): Potentiodynamic polarization parameters of compound C12P in 1M HCl at 25 °C

Sample		E_{corr} (i=0) mV	I_{corr} mA/cm²	b_a mV	b_c mV	η%
C12P	Blank (1M)HCl	-569.600	0.233	166.700	-120.700	0.000
	75 ppm	-543.200	0.128	165.700	-134.100	44.936
	150 ppm	-553.800	0.120	159.000	-119.800	48.369
	225 ppm	-578.800	0.109	370.000	-111.000	53.219
	300 ppm	-580.500	0.071	96.500	-103.800	69.657
	375 ppm	-577.000	0.063	83.000	-105.000	73.133

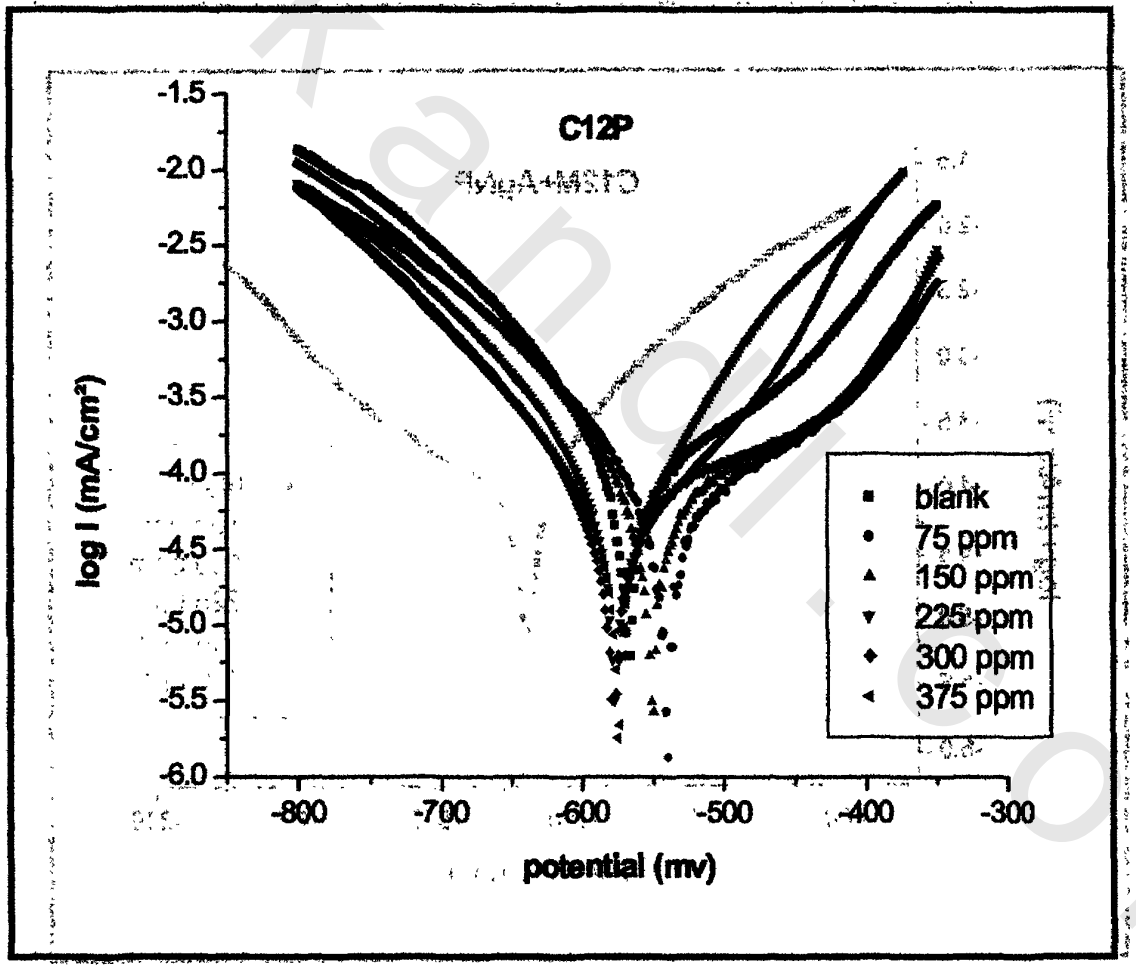

Figure (72). Tafel line for the carbon steel sample in 1 M HCL and at different concentrations of compound (C12P)

Table (18): Potentiodynamic polarization parameters of compound C12P with AgNPs in 1M HCl at 25 ^{o}C

Sample		E_{corr} (i=0) mV	I_{corr} mA/cm^2	b_a mV	b_c mV	η%
C12P+AgNPs	Blank (1M)HCl	-569.600	0.233	166.700	-120.700	2.725
	75 ppm	-563.300	0.116	172.000	-123.300	50.258
	150 ppm	-583.500	0.107	102.900	-119.200	53.948
	225 ppm	-582.100	0.079	100.100	-108.200	66.008
	300 ppm	-582.800	0.061	107.800	-112.100	73.948
	375 ppm	-587.200	0.055	201.400	-113.300	76.437

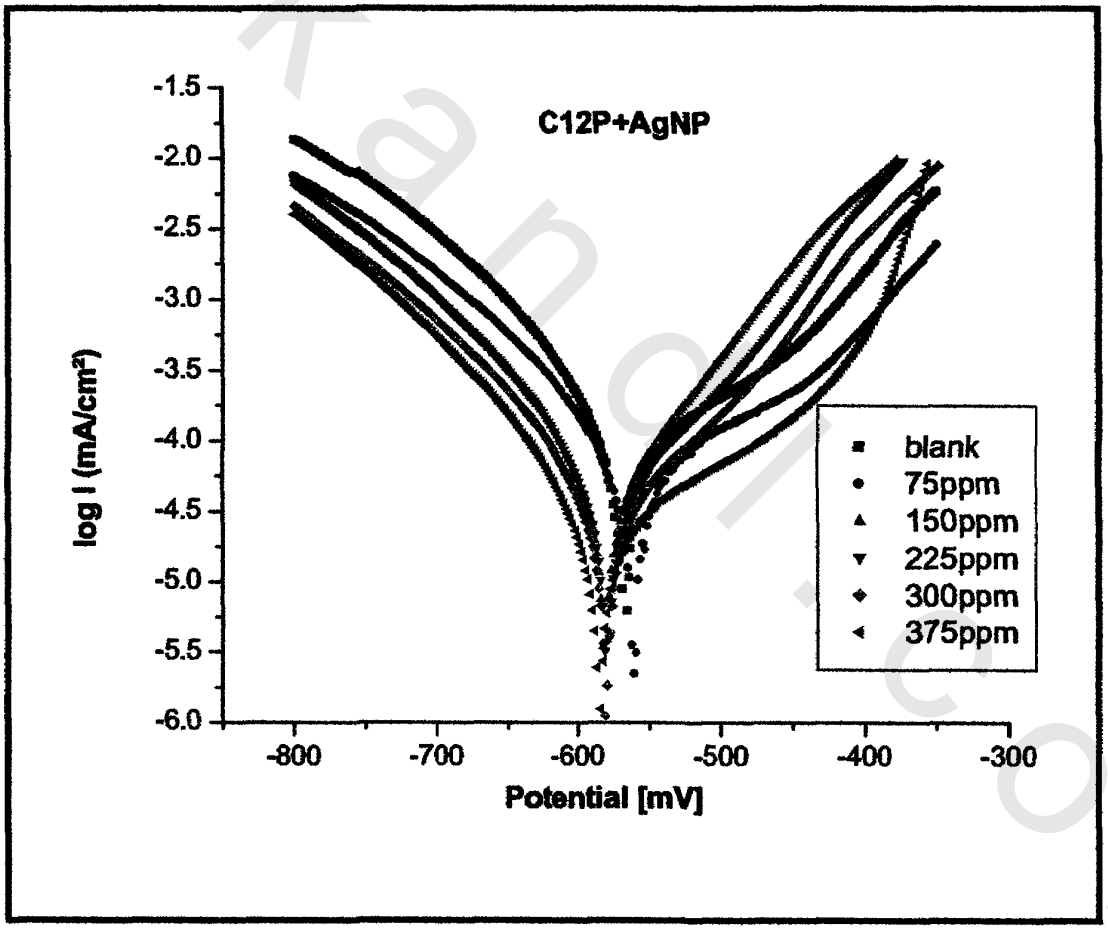

Figure (73). Tafel line for the carbon steel sample in 1 M HCL and at different concentrations of compound C12P with AgNPs

4.4.3. Energy Dispersive Analysis of X-rays (EDAX)

The protective film formed on carbon steel surface was analyzed using an energy dispersive analysis of X-ray technique (EDAX) as shown in Figure 74. The spectrum obtained by EDAX indicated that carbon steel sample immersed in 1 M HCl solution was failed in the absence of inhibitor molecules because it was severely weakened by external corrosion as shown in Figure 74 (a). By addition of 375 ppm of 12-(3-amino phenoxy) dodecane-1- thiol (C12M), the surface of carbon steel sample was greatly improved due to formation of protective film of the surfactant molecules as indicated by the decrease of iron band in Figure 74 (b).

The appearance of two bands of silver and the strong decrease in iron band in the presence of 375 ppm of 12-(3-amino phenoxy) dodecane-1- thiol self-assembled on silver nanoparticles (C12M+AgNP) as shown in Figure. 74 (c).By addition of 375 ppm of poly 12-(3-amino phenoxy) dodecane-1- thiol (C12P), the surface of carbon steel sample was greatly improved due to formation of protective film of the surfactant molecules as indicated by the decrease of iron band in Figure 75 (a). The appearance of two bands of silver and the strong decrease in iron band in the presence of 375 ppm of poly 12-(3-amino phenoxy) dodecane-1- thiol self-assembled on silver nanoparticles (C12P+AgNP) as shown in Figure 75(b) indicated that the protective film formed was strongly adherent to the surface, leading to a high degree of inhibition efficiency this is the same in case of poly 12-(3-amino phenoxy) dodecane-1- thiol (C12P) as shown in Figure 75 **[Amin, 2006, Migahed et al., 2009].**

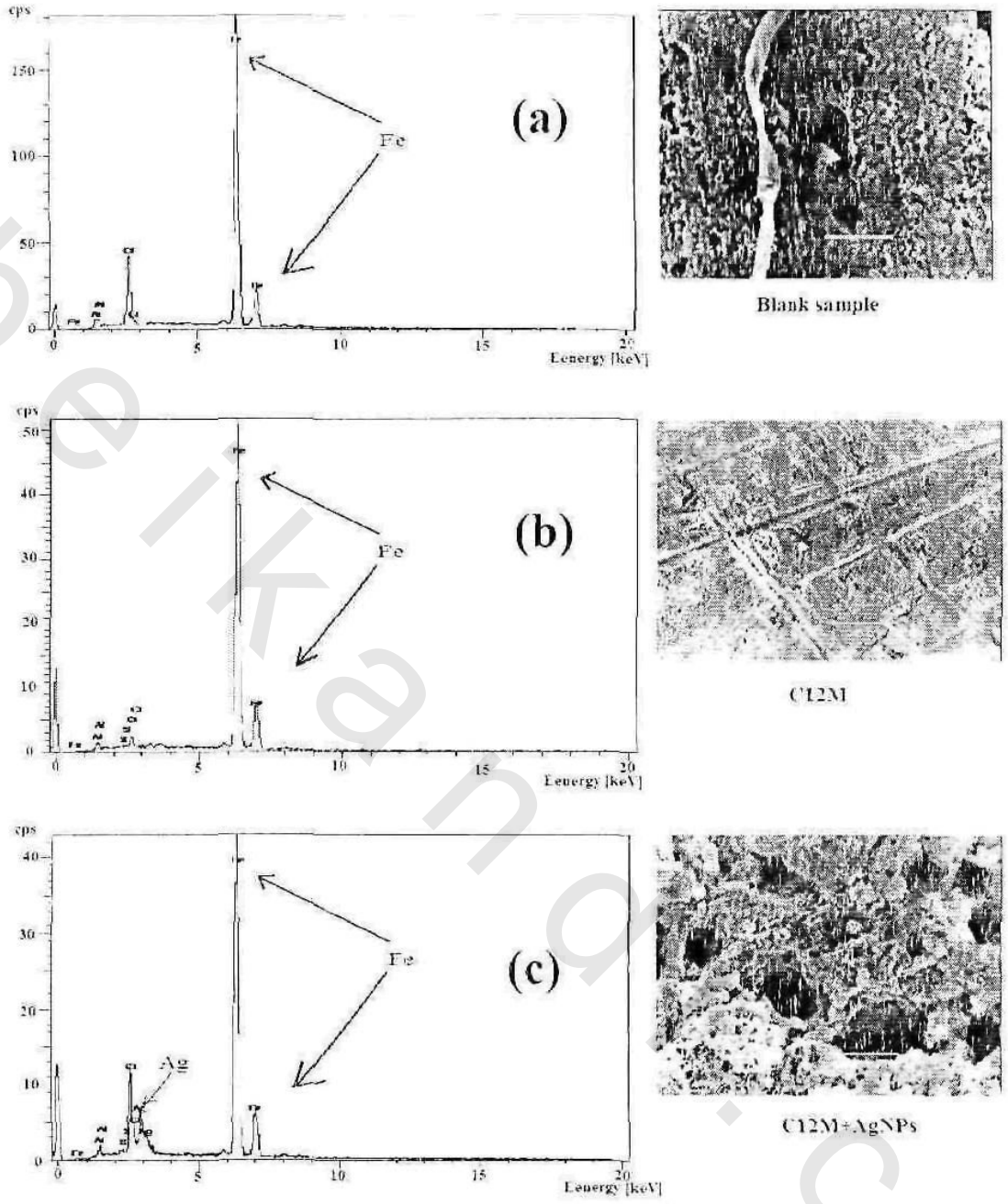

Figure (74) Energy Dispersive Analysis X-rays (EDAX) of carbon steel samples: (a) After immersion in 1 M HCl solution for 24 h. (b) After immersion in 1 M HCl solution for 24 h in the presence of C12M. (C) After immersion in 1 M HCl solution for 24 h in the presence of C12M self-assembled on silvernanoparticles.

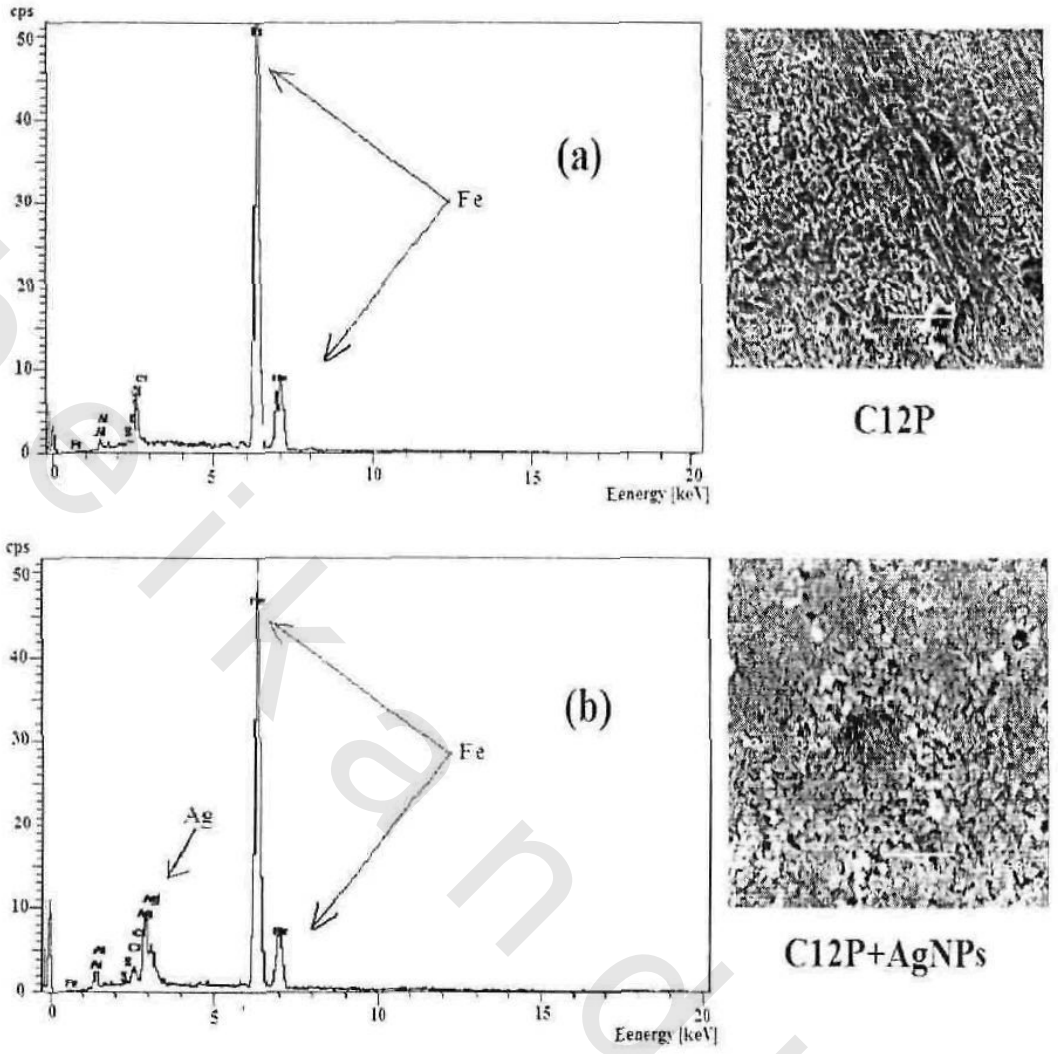

Figure (75) Energy Dispersive Analysis X-rays (EDAX) of carbon steel samples: (a) after immersion in 1 M HCl solution for 24 h in the presence of C12P. (b) after immersion in 1 M HCl solution for 24 h in the presence of C12P self-assembled on silver nanoparticles.